Stony Brook University

Correlating Structure and Function in Class A GPCRs

A Dissertation Presented

by

Joseph A. Goncalves

to

The Graduate School

in Partial Fulfillment of the

Requirements

for the Degree of

Doctor of Philosophy

in

Molecular and Cellular Biology

Stony Brook University

August 2012

Stony Brook University

The Graduate School

Joseph A. Goncalves

We, the dissertation committee for the above candidate for the Doctor of Philosophy degree, hereby recommend acceptance of this dissertation.

Steven O. Smith, Ph. D

Professor and Director of Structural Biology

Department of Biochemistry and Cell Biology

Suzanne Scarlata, Ph. D

Professor, Department of Physiology and Biophysics

James Konopka, Ph. D

Professor, Department of Molecular Genetics and Microbiology

Mark Bowen, Ph. D

Assistant Professor, Department of Physiology and Biophysics

Philip J. Reeves, Ph. D

Lecturer in Biochemistry, School of Biological Sciences, University of Essex

This dissertation is accepted by the Graduate School

Charles Taber

Interim Dean of the Graduate School

Abstract of the Dissertation

Correlating Structure and Function in Class A GPCRs

by

Joseph Goncalves

Doctor of Philosophy

in

Molecular and Cellular Biology

Stony Brook University

2012

Class A G protein-coupled receptors (GPCRs) serve as the gatekeepers for cell signaling in eukaryotes. With over 4% of the human protein-encoding genome dedicated to their expression, GPCRs are accountable for a variety of physiological responses including, vision, vasodilation, and cell migration. These receptors all contain seven transmembrane helices and a number of conserved residues suggesting a universal activation mechanism.

In order to understand GPCR activation, it is essential to delineate the structural differences between ligand-bound receptor conformations. Despite the breadth of biophysical studies conducted to date, how ligand binding is coupled to receptor activation remains to be elucidated. In this thesis, solid-state NMR studies are presented that target conformational changes in the low light visual pigment rhodopsin, a prototypical GPCR. Rhodopsin is activated by a light-induced 11-*cis* to *trans* isomerization of a covalently bound retinal chromophore. The experimental data presented define global structural changes that couple receptor activation with the binding of downstream signaling targets. Activation-induced changes are described in the region of transmembrane helices H5 and H6. First, NMR distances measurements are used to temporally separate the motion of H6. Using $^{13}C\ldots^{13}C$ dipolar couplings we observe a rotation of transmembrane helix H6 upon formation of Meta I. Meta I is the inactive predecessor of the signaling competent state, Meta II. Rotation of H6 in Meta I reflects the disruption of a salt

bridge between Arg135$^{3.50}$ and Glu247$^{6.40}$ prior to displacement of the transmembrane helix in Meta II, which is required for coupling to heterotrimeric G protein. In addition, we show that H5 undergoes a rotation in the transition to Meta II. Specifically, we observe NMR contacts between Tyr223, Tyr306, Met257, and Arg135 that reveal a close association between these residues in the active Meta II state. Rotation of H5 allows a direct interaction to form between signature-conserved residues Tyr223$^{5.58}$ and Arg135$^{3.50}$. Fluorescence spectroscopy is used to measure the rate of active state decay. We find that the Tyr223$^{5.58}$ and Arg135$^{3.50}$ interaction is crucial in stabilizing the active conformation of H5. The structural studies on rhodopsin are extended to the ligand-activated β_2-adrenergic receptor. We use NMR to probe the rotational orientation of transmembrane helix H5 in the presence of various ligands. The data show a graded rotation of H5 that correlates with ligand efficacy. Together, the structural studies on rhodopsin and the β_2-adrenergic receptor reveal that H5 rotation is a common element of GPCR activation.

TABLE OF CONTENTS

LIST OF ABBREVIATIONS

ATD, amino-terminal domain

β2-AR, beta 2-adrenergic receptor

C1-C20, positions for carbon nuclei in retinal

cGMP, cyclic guanidine monophosphate

IL1 – IL3, intracellular loop regions of G protein-coupled receptors

CP, cross polarization

DARR, dipolar assisted rotational resonance

DDM, nβ-d-dodecyl –maltoside

DMEM, Dulbecco's Modified Eagle medium

DOPC, dioleoylphosphotidylcholine

DOPE, dioleoylphosphotidylethanolamine

EL1 – EL3, extracellular loop regions of G protein-coupled receptors

EPR, electron paramagnetic resonance

FBS, fetal bovine serum

GDP, guanidine diphosphate

GMP, guanidine monophosphate

GPCR, G protein-coupled receptor

GRK, G protein-coupled receptor kinase

GTP, guanidine triphosphate

H1 - H8, helices 1 through 8 in G protein coupled receptors

HPLC, high performance liquid chromatography

FTIR, Attenuated total reflection infrared spectroscopy

MAS, magic angle spinning

MD, molecular dynamics

Meta II, metarhodopsin II

NMR, nuclear magnetic resonance

ppm, parts per million

PBS, phosphate-buffered saline

PDE, phosphodiesterase PSB, protonated Schiff base

ROS, rod outer segment

UV-Vis, ultraviolet-visible

WT, wild-type

LIST OF FIGURES

LIST OF TABLES

ACKNOWLEDGEMENTS

Several people have had integral roles in the work presented in this thesis. I would like to extend a special thank you to each of them. To Markus Eilers, an assistant research professor for his integral role in sample preparation. Markus was responsible for all the cell culture aspects of expressing many of the isotope-enriched rhodopsin samples. To Aashish Patel and Evan Crocker former members of the Smith lab that established the protocols for sample preparation used to date. To Shivani Ahuja, with whom I worked closely for the first three years of my time here at Stony Brook. Shivani showed me how to purify rhodopsin as well as run and interpret NMR experiments. She also conducted many of the NMR data included in this thesis to characterize Meta I. To Prof. Phil Reeves from the University of Essex, whose lab generated the stable cell lines used for inducible receptor expression. Moreover, the Reeves lab conducted the transducin activity and Meta II decay assays that helped to put the structural features of several rhodopsin mutants in the context of receptor function. To Mordechai Sheves at a Weizmann institute for preparing ^{13}C-enriched retinal. To Prof. Reiner Vogel and Katrina Zaitseva from the University of Freiburg for providing FTIR spectroscopic data that helped us understand the kinetics of several rhodopsin mutants. To Prashen Chelikani from the University of Manitoba, who generated the β_2AR stable cell line that was used to collect data presented in this thesis. A special thanks is also in order for Brian Kobilka at Stanford University. Prof. Kobilka provided invaluable advice on the purification strategies, various ligands and purified Nb80 for the β_2AR work. Particularly, Aashish Manglik from the Kobilka lab has helped in constructing a FLAG-tagged β_2AR stable cell line. To Martine Ziliox, the NMR facility manager at Stony Brook University. Martine serves the indispensible role of making sure the spectrometers are up and running at all times. Her extensive knowledge of hardware and pulse program syntax makes her an invaluable asset. Trained as a physicist, she also provides clear and concise explanations for the fundamental principles of NMR in a manner that can be easily understood by the non-specialist. Lastly I thank Prof. Steven O. Smith. Without his support and access to his collaborators mentioned above, this work would not have been possible. I also thank Prof. Smith for his immense role in research design and manuscript preparation.

CHAPTER 1: INTRODUCTION

1.1. G protein-coupled receptors: a superfamily of integral membrane receptors.

The superfamily of G protein-coupled receptors (GPCRs) comprises an extensive group of integral membrane proteins that are essential for a wide variety of cell signaling pathways. Members of the GPCR superfamily share a common secondary structure consisting of seven transmembrane helices that are bridged by extended loop regions, which help to make up both the intracellular and extracellular surface of the receptor. GPCRs also share a common class of intracellular binding partners in the eponymous heterotrimeric G proteins (Gαβγ) whose α subunits (Gα) are bound to guanosine diphosphate (GDP). Upon activation, the cytosolic surface of GPCRs interacts with Gα to induce guanine nucleotide exchange. In its GTP-bound form, Gα dissociates from the βγ subunit and both moieties interact with downstream signaling targets to propagate the signal of ligand binding.

In spite of the global similarities in both topology and intracellular binding partners, GPCRs have evolved to recognize and transduce an extraordinarily broad range of signals that includes light, Ca^{++}, small organic molecules and large peptide hormones. These receptors are exclusive to eukaryotes and are found in both vertebrates as well as invertebrates (*1*). GPCRs can be divided into six classes (A-F) based on sequence homology and functional similarity (*1-3*).

The class A (rhodopsin-like family) receptors respond to the presence of diverse stimuli ranging from light to various ligands, which include small molecule amines, and hormones. Class B (Secretin and Adhesion families) receptors are activated by peptides of the glucagon hormone family (*4, 5*). Receptors in class C (Glutamate family) are composed of the metabotropic glutamate receptors, which are characterized by a large N-terminal ligand-binding domain (*6*) that is structurally homologous to the amino terminal domain of the ligand-gated ionotropic glutamate receptors in postsynaptic neuronal membranes (*7*). Pheromones (e.g. α-factor) secreted by *Saccharomyces cerevisiae* bind to class D GPCRs (e.g. STE2) during the mating process. Similar mechanisms are in place for mating of several fungi (*8*). Class E receptors have been implicated in the chemotactic migration of slime mold and can potentially be exploited as antifungal targets (*9, 10*). Class F (Frizzled/smoothened/taste2 family) contains

receptors in the Wnt signaling pathway (*11*), which perform indispensable roles in embryonic development (*12*).

The majority of GPCRs are categorized as class A receptors. In the GPCR database, there are over 20,000 class A sequences from various species. 952 of 1061 GPCRs in the human genome are in class A, most (509) of which are involved in olfaction. Non-olfactory class A GPCRs are further divided among 19 subfamilies including the well-studied visual and small molecule amine receptors, as well as hormone and peptide receptors. Despite the breadth of the class A subfamily, there exists a degree of sequence conservation among these receptors. Furthermore, the class A receptors share similar mechanisms of receptor downregulation. Activated receptors are targeted for phosphorylation by one of seven related G protein-coupled receptor kinases (GRK1-7) (*13-16*). Subsequently, these post-translational modifications serve as docking sites for yet another homologous class of proteins, arrestin(*17-20*). Once bound to a receptor, arrestin molecules recruit components of the clathrin-mediated mechanism for endocytosis. The fact that arrestin molecules from the retina are able to desensitize β_2 adrenergic receptor (β_2AR) signaling underscores a common mechanism by which class A GPCR signaling is down-regulated (*21, 22*).

In terms of their pharmacology, members of the class A GPCR subfamily currently make up over 25% of the proteome accessible to small molecule drugs (*23*). There are a number of factors that make class A GPCRs such a predominant pharmacological target. First, they are widely involved in a variety of cellular processes. In addition, their location on the cell surface renders them accessible to drug binding. Furthermore, there are several clinical mutations in GPCRs that are associated with pathologies ranging from asthma and allergies to Parkinson's disease (*24, 25*). These mutations modulate activity and the resulting phenotypes are associated with the aberrant signaling properties of non-native receptors. In the visual system for example, mutations in rhodopsin can result in autosomal dominant retinitis pigmentosa, an inherited human disease that causes progressive retina degeneration due to the misfolding of the visual receptor, or congenital night blindness, which is due to constitutive receptor activation (*26*).

The amine subfamily of receptors (including the noradrenaline, dopamine, histamine, and 5-hydroxytryptamine receptors) is the largest drug target among GPCRs. Saunders (*27*) estimated that of the 35 top GPCR prescription drugs in 2003, 24 ligands targeted monoaminergic

receptors. Inhibitors of the angiotensin-II receptor were a distant second in the number of drugs on the market. Over the past seven years, the drug targets have expanded well beyond this limited set. For example, CCR5 and CXCR4 and their cognate chemokine agonists have been implicated in various inflammatory and autoimmune conditions as well as cancer. CXCR4 has also been shown to be crucial for embryonic development. Furthermore, CCR5 (*28, 29*) and CXCR4 (*30, 31*) are the major co-receptors used by HIV-1 for entry into host cells and specific entry inhibitors targeting these receptors have emerged as a new class of anti-HIV-1 drugs. Maraviroc (UK-427,857) is a potent antagonist of the CCR5 receptor that prevents HIV entry and is currently one of the only small molecule inhibitors available for HIV treatment (*32*).

1.2. Overall structure and activation mechanism.

Models of GPCR activation have been based on a two-state receptor model (*33, 34*). In these models, ligands modulate an equilibrium between two distinct conformations of the receptor. Under the framework of the two-state model, constitutive activity can be explained by an agonist-independent conversion from an inactive (R) state to an active (R*) state. Recently, data suggesting the existence of multiple conformational states have emerged that call for a reevaluation of the two-state model. For example, biochemical data have shown that an activated receptor is often capable of coupling to a number of heterotrimeric G proteins (*35*) and that different signaling cascades can be activated from a single receptor depending on the nature of the bound agonist (*36*).

The challenge is to now unravel what appears to be a continuum of possible conformations with varying degrees of activation selectively stabilized by different ligands (*37*). A crucial step in this process is to correlate cell-based activity data with structural characterization of differentially activated receptors. In the following subsections, a survey is presented of the high-resolution structural data that have contributed our current understanding of GPCRs and their activation mechanism. The current body of structural data available for GPCRs is dominated by X-ray crystallography. However, solid-state nuclear magnetic resonance (NMR) spectroscopy has also made a significant contribution. Together, these two high-resolution techniques provide a framework for understanding the wide range of biochemical (*38-42*) data in the literature, as well as biophysical data obtained from electron paramagnetic resonance (EPR) (*43-47*),

fluorescence (*48-50*), UV absorbance (*51, 52*), Fourier transformed infrared (FTIR) (*53-61*), and resonance Raman spectroscopy (*62-64*).

The subsections below present a survey of the structural data that currently describes the activation mechanism of class A GPCRs. For clarity, the relevant literature is discussed in the context of specific regions of the receptor. For each region, open questions for future pursuits are enumerated.

1.2.1. N terminus and extracellular loops.

In GPCRs, the peptide sequence prior the start of α-helical secondary structure in transmembrane helix H1 is variable in length and structure. Nevertheless, the N-terminal region (ATD) of GPCRs contains structural modules that are targets of post translational modification and ligand binding. Regions of the ATD have also been implicated in homodimerization of the bradykinin B_2 receptor (*65*).

Several Asn residues in the ATD fall within the consensus sequence for N-linked glycosylation. Post translational receptor glycosylation is required for proper trafficking in a number of GPCRs including the gonadotropin-releasing and luteinizing hormone receptor (*66*), as well as the neurokinin receptor (*67*). In other cases, such as the β_2AR (*68*), sugar moieties in the ATD influence ligand affinity.

There are several examples where the ATD is directly involved in ligand binding. For instance, crystal structures of soluble forms of the ATD from the metabotropic glutamate receptor have been determined which show a 'Venus flytrap' moiety in its open and closed state (*69, 70*). In addition, chemokine receptors operate under a two-step ligand binding process, whereby regions of chemokines associate with the ATD of their cognate receptors prior to interacting with the transmembrane core (*71*). In one unique receptor, the PAR (protease-activated receptor) the native peptide ligand is a component the ATD and activation is induced by a proteolytic event, which allows the tethered ligand to enter the binding pocket (*72*).

In rhodopsin, the ATD contains two stretches of residues that adopt β-sheet secondary structure (β1 and β2). In addition there are two N-linked glycosylation sites at Asn2 and Asn15, the latter of which is required for proper folding and receptor activation (*73*). Epitope mapping

reveals that binding of antibodies to the ATD results in a decrease in the dark state stability of rhodopsin (*74*). In addition, several mutations associated with autosomal dominant retinitis pigmentosa are found in the extracellular region. The implication is that ATD is more than a flexible region of GPCRs. As such, it will warrants further inquiry.

1.2.2. H1-H4 transmembrane core.

Much of the biophysical data that currently describes GPCR activation reveal structural changes predominantly in transmembrane helices H5, H6 and H7. One of the common features of H5-H7 is that each of the three helices contains a conserved proline residue, whose presence is known to disrupt secondary structure in α-helices (*75, 76*). In contrast, there are no conserved proline residues on H1-H4. In addition, the interfaces between H1-H4 are lined with a number of small residues (Gly, Ala, Ser), whose individual conservation is low but rises to over 90% when considered as a group. It has been proposed that the presence of these so-called 'group conserved' residues helps to mediate close packing interactions between α-helices (*77*). In the case of rhodopsin, site-directed mutagenesis of $Gly121^{3.36}$, a group conserved residue, compromises thermal stability of the inactive state (*78*). (Note, superscript denotes Ballesteros-Weinstein numbering. The first digit identifies the transmembrane helix. The remaining digits describe the proximity of a particular residue to the most conserved amino acid in the corresponding transmembrane helix, which is denoted 50 (*79*)). In the β_2AR, point mutations that introduce larger residues at group conserved positions on transmembrane helix H4 decreased ligand affinity (*80*). The deleterious effects of increasing the side chain volume at group conserved positions in the β_2AR were rescued by introducing smaller residues at neighboring positions within the H1-H4 core (*80*). When coupled with the lack of proline residues, group conservation within H1-H4 supports that a stable tetrad core remains relatively static upon receptor activation.

Interestingly, there are a number of studies that would argue for a pivotal role of transmembrane helix H3 in receptor activation and therefore challenge the idea of a stable H1-H4 core. For rhodopsin, activation-induced structural changes have been observed within the region of the conserved E/DRY motif at the cytosolic end of H3 in rhodopsin (*59*). Moreover, the rhodopsin activation mechanism is known to include an internal proton transfer between the retinal Schiff base linkage and a conserved glutamate residue on H3 (*60, 81, 82*). In the

dopamine D2 receptor, regions of H3 have been implicated in ligand binding (*83-85*). Perhaps one of the more compelling pieces of structural data in support of H3 motion comes from a direct comparison of active (*86*) and inactive (*87*) crystal structures of the β_2AR where a ratcheting motion is observed in the interface between transmembrane helices H3 and H6, which involves a motion of both helices (*86*). Nevertheless, whether or not H3 motion is a feature of GPCR activation remains an open question.

1.2.3. H5.

A variety of biophysical and biochemical studies have been conducted on active GPCRs to map the binding site of the heterotrimeric G protein. For rhodopsin, peptide mapping and crosslinking experiments have specifically implicated the second and third intracellular loop regions (IL2 and IL3, respectively). Studies have demonstrated that the interactions between active rhodopsin and transducin (G_t, the G protein associated with visual receptors) block the binding of antibodies whose epitopes are on IL2 and IL3 (*88*). Of note, antibodies designed to target the cytoplasmic surface of rhodopsin effectively inhibit the binding of G_s to β_2AR (*89*) and suggest that, despite a lack of sequence conservation, the cytosolic surfaces of class A GPCRs are similar. In 1994, a study conducted by the group of Heidi Hamm demonstrated that peptides designed to mimic IL3, were remarkably effective in disrupting the interactions between transducin and the active state of rhodopsin (*90*). In contrast, the consequence of occluding IL2 was moderate (*90*). The dominant role of IL3 in the binding of heterotrimeric G protein to active GPCRs is further demonstrated by site directed mutagenesis of both the β_1AR and β_2AR (*91*) as well as the muscarinic acetylcholine receptor (*92*).

In order for ligand binding at the extracellular surface to modulate the conformation of IL3, structural changes must be transmitted through the adjoined transmembrane helices, H5 and H6. The structure of active rhodopsin in complex with undecapeptides corresponding to the carboxy-terminus of transducin reveals specific interactions between the peptide and the cytosolic ends of transmembrane helices H5 and H6 (*93-95*).

The cytosolic end of transmembrane helix H5 contains a $Y(x)_7K(R)$ motif which is conserved throughout class A GPCRs. The $Y(x)_7K(R)$ motif contains a pair of conserved residues whose side chains form interactions that help to stabilize an active receptor conformation. Mutations in

this region have been shown to significantly destabilize the active state of rhodopsin (*96*) and stabilize the inactive state of the β_1AR (*97*). In rhodopsin, the two corresponding residues in the $Y(x)_7K(R)$ motif are Tyr223$^{5.58}$ and Lys231$^{5.66}$. In the dark, neither of these residues forms interactions within the receptor. Inactive crystal structures of ligand-activated GPCRs also fail to shown any interactions involving the $Y(x)_7K(R)$ motif. The implication is that sequence identity of the $Y(x)_7K(R)$ motif is maintained throughout GPCRs for the purpose of stabilizing active receptor conformations.

On the extracellular surface, residues on H5 interact with the β-ionone ring in rhodopsin (i.e. Met207$^{5.42}$, His211$^{5.46}$ and Phe212$^{5.47}$) (*98*). Upon retinal isomerization, these interactions are modulated in concert with changes in the interhelical hydrogen bonding network between transmembrane helices H3 and H5 (*99, 100*). A similar mechanism may be at work in the amine receptors where a triad of conserved serine residues interact with the hydrogen moieties of aminergic ligands (*101-105*). The goal is now to understand how specific interactions between ligands and the residues on H5 result in the cytosolic change required to form the active state interactions of $Y(x)_7K(R)$ motif. An allosteric coupling of these two microdomains would provide insights into how ligand binding at the extracellular surface modulates the structure of IL3 to allow formation of the ternary signaling complex (i.e. ligand, receptor, and heterotrimeric G protein).

1.2.4. H6.

One of the best documented features of the GPCR activation mechanism is a significant motion of the cytosolic end of transmembrane helix H6 away from H3. This motion was first characterized by electron paramagnetic resonance measurements of rhodopsin containing nitroxide spin labels attached to the cytoplasmic end of transmembrane helix H6 (*43*). Roughly concurrent with the EPR measurements, work from the group of Henry Bourne demonstrated that an engineered metal ion binding site, designed to restrict the motion of H6 with respect to H3, blocks rhodopsin activation (*106*). Displacement of H6 in rhodopsin is confirmed by crystallographic studies of putative active receptor conformations (*93, 94, 107, 108*).

The motion of transmembrane helix H6 seems to be a common feature of activation throughout GPCRs. For instance, in 1997, the Kobilka lab observed local changes in the

environment of several cysteine-linked fluorophores upon agonist bonding to the β_2AR (*109*). These changes were subsequently assigned to Cys125$^{3.44}$ and Cys285$^{6.47}$ and interpreted as structural perturbations on H6 brought about by receptor activation (*110*). Interestingly, Javitch *et al.* (*111*) demonstrated that the sidechain of Cys285$^{6.47}$ becomes accessible to the bulk solvent in the active conformation of the β_2AR. Comparisons of active (*112, 113*) and inactive (*87, 114*) crystal structures of the β_2AR further support the idea that H6 motion is a common theme of GPCR activation.

An active focus in the field of GPCR research is to determine precisely how ligand binding results in the necessary structural changes that induce the motion of transmembrane helix H6. Since H6 motion appears to be a common feature of GPCR activation, it stands to reason that the residues mediating helix motion are conserved. The most conserved residue of transmembrane helix H6 is a proline, which induces a kink in the backbone of the transmembrane helix. In addition, Pro$^{6.50}$ is a part of the conserved CWxP motif. A second set of conserved residues of H6 is an aromatic cluster that includes Trp$^{6.48}$, of the CWxP motif, as well as Phe$^{6.44}$, Trp$^{6.48}$, Phe$^{6.51}$, and Phe$^{6.52}$.

Residues from both the CWxP motif and the aromatic cluster form the basis of a putative rotamer toggle switch. The idea is that the side chains of residues within the aromatic cluster make specific contacts with ligands to propagate structural changes along the transmembrane helix (*115*). In 2002, Shi *et al.* proposed a mechanism by which the side chain rotameric states of both Trp$^{6.48}$ and Phe$^{6.52}$ are coupled and change during receptor activation. It should be noted that in the case of rhodopsin, the residue at position 6.52 is an alanine. However, the β-ionone ring of the retinal chromophore is in direct contact with Trp265$^{6.48}$. As such, it is assumed that the β-ionone ring, together with Ala269$^{6.52}$, plays the role of Phe$^{6.52}$ (*116*). Side chain dynamics in the region of the aromatic cluster are poised to modulate the backbone kink induced by Pro$^{6.50}$. Moreover, the conserved Cys at position 6.47 is able to form weak hydrogen bonds with the different backbone carbonyls of H6 depending on its side chain rotameric state (*111*). These hydrogen bonds mediate the backbone distortion about Pro$^{6.50}$ to provide a link between the CWxP motif and motion of the cytoplasmic part of transmembrane helix H6.

Changes in the side chain rotamer states of residues within the aromatic cluster have been a point of contention in the field. Specifically, the side chain orientation of Trp$^{6.48}$ is virtually identical in all GPCR crystal structures. However, various biophysical studies of rhodopsin including UV/Vis (*52*) and linear dichroism spectroscopy (*51*) are consistent with local changes in Trp265$^{6.48}$. Moreover, cryo-electron microscopy of an early intermediate in the photoactivation cycle of rhodopsin reflects a change in the electron density associated with Trp265$^{6.48}$ (*117*). As a result, how ligand binding induces the large scale displacement of transmembrane helix H6 during GPCR activation is a question that still remains to be answered.

1.2.5. H7.

Transmembrane helix H7 contains a highly conserved NPxxY motif. In the case of rhodopsin, both Asn302$^{7.49}$ and Tyr306$^{7.53}$ of this motif participate in interactions that stabilize the inactive conformation. These residues are also in a position to trigger receptor activation via "microswitches" (*118, 119*). Asn302$^{7.49}$ participates in a hydrogen bonding network with Ala299$^{7.46}$ and Ser298$^{7.45}$ in the preceding helix turn. These three residues also form hydrogen bonds to the side chains of Asn55$^{1.50}$ and Asp83$^{2.50}$, both of which are highly conserved throughout class A GPCRs. The side chain of Asn302$^{7.49}$ also participates in a water-mediated hydrogen bonding network with the indole nitrogen of Trp265$^{6.48}$. From the cytosolic surface, the sidechain of Asn302 is in a hydrophobic pocket consisting of Leu76$^{2.43}$, Leu79$^{2.46}$, Leu128$^{3.43}$, Leu131$^{3.46}$, and Met257$^{6.40}$. Both Leu79$^{2.46}$ and Leu128$^{3.43}$ are strictly conserved (94% and 78% respectively) and Ala124$^{3.39}$ is group conserved (72%) (*120*). Mutation of either Leu79$^{2.46}$ or Leu128$^{3.43}$ is associated with constitutive activity in rhodopsin (*121*) and various other GPCRs (*122-124*). Together with the dark state crystal structure, the mutational data argue that the close packing interactions involving Asn302 and its neighboring residues helps to stabilize the dark state of rhodopsin.

Also in the dark state of rhodopsin, Tyr306$^{7.53}$ forms a hydrogen bonding to the side chain of Asn73^{IL1} at the cytoplasmic end of H2. Asn73^{IL1} has been identified as a critical residue for the interaction of active rhodopsin with arrestin, a prerequisite for clathrin-mediated endocytosis (*125*). In the dark, interaction with Tyr306 likely sequesters the side chain of Asn73 to prevent arrestin binding in the absence of receptor activation.

In 2008 Ernst and Hoffman obtained well ordered crystals of opsin. Opsin is formed when the Meta II intermediate decays and releases the agonist all-*trans* retinal from the retinal binding site. The opsin crystal structure provided the first explanation for how the structural changes on the extracellular side of rhodopsin are transmitted to the cytoplasmic side of transmembrane helix H7 through the conserved NPxxY motif (*95, 107*). Due to the outward rotation of H6, the side chain of Asn302$^{7.49}$ is no longer hydrogen bonded to Trp265$^{6.48}$. Concurrently, the side chain Tyr306$^{7.53}$ shifts into a pocket vacated by Met257$^{6.40}$ (*126*).

In rhodopsin, the retinal chromophore is covalently bound to the side chain of Lys296$^{7.43}$ through a Schiff base linkage. In the dark, the retinal Schiff base linkage is protonated and its protonation state is maintained by a counterion (Glu113$^{3.28}$) on transmembrane helix H3, Glu113$^{3.28}$. A hallmark feature of rhodopsin activation is an internal proton transfer from the protonated Schiff base to the carboxylate side chain of Glu113$^{3.28}$. To date, no mechanism has been proposed to explain the requirement for Schiff base deprotonation. An open question is whether or not the structural changes at the cytosolic end of transmembrane helix H7 are associated with an Schiff base deprotonation at the extracellular surface.

1.2.6. H8 and the C terminus.

After the breakpoint of transmembrane helix H7, a short unstructured loop region (IL4) is followed by an amphipathic helix (H8) that runs perpendicular to the bilayer normal. Post translational palmitoylation of cysteine residues serve as hydrophobic anchors to tether H8 to the cell membrane in rhodopsin, as well as other GPCRs (*127*). H8 and IL4 have been shown to be involved in transducin binding to rhodopsin (*128*). Furthermore, H8 has been shown to mediate the interaction between active rhodopsin and visual arrestin (*129*). How the structure of H8 is altered upon activation to allow for its interaction with downstream signaling targets is not well understood.

One possibility is that activation-induced conformational changes are transduced from H7 through the NPxxY motif to H8. Specifically, there exists an electrostatic interaction between the aromatic side chains of Tyr$^{7.53}$ and a conserved phenylalanine residue on H8. The delocalized π-electrons from the aromatic moieties of both residues restricts side chain motion. This interaction is broken in upon GPCR activation. In 2003, Fritze *et al* (*130*) revealed that substituting an

alanine residue at position 7.53 rescued the ability of rhodopsin to populate the active conformation in the presence of a retinal analogue that stalls the photoactivation process. In the inactive conformation, this stacking interaction may serve to restrict the motion of H8 and prevent premature complex formation with either arrestin or heterotrimeric G protein.

1.3. Dissertation outline.

In this thesis, solid-state NMR studies are presented that target conformational changes brought about by GPCR activation. Chapter 2 presents a detailed protocol for generating samples along side a description of the NMR methods. For clarity, a brief background of NMR is provided with its scope limited to the data presented herein. The experimental data presented in subsequent chapters define global structural changes that couple receptor activation with the binding of downstream signaling targets. Chapters 3 and 4 discuss the activation-induced changes on H5 and H6, respectively. In Chapter 5 we investigate structural changes on the extracellular surface of rhodopsin.

CHAPTER 2: MATERIALS AND METHODS.

2.1. Sample preparation.

Many of the challenges that make the structural characterization of GPCRs difficult are associated with sample preparation. The first issue is one of expression. With the noted exception of rhodopsin, it is not practical to obtain large quantities of GPCRs from their primary tissue sources. Heterologous expression in HEK293 cells facilitates large-scale production of functional GPCRs with the appropriate post-translational modifications that are often required for proper receptor folding. The second issue has to do with finding an adequate representation of the native membrane environment of GPCRs in order to preserve receptor function. At a minimum, micelles of amphipathic detergent molecules are required to solubilize the hydrophobic surface of GPCRs and prevent formation of insoluble aggregates of non-functional receptor.

In the following subsections, I describe the methods used to generate isotope-enriched samples of GPCRs that are both functional and of sufficient quantity for structural studies using NMR spectroscopy. The approach described herein has been extensively applied to rhodopsin (*131-134*) and has shown promise for both CCR5 (*135*) and β_2AR (*136, 137*).

2.1.1. Generation of tetracycline-inducible cell lines.

The overexpression of membrane proteins has the tendency to disrupt membrane integrity, resulting in cell death and a low protein yield. To combat this, stable cell lines are generated where overexpression can be induced upon the addition of an exogenous agent. By allowing cells to proliferate prior to induction, one can maximize the target protein yield. HEK293S cells are first transfected with the pCDNA6-TR plasmid (Invitrogen), which contains the gene for the tet operon repressor protein (TetR) and confers resistance to blasticidin. The plasmid (30 μg) is dissolved in 500 μL of 250 mM $CaCl_2$ and mixed (dropwise while vortexing) with 500 μL of a solution containing 100 mM N,N-bis(2-hydroxyethyl)-2-aminoethanesulphonic acid, 500 mM NaCl, and 3.0 mM Na_2HPO_4 at pH 7.02. The mixture is incubated for 1 min at room temperature and then added directly to the HEK293S cell plate. The cells are then transferred to a humidified incubator and incubated under 1.5% CO_2 at 35 °C for 19 h. Stably transfected cell lines are isolated and selected using blasticidin (5 μg/mL) selection.

Second, cells resistant to blasticidin are transfected with the pACMV-TetO plasmid (*134*), into which the GPCR gene of interest has been subcloned. Using this construct, GPCR expression is governed by the CMV promoter sequence that contains a binding site for the tet repressor protein. Binding of the tet repressor protein to its cognate sequence in the CMV promoter inhibits expression of the target gene. Expression is induced when the interaction between the tet repressor protein and its binding site is disrupted by addition of tetracycline to the media. Cell lines stably transfected with this plasmid are subsequently selected using G418 (2 mg/mL) and individual colonies appearing after 14 days are isolated and expanded in triplicate to 10^7 cells in 10-cm-diameter culture dishes. Cells from one dish are stored in liquid nitrogen. The two other dishes are used to determine the inducible GPCR expression levels. Of these two dishes, one is supplemented with growth medium alone. The other dish is supplemented with growth medium containing both tetracycline (2 μg/mL) and sodium butyrate (5 mM) (*134*).

2.1.2. Large-scale expression of stable isotope-enriched GPCRs.

For large-scale production of GPCRs, a bioreactor (New Brunswick Scientific Celligen Plus or BioFlo310) is used in order to control pH and O_2 during cell growth. Starter cultures are grown adherently on 15 cm dishes using DMEM (*138, 139*) containing 1.7 mM Ca^{2+} and supplemented with 10% heat inactivated fetal bovine serum as well as penicillin (100 units/mL) and streptomycin (100 μg/mL). At about 70% confluence, cell monolayers are fed with the same medium except with a Ca^{2+} concentration of 680 μM (*132*). Once the cells reach ~90% confluence, the cells are trypsinized and resuspended in suspension growth medium.

The bioreactor is inoculated using six such culture dishes per liter (~1.5 x 10^8 cells) (*132*). The growth vessels (14-liter capacity) are equipped with pitch blade impellers and primed for use as directed by the manufacturer. The growth parameters are set to 37 °C, pH 7, and 50% dissolved oxygen. The medium is modified specifically to promote suspension growth and enable isotope labeled amino acid incorporation. Specific amino acids are replaced by ^{13}C- and/or ^{15}N-labeled amino acids (depending on the experiment) and the calcium concentration is reduced to 340 μM (*132*). This medium is supplemented with 10% dialyzed (MWCO), heat-inactivated fetal bovine serum (*132*), Pluronic F-68 (0.1%), dextran sulfate (300 mg/L), penicillin (100 units/mL) and streptomycin (100 μg/mL). The addition of dextran sulfate prevents aggregation during suspension growth and promotes protein expression (*140*), while

addition of surfactant Pluronic F-68 preserves membrane integrity and combats the shearing forces resulting from cell agitation. On the fourth day after inoculation, cells are supplemented with glucose (2.4 mg/L). The following day, expression of the target gene is induced with tetracycline (2 μg/L, final concentration) and sodium butyrate (5 mM, final concentration). These are dissolved in ultrapure water, filtered and fed slowly into the cell suspension. Cells are typically harvested on day 7, and the cell pellets are stored at -80 °C.

2.1.3. Purification and membrane reconstitution of GPCRs.

The contents of the bioreactor vessel are siphoned into an ice-cold container. Cells are then separated from spent growth medium by centrifugation at 4,000 x g for 10 min at 4 °C. Cell pellets are washed twice by suspension in ice-cold PBS (pH 7.2) supplemented with protease inhibitors (400 mM PMSF, 50 mg/mL benzamidine) and harvested via centrifugation at 4,000 x g for 30 min at 4 °C. For ligand-activated GPCRs, cell pellets from the second wash step are snap-frozen in liquid nitrogen and stored at -80 °C. For rhodopsin, all subsequent steps are carried out in the dark. Cells are suspended in PBS (pH 7.2) with 400 μM PMSF and benzamidine (50 μg/mL) and 125 nmol of 11-*cis* retinal from a 10 mM ethanol stock is added per gram of cell pellet. The cell suspension is then incubated in the dark at 4 °C with nutation. After 2 h, an additional 125 nmol of 11-*cis* retinal (see 2.1.4) is added per gram of pellet and nutation is continued for another 2 h. The cells are harvested by centrifugation at 4,000 x g for 10 min at 4 °C after a total of 4 h and stored at -80 °C.

Frozen cell pellets are thawed on ice and suspended in ice-cold PBS (pH 7.2) with 1% (w/v) n-β-D-dodecylmaltopyranoside (DDM). The resulting cell suspension is homogenized with several passages through an 18-gauge needle. Membrane solubilization occurs during a subsequent incubation, the conditions of which are a function of protein stability and subject to optimization on a case-by-case basis. For instance, the β_2AR was be solubilized at 4 °C in the presence of protease inhibitors (*114*), whereas CCR5 required the addition of lipids and cholesterol hemisuccinate in order to retain function (*141*). Detergent solubilized lysates are separated from the remaining cell debris via centrifugation for 30 min at 25,000 x g at 4 °C.

Detergent-soluble lysate is applied to a 1D4-sepharose column via gravity flow and the rho-tagged GPCR is immunoprecipitated (*142*). The column is then washed with 10 volumes of

0.02% DDM in PBS (pH 7.2). A subsequent wash step with 0.02% DDM in sodium phosphate (2 mM) buffer (pH 6.0) is used to equilibrate the column for elution. The receptor is then eluted from the 1D4-column with 0.02% DDM in sodium phosphate buffer (pH 6.0) supplemented with a nonapeptide (100 mM) whose sequence corresponds to the nine carboxyl-terminal residues of rhodopsin (TETSQVAPA). Protein-containing elution fractions are subsequently pooled and concentrated in a centrifugal device (AmiCon, MWCO-30 kDa).

A challenge that one faces when studying GPCRs is to put the data in the context of a physiological membrane bilayer. As such, data are collected in an environment that approximates a cell membrane. First order, the most accurate reconstitution media are lamellar vesicles of lipids extracted from ROS. However, The size of lipid vesicles ranges from tens of nanometers to several hundred micrometers.

Much of the data in this thesis were collected using solid-state NMR spectroscopy. One of the major limitations for solid-state NMR spectroscopic studies of GPCRs is low sensitivity. The observable signal in an NMR experiment relies on small differences in population between two spin states (*143*). As a result, highly concentration solutions of isotope-enriched receptor need to be generated. Since we are limited in terms of sample volume, adding lipids would decrease the amount of receptor that could be present in a given sample. As such, there is a trade off between a rigorous reproduction of the native membrane bilayer and sensitivity of the NMR experiment.

Detergents provide an efficient means to solubilize integral membranes for the purpose of purification. Moreover, the size of a DDM micelle is on the order of 50 Å, which allows highly concentrated samples of reconstituted receptor to be generated (*144*). However, one is still forced to verify both ligand binding and the ability to interact with downstream signaling targets. Retinal binding to rhodopsin in DDM is revealed by UV/Vis spectroscopy. Specifically, we conduct a regeneration experiment in which we illuminate rhodopsin in the presence of 11-*cis* retinal and then monitor the absorbance at 500 nm over time to assess whether or not the pigment is regenerated. By illuminating through a high pass filter with a cutoff of 495 nm, we ensure that the free 11-*cis* retinal is not isomerized during the photoactivation step. Within thirty minutes of photoactivation, over 80% of the rhodopsin is regenerated, suggesting that the binding of retinal to rhodopsin in DDM is comparable to cell membranes (*100, 133*). The ability of Meta II in detergent micelles to activated transducin is demonstrated by intrinsic changes in the

fluorescence of Trp residues in $G_t\alpha$ upon activation (*145*). It should be noted that mixed micelles consisting of DDM, POPC and POPS facilitate the binding of the heterotrimer G_t to photoactivated rhodopsin (*146*). However, this is likely do specific lipid-transducin interactions rather than altering receptor conformation.

For ligand activated receptors, functional characterization of the purified protein is assessed by monitoring ligand binding using a variety of detection methods. For example, cognate ligands that have been isotope-enriched (e.g. ^3H) can be incubated with purified receptor where specific binding can be assessed using a scintillation counter (*147*). Alternatively, purified receptors can be immobilized on glass slides and ligand binding can be quantified using surface plasmon resonance (*148-151*).

For the β_2AR, the ligand binding kinetics of DDM-solubilized receptor is comparable to what is observed in biological membranes (*152*). Furthermore, provided the right ionic strength and pH (500 mM NaCl and pH7, respectively), the receptor retains it ability to activate Gs after immunopreciptation and purification. The Kobilka lab used the same conditions to purify receptor when determining crystal structures of the β_2AR at various stages of activation (*153*).

2.1.4. HPLC purification of 11-cis retinal.

The 11-*cis* isomer of retinal is obtained from a mixture of isomers via high-pressure liquid chromatography using an Econosphere silica 10μm column from Alltech (length 250 mm, ID 10 mm) (*132*). 40 mgs of all-*trans* retinal powder was first dissolved in 500 μl acetonitrile. Due to the hydrophobic nature of the chromophore, the acetonitrile is first dried using anhydrous calcium chloride. The solution was then subject to a 20 min illumination step with white light. During this process, the all-*trans* retinal adopts a variety of low energy isomeric states. The acetonitrile is subsequently removed from the mixture under a low flow of argon gas and the resulting film is suspended in the chromatographic mobile phase, 96% hexane (dried) and 4% ethyl acetate (dried). The solution is then passed through a 0.2 μm filter and stored on ice for the duration of purification.

The Econosphere silica column is equilibrated with 240 milliliters of the mobile phase at a flow rate of 8 ml/min. Injection volumes of 1ml are prepared via diluting the 200-400 μl of the stock isomeric mixture with hexane. The precise dilution is a function of retinal concentration

and column resolution, which varies between preparations. The flow-through of the column was passed through an inline UV/Vis detector and the absorption was monitored at 365 nm and 340 nm. The peak corresponding to 11-*cis* retinal has been previously assessed on the basis of its ability to enter the retinal-binding pocket of rhodopsin and generate a pigment with the appropriate λ max (498 nm). 11-*cis* retinal is collected in a round bottom flask and stored on ice between injections to prevent thermal isomerization. Pooled 11-*cis* retinal fractions are subsequently dried under a low flow of argon gas, suspended in 100% ethanol and diluted to the desired concentration.

2.1.5. Functional characterization for rhodopsin: Assay for Meta II stability.

Given their aromatic nature, monitoring the fluorescence of tryptophan residues serve as convenient internal probe for changes in protein structure. In its all-*trans* conformation, the retinal is characterized by an absorbance profile that significantly overlaps with the fluorescence emission of tryptophan. In rhodopsin, the β-ionone ring of 11-*cis* retinal is closely packed against the indole sidechain of Trp265. As a result, Trp265 fluorescence is quenched by all-*trans* retinal. As Meta II decays and the Schiff base linkage is hydrolyzed, retinal exits the binding pocket and the quenching interaction is lost. Therefore, monitoring tryptophan fluorescence in rhodopsin as a function of time after illumination reports on the rate of Schiff base hydrolysis and Meta II decay. In order to measure Meta II decay rates via tryptophan fluorescence, a 250 nM solution of rhodopsin is illuminated using a 495 nm long pass filter at 20 °C in 10 mM BTP, pH 6 containing 0.1% DDM. The tryptophan residues of rhodopsin are exited with a monochromatic light at a wavelength of 280 nm. Fluorescence increase was monitored at 330 nm every 30 s for 7200 s using a 2 s integration time. Slit widths for excitation and emission were 2 nm and 15 nm respectively. Fluorescence intensity is subsequently normalized to the maximum level achieved during the time course of the measurement. The adjust fluorescence data plotted as a function of time and fit a monoexponential function with a time constant that reflects the rate of Schiff base hydrolysis (*154*).

2.2 Solid-state NMR spectroscopy.

NMR spectroscopy exploits the ability of high-powered RF pulses to manipulate spin states, an intrinsic property of subatomic particles. In a static field, the spin states of magnetically active nuclei are distributed about their respect energy levels such that there is a net magnetic moment.

Upon RF irradiation, the spin states are perturbed and net magnetic moment will precess about the main magnetic field to induce a current in the sample coil. The resulting current is lost as the spins return to their equilibrium populations to generate a free induction decay (FID). The FID reports the amplitude of the current generated for all the magnetic moments in the sample as a function of time, making it difficult to interpret the properties of individual nuclear spins. After Fourier transformation, the individual spins are resolved from one another on the basis of their respective precession frequencies.

In the following subsection, detailed protocols for the NMR applications utilized in this work are described. In order to put the data in context, a background summary of the relevant concepts is first provided.

2.2.1. Chemical shift and dipolar couplings.

The structural data provided herein have been predominantly derived by observing two nuclear spin interactions: the chemical shift and the dipolar interaction. The chemical shift describes interactions between the nuclear spin and the external magnetic field through the electrons surrounding the nucleus. During an NMR experiment, the external magnetic field polarizes the electron cloud surrounding the nucleus to generate a magnetic moment (*143*). The resulting magnetic moment acts to shield nuclear spins from the external field, thereby modulating their respective precession frequency. As such the chemical shift provides intrinsic information about the electrostatic environment of a particular nucleus. On the other hand, dipolar couplings are through space interactions between nuclear spins, the intensity of which can be interpreted to obtain spatial restraints for tertiary (and quaternary) protein structure.

The chemical shift is an orientation-dependent interaction defined by three values (σ_{11}, σ_{22} and σ_{33}), which generally span over tens of kHz. Under rapid Brownian motion, the chemical shift interaction is averaged to its isotropic value resulting in narrow, well-resolved resonances that are typically seen in the solution spectra of small proteins. Given the sensitivity of the chemical shift interaction to the local environment, accurate chemical shift measurements report secondary structure, hydrogen bonding and partial charge interactions. Therefore, having the necessary resolution to obtain isotropic values for individual nuclei provides a great deal of structural information. In addition to the intrinsic value of chemical shift measurements, spectral

resolution is essential for the multidimensional internuclear correlation experiments. In solid-state NMR spectroscopy, samples are static and the resulting chemical shift anisotropy plagues spectra with broad lines that represent the full range of the chemical shift interaction. Such line-widths compromises spectral resolution and would, without remedy, severely limit the utility of biomolecular solid-state NMR spectroscopy.

A mathematical description of the chemical shift interact anisotropy reveals a $1\text{-}3\cos^2\theta$ dependence, where θ is the angle between the chemical shift tensor and main magnetic field vector. As such, if the axis of rotation is set to 54.7°, the chemical shift is average to zero (*155*). However, in order to ensure that the net magnetization does not undergo significant relaxation within a single rotor period, the sample must be spun at a frequency that approaches the strength of the chemical shift anisotropy (10-25 kHz) (*156*). At sufficient (magic angle spinning) MAS rates, NMR spectra collected on crystalline samples produce spectra with narrow Gaussian-shaped lines.

An additional component of line broadening in solid-state NMR spectra is the dipolar coupling. Dipolar couplings are described as a direct interaction between the magnetic dipole moments that are associated with individual nuclear spins. Polarization transfer between coupled spins results in splitting and enhances the rate of relation, both of which compromise line widths in static samples. The strength of a particular dipolar interaction is governed by a three criteria: the identity of the nuclei involved as described by the gyromagnetic ratio, the angle made between the axis of the coupled spins and the main magnetic field, and the internuclear distance that separates the two coupled spins. As with chemical shift anisotropy, the angular dependence of the dipolar interactions also scales as $1\text{-}3\cos^2\theta$.

In biological samples, the main nuclei of interest are ^{13}C, ^{15}N and ^{1}H. The gyromagnetic ratio of ^{1}H is 4 times higher than that of ^{13}C and 10 times that of ^{15}N. As such, heteronuclear dipolar couplings between ^{1}H and either ^{13}C or ^{15}N result make it a difficult to observe these nuclei. In order to achieve MAS rates that are sufficient to average such large interactions, small sample volumes are required. For high molecular weight proteins, reducing the sample volume decreases sensitivity. To combat this, one can use high power RF irradiation to equilibrate the net proton magnetization during acquisition, which averages the associated dipolar couplings to zero.

Various pulse programs have been established for this purpose (*157-160*). Initial decoupling strategies involved a continuous wave of ^{1}H irradiation during acquisition. Subsequent improvements involve composite pulses trains with both frequency and phase modulations (*160*). For the purpose of our experiments we use SPINAL 64 (*161*).

2.2.2. Cross polarization.

For several reasons protons are the most frequently exploited nuclei in protein structure determination by NMR (*162, 163*). First, protons represent the most abundant nuclei. Second, unlike carbon and nitrogen, the naturally abundant isotope (^{1}H) is magnetically active thereby circumventing the need for the isotope-enrichment. Third, protons have the highest gyromagnetic ratio of all the relevant isotopes one would observe in biomolecular NMR. Since the gyromagnetic ratio represents the magnetic susceptibility of a particular nucleus, protons exhibit the highest degree of polarization in a static field. Therefore, one can maximize the amount of data collected per unit of time by directly observing protons.

However, in the absence of isotropic motion, strong homonuclear couplings make it impractical to collect and interpret ^{1}H spectra. Even in solution spectra, residual ^{1}H-^{1}H dipolar line broadening introduced when the molecules being investigated are beyond 40 kDa with correlation times that exceed the nanosecond regime and are unable to average out the dipolar coupling (*164*). In solids, the full range (~70 kHz for ^{1}H-^{1}H) of the dipolar interaction is present and the sample volumes required to obtain MAS rate sufficient for motional averaging would make the timescale of spectral acquisition impractical.

All of the NMR data presented in this thesis involves detection of either ^{13}C or ^{15}N magnetization. In addition to requiring isotope-enriched samples, observation of ^{13}C and ^{15}N magnetization is hampered by two intrinsic properties. Specifically, both nuclei have low gyromagnetic ratios and long relaxation times. The net result is a decrease in sensitivity coupled with longer acquisition times. To combat this, one can use a technique known as cross polarization (CP) (*165-167*). During CP, ^{1}H magnetization is prepared and used to polarize the nuclear spins of less sensitive nuclei through the dipolar coupling (i.e. ^{13}C and ^{15}N), thereby increasing the sensitivity. The ability of ^{1}H magnetization to polarize ^{13}C nuclear spins is enhanced by strong heteronuclear ^{13}C-^{1}H dipolar couplings. As such, there is an inherent

distance dependence in the rate of polarization transfer, and ^{13}C nuclei that are close to neighboring ^{1}H are easiest to cross polarize. To a certain point of saturation, the efficiency of CP scales with the time that both nuclei are being simultaneously irradiated (*168*). Using CP times on the order of 2-3 ms is sufficient to allow maximum transfer. Shorter contact times (80-100 μs) can be used to limit the transfer to nuclei that are directly bonded (*169*), which is useful in order to make assignments for peptide backbone nuclei in the solid-state. In addition to the increased sensitivity, the relaxation rate is governed by the proton magnetization decay, which occurs on a much faster time scale and allows data acquisition to be expedited. When combined, CP and MAS can produce high-resolution spectra on milligram quantities of GPCRs (*132, 170-173*).

2.2.3. ^{13}C Difference spectroscopy.

Figure 2.1A presents a 1D ^{13}C CPMAS spectrum of isotope-enriched rhodopsin in DDM micelles. The spectrum was collected at an MAS rate of 10 kHz with CP times of 2 ms with and composite two-pulse phase modulated (SPINAL 64) ^{1}H decoupling used during the acquisition time of 50 μs. The high concentrations of detergent that are used during sample preparation results in an overwhelming contribution of natural ^{13}C abundance to the spectrum. In addition, the chemical shift dispersion for the individual atoms is small relative to the line-widths, resulting in considerable overlap, which makes it difficult to assess chemical shift changes between spectra. However, events that cause variations of chemical shift reflect significant structural events that are associated with GPCR activation.

Difference spectroscopy provides a method to isolate the NMR resonances of amino acids whose chemical shift changes upon receptor activation. Figure 2.1B presents the ^{13}C NMR difference spectrum between the inactive and active states of rhodopsin using MAS. For this experiment, receptors are isotopically labeled in HEK293S cells by introducing ^{13}C-enriched tyrosine, glycine and methionine into the growth media. Changes in chemical shifts are observed for each type of amino acid upon activation. By comparing the wild type difference spectrum with difference spectra of site-specific mutants, the observed NMR resonances can be assigned to specific amino acids in the protein. For example, there are two distinct negative peaks in the spectral region corresponding to the $^{13}C\zeta$-resonances of tyrosine. These peaks indicate that at least two tyrosines in the active metarhodopsin II intermediate have changed chemical environment. Herzfeld and colleagues (*174*) have shown that the $^{13}C\zeta$-tyrosine chemical shift is

sensitive to hydrogen bonding of the Cζ-OH hydroxyl group with a downfield shift reflecting an increase in hydrogen bonding. The loss of the upfield tyrosine resonance in metarhodopsin II upon mutation of Tyr206 to phenylalanine allows one to assign this resonance to a specific amino acid (*172*). The upfield position of the chemical shift suggests that this tyrosine becomes more weakly hydrogen bonded upon activation (*172*).

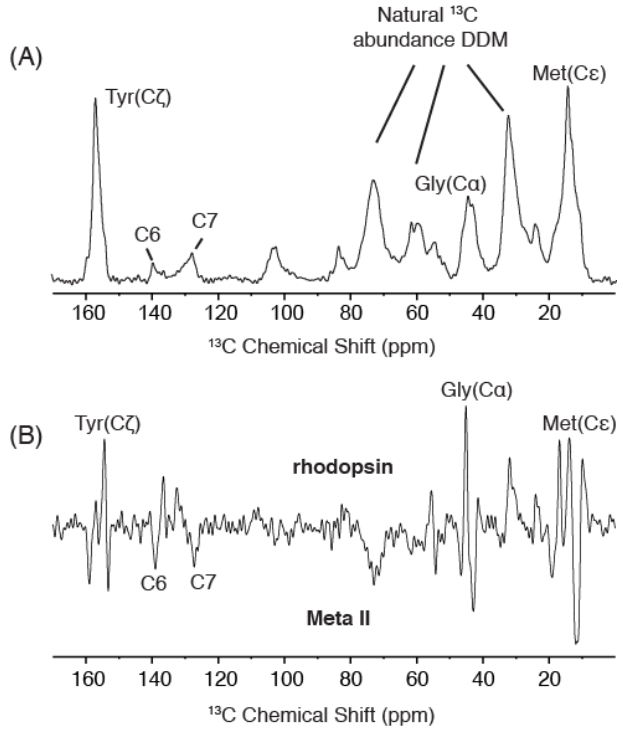

Fig. 2.1. ^{13}C Difference spectroscopy. *(A) One dimensional ^{13}C MAS spectrum of rhodopsin solubilized in DDM are shown. The receptor was ^{13}C labeled with $^{13}C\zeta$ -tyrosine, $^{13}C\alpha$-glycine and $^{13}C\varepsilon$-methionine and regenerated with $^{13}C6,C7$-retinal. The spectrum was obtained with a MAS frequency of 10 kHz and a sample temperature of 250 K on a Bruker Avance 600 MHz spectrometer. The contribution of DDM in the sample can be reduced by reducing the concentration of detergent in the final step of purification. (B) One dimensional ^{13}C MAS difference spectrum between rhodopsin and metarhodopsin II.*

2.2.4. Dipolar recoupling experiments.

Background. Weaker dipolar interactions such as the hetero- and homonuclear couplings between ^{13}C and ^{15}N are on the order of 10 kHz. These interactions are the basis for structure determination in solid-state NMR spectroscopy. By observing polarization transfer through the dipolar coupling between two nuclei, one can obtain tertiary restraints based on the distance dependence of the dipolar coupling. However, even at modest MAS rates of 8-10 kHz, hetero- and homonuclear dipolar couplings between ^{13}C and ^{15}N nuclear spins are averaged to zero. In order to take extract in intrinsic internuclear distance information provided by these interactions, steps must be taken to reintroduce the dipolar interaction prior to spectral acquisition.

The past few decades have brought forth a variety of methods to reintroduce dipolar couplings in the MAS experiment (*175-179*). A number of 2D recoupling solid-state NMR sequences have also been introduced for obtaining long-range distance information by measuring weak dipolar couplings (*176, 179*). We found dipolar assisted rotational resonance (DARR) NMR to be the most effective method to obtain distances in ^{13}C-labeled membrane proteins (*180*). Figure 2.2 presents a two-dimensional ^{13}C DARR spectrum of rhodopsin, with selective ^{13}C-enrichment, that illustrates this method. The ^{13}C, ^{13}C correlation spectrum is shown as a contour plot where the resonances along the diagonal correspond to the 1D spectrum shown in figure 2.1 (panel A), whereas off diagonal cross peaks represent polarization transfer between nuclei whose chemical shift values are given by the f1 and f2 dimensions. The strongest cross peaks are observed between the directly bonded C6 and C7 carbons of the retinal polyene chain. Moderate cross peaks are observed between the ^{13}C6, ^{13}C7 retinal resonances and the ^{13}Cε-resonance of Met207, while a weak cross peak is observed between the ^{13}Cε resonance of Met86 and the ^{13}Cα resonance of Gly121.

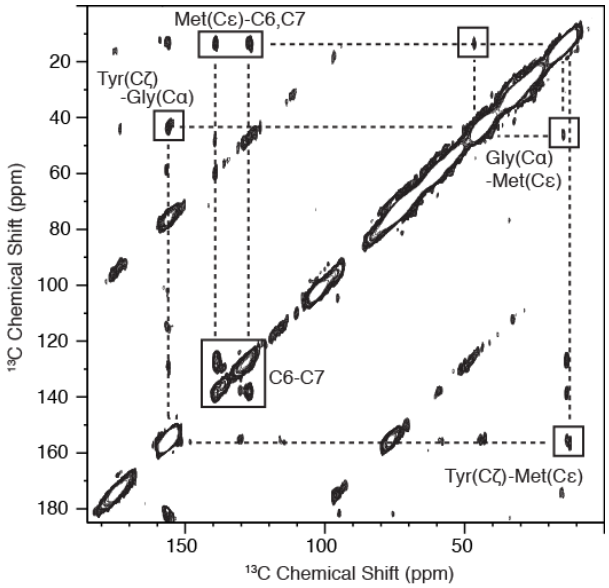

Fig. 2.2. 2D ^{13}C Dipolar recoupling spectra. *^{13}C DARR spectrum of isotope-enriched rhodopsin in the dark. The spectrum was acquired at ^{13}C frequency of 150 MHz under MAS of 10 kHz. During the 600 ms of DARR mixing time. Off diagonal cross peaks arise via polarization transfer between neighboring nuclei.*

Cross peak quantitation. While it holds true that the intensity of the cross peaks is related to internuclear distance, polarization transfer through the dipolar coupling is facilitated in nuclei that are relatively close in chemical shift. As a result, it can be difficult to evaluate distances in a

quantitative fashion. Nevertheless, we find that dipolar-assisted rotational resonance (DARR) allows polarization transfer in a manner that is relatively insensitive to the chemical shift difference (*179*). As such, the chief determinant of off-diagonal cross peak intensity is the internuclear distance.

A challenge when interpreting changes in dipolar coupling strength is to normalize the spectra whose crosspeaks are being evaluated. It is often difficult to interpret relative intensities simply by looking at contours plots in a 2D spectrum. One way to circumvent this is to extract a row from the indirection dimension (y axis) at the frequency of a particular nucleus. The majority of the intensity in the resulting row is at the frequency at which it was extracted (i.e. the main y=x diagonal). Any other peak corresponds to nuclei that exchanged polarization with the main diagonal resonance.

In order to interpret changes in internuclear distance between spectra collected on two receptor conformations we begin by extracting the relevant rows that contain the crosspeak of interest from the 2D spectrum. If a crystal structure is available, the distance measured between two nuclei can be correlating with a particular dipolar coupling from a 2D spectrum. For example, in rhodopsin we observe a ^{13}Cε-Met - ^{13}Cζ Tyr crosspeak that has been assigned to a dipolar coupling between Met207$^{5.42}$ and Tyr191^{EL2} (Fig. 2.3A). The intensity of this crosspeak can be correlated with the internuclear distance as measured from the crystal structure. The ability to cross-reference dipolar coupling strengths with distance measurements provides a means of obtaining semi-quantitative distance restraints.

Subsequently, we must address how well we can distinguish various internuclear distances from one another by comparing crosspeak intensity (i.e. resolution). The strategy is to use a mixing time long enough to obtain maximum polarization form weak dipolar couplings. In doing so, we maximize the observable difference in crosspeak intensity for two internuclear distances in the shortest amount of time.

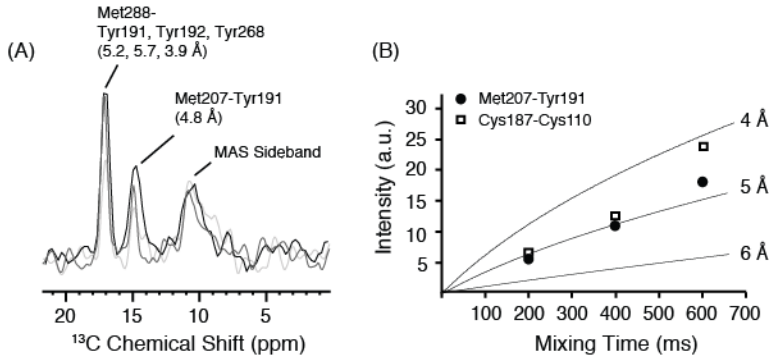

Fig. 2.3. DARR NMR measurements of internuclear distance. *(A) One-dimensional slices extracted from 2D DARR NMR spectra. The slices are taken through the off-diagonal cross peaks between ^{13}Cε-Met and ^{13}Cζ-Tyr and highlight the intensity changes that occur with mixing times of 200 (light grey), 400 (grey) and 600 (black) ms. (B) Intensity build up curves from DARR NMR measurements on rhodopsin labeled with ^{13}Cε-Met, ^{13}Cζ-Tyr and ^{13}Cβ-Cys.*

Figure 2.3 presents standard DARR mixing curves based on measurements of distances from the rhodopsin crystal structure. The buildup of intensity for two resolved sites in rhodopsin is shown. The Cβ-Cys110 to Cβ-Cys187 distance is 4.43 Å. The Cε-Met207 to Cζ-Tyr191 distance is 4.87 Å (*181*). As such, a mixing time of 600 ms is sufficient for us to differentiate internuclear distances that differ by 0.3-0.5 Å.

CHAPTER 3. STRUCTURAL CHANGES IN TRANSMEMBRANE HELIX 5 UPON GPCR ACTIVATION.

3.1. Rhodopsin

Rhodopsin, the vertebrate photoreceptor for vision under dim light, belongs to the large, pharmaceutically important superfamily of G protein-coupled receptors (GPCRs). The photoreactive chromophore in rhodopsin is the 11-*cis* isomer of retinal, which is covalently linked to Lys296$^{7.43}$on the intradiscal (or extracellular) side of the receptor. Absorption of light drives the 11-*cis* to *trans* isomerization of the retinal within a tight binding pocket. The conformational changes that occur in this process must be transmitted through the membrane-spanning portion of the bilayer to the intracellular surface in order to open up the binding site for the heterotrimeric G protein, transducin. The crystal structure of the dark, inactive state of the visual pigment rhodopsin (*98*) reveals a tightly packed bundle of seven transmembrane (TM) helices, but offered few clues as to how the helices move upon light activation.

Site directed spin-labeling studies by Hubbell and coworkers (*43, 47*) showed that the largest change in the seven TM helix bundle involves an outward rotation and displacement of transmembrane helix H6, consistent with an increase in volume of the receptor upon activation (*182, 183*). The challenge for obtaining a high-resolution structure of the active metarhodopsin II (Meta II) intermediate has been that light activation causes the dark state crystals of rhodopsin to dissolve (*184*), suggesting that the structural changes are sufficiently large to disrupt crystal packing. Salom *et al.* (*185*) were able to isolate crystals that could be light activated. They determined the structure of a photointermediate of rhodopsin containing retinal with a deprotonated Schiff base (SB) (*186*). The structure did not exhibit the large helix motions characteristic of the activated receptor, suggesting that this intermediate corresponds to the Meta II substate (Meta IIa) (*187*), which is formed prior to helix motion (*46*). The motion of H6 precedes proton uptake by Glu134 and formation of the Meta IIbH^+ substate (*46*).

Motion of H6 is also observed in the crystal structure of opsin at low pH (*107*). The outward motion of H6 revealed by the opsin crystal structures (*95, 107*) are similar in magnitude (~6 Å) to the change observed by site directed spin labeling studies (*47*). Under physiological conditions (e.g. COS cells at pH 7.2 (*78*) and ROS at pH 8 (*188*)), opsin has low (≤1%), but detectable,

basal activity. At pH 4, FTIR difference spectra of opsin exhibit vibrational bands characteristic of Meta II (*189*) suggesting that opsin adopts a conformation that is similar to the active state. In line with the FTIR results, the crystal structure of opsin obtained at pH 6 appears to retain many features that are characteristic of Meta II (Fig. 3.1). In fact, a more recent crystal structure of opsin (*95*) contains the bound C-terminal peptide of the Gα subunit from transducin in a conformation similar to that observed in solution NMR studies on the activated Meta II intermediate (*190, 191*).

One of the most striking features of the opsin structure is that the ionic lock involving Glu134$^{3.49}$-Arg135$^{3.50}$ of the conserved ERY sequence on H3 and Glu247$^{6.30}$ on H6 is disrupted (Fig. 3.1B). Instead, Arg135$^{3.50}$ is extended toward Met257$^{6.40}$, Tyr223$^{5.58}$ and Tyr306$^{7.53}$. Both Tyr223$^{5.58}$ and Tyr306$^{7.53}$ have strong sequence identity through the class A family of GPCRs. Tyr306$^{7.53}$ is part of the highly conserved NPxxY motif on the cytoplasmic side of H7 and is thought to impart stability of the inactive receptor (*130*). Tyr223$^{5.58}$ is unusual in that it is oriented away from the helical bundle in the inactive, dark receptor, but rotates in toward the ionic lock in the opsin crystal structure. While Tyr306$^{7.53}$ of the NPxxY sequence has been characterized extensively, the first suggestion that Tyr223$^{5.58}$ plays a critical role in receptor activation came from the crystal structure of opsin.

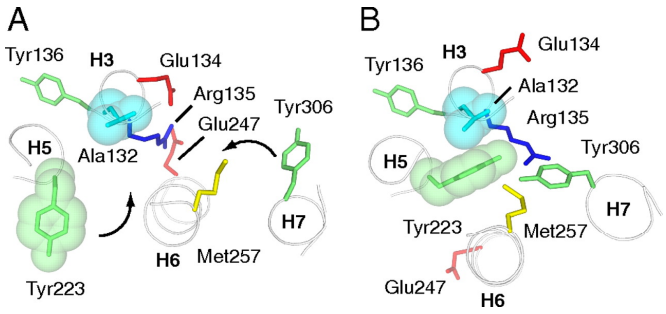

Fig. 3.1. Comparison of the rhodopsin and opsin crystal structures in the region of the ionic lock. *(A) Structure of rhodopsin in the region of the ionic lock as viewed from the extracellular surface. (B) Structure of opsin at low pH in the same orientation as in A. The side chains of Tyr223$^{5.58}$ and Tyr306$^{7.53}$ are rotated inward toward the helical bundle where they are within hydrogen bonding distance of Arg135$^{3.50}$. Ala132$^{3.47}$ is the most highly group-conserved residue in class A GPCRs.*

Solid-state NMR spectroscopy provides a unique way of following the structural transitions from rhodopsin to Meta II (*171, 172*). NMR measurements can be made on rhodopsin in fluid

membrane, which facilitates the conformational changes associated with the formation of the Meta II intermediate. To date, the majority of the NMR work has focused on the retinal-binding pocket. Here, we use solid-state NMR spectroscopy to determine the structure of the ionic lock region in Meta II and fluorescence spectroscopy to characterize the rates of Meta II decay in mutants of rhodopsin where three highly conserved tyrosines (Tyr136$^{3.51}$, Tyr223$^{5.58}$ and Tyr306$^{7.53}$) on the cytoplasmic side of the receptor have been sequentially mutated to phenylalanine. Our experiments on Meta II stability and transducin activation provide insights into the roles of these three conserved tyrosine residues on the intracellular surface that appear to orchestrate receptor activation. In addition, we show that Tyr223$^{5.58}$ has a more substantial contribution to the stability of Meta II and transducin activation than either Tyr136$^{3.51}$ or Tyr306$^{7.53}$.

3.1.1. The open state of the ionic lock in Meta II.

The outward rotation of H6 observed in the opsin crystal structure places the side chain of Met257$^{6.40}$ in close proximity to Arg135$^{3.50}$. The ^{15}N chemical shifts of the Nη_1, Nη_2 and Nε side chain nitrogens and the ^{13}C chemical shift of the Cζ carbon were measured to address the changes in the environment of Arg135$^{3.50}$ upon Meta II formation. The arginine ^{15}N chemical shifts are sensitive to the protonation state and environment of the guanidinium group (*192*), and one can envisage that when the interactions between Glu134$^{3.49}$, Arg135$^{3.50}$, and Glu247$^{6.30}$ are broken the guanidinium side chain of Arg135$^{3.50}$ undergoes a change in electrostatic environment. For example, Arg82 within the TM domain of bacteriorhodopsin is situated between several acidic residues including Asp85. The ^{15}N chemical shifts of the N$\eta_{1,2}$ resonances are not resolved in the ground state, but exhibit a distinct splitting in the M photointermediate (*192*). The splitting is attributed to changes in the charge distribution within the Arg82 guanidine group after the Asp85 carboxyl group becomes protonated and Arg82 rotates toward the extracellular surface.

The ^{15}N and ^{13}C spectra of arginine-labeled rhodopsin and Meta II are presented in Fig. 3.2. There is no chemical shift resolution in the ^{15}N resonances of the arginine Nη_1, Nη_2 and Nε nitrogens in either rhodopsin or Meta II, and there is only a slight (<1 ppm) shift in the ^{13}Cζ resonance. The lack of significant changes indicates that the protonation state of Arg135$^{3.50}$ has not changed and suggests that the electrostatic environment surrounding Arg135$^{3.50}$ is similar in

the inactive and active states. These results suggest that either there are no large changes in the receptor structure, as suggested by the crystal structure of a rhodopsin photoproduct with a deprotonated retinal SB, or that disruption of the full charge-charge interactions within the Glu134$^{3.49}$-Arg135$^{3.50}$-Glu247$^{6.30}$ ionic lock are compensated by partial charge interactions that result in no substantial change in the ^{15}N or ^{13}C chemical shifts of Arg135$^{3.50}$.

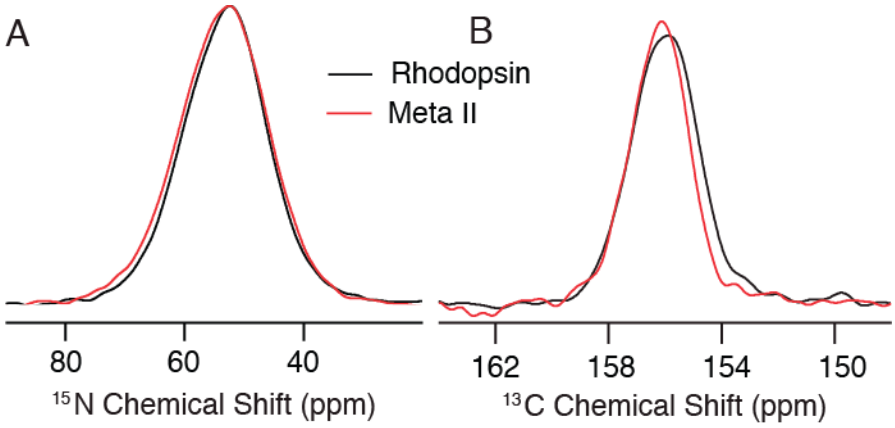

Fig. 3.2. ^{15}N (A) and ^{13}C (B) chemical shifts as a probe of the environment and protonation state of Arg135$^{3.50}$. *There are seven arginines in rhodopsin. Arg135$^{3.50}$ is thought to be the only arginine that experiences an appreciable change in environment upon photoactivation. Magic angle spinning NMR spectra illustrate that the ^{15}N and ^{13}C chemical shifts of the guanidinium group of arginine do not change appreciably between rhodopsin (black line) and metar- hodopsin II (Meta II) (red line). The arginine $N\eta_{1,2}$ resonances of Meta II appear to overlap those seen in rhodopsin, indicating that Arg135$^{3.50}$ remains protonated and is in a similar hydrogen bonding environment despite data supporting neutralization of the ionic lock upon receptor activation (48, 59). Petkova and coworkers (192) found that the guanidinium nitrogen atoms of the protonated arginine side chain are generally involved in hydrogen bonding interactions and exhibit chemical shifts ranging from 68.9 to 56.3 ppm for the ε-nitrogen, from 62.0 to 45.6 ppm for the downfield η resonance, and from 46.8 to 34.2 ppm for the upfield η resonance. The differences in the Nη chemical shifts are attributed to asymmetry in hydrogen bonding and can be almost as large as the >40-ppm differences observed upon deprotonation (193). The NMR data presented here along with the crystal structure of opsin (107) indicate that the protonated Arg1353.50 side chain is stabilized in a symmetric fashion by hydrogen bonding interactions with Glu134$^{3.49}$, Tyr223$^{5.58}$, and Tyr306$^{7.53}$. The chemical shift measurements of arginine and tyrosine indicate that Arg135$^{3.50}$ is charged and that Tyr223$^{5.58}$ and Tyr306$^{7.53}$ are neutral. In the crystal structure of opsin, the Gα peptide is observed to bind in a helical conformation with the negatively charged C terminus most closely associated with Lys311 on H8 of rhodopsin. Gα binding does not appear to be driven by the electrostatic environment created by a protonated arginine side chain. ^{15} N chemical shift measurements (panel A) were collected by Shivani Ahuja.*

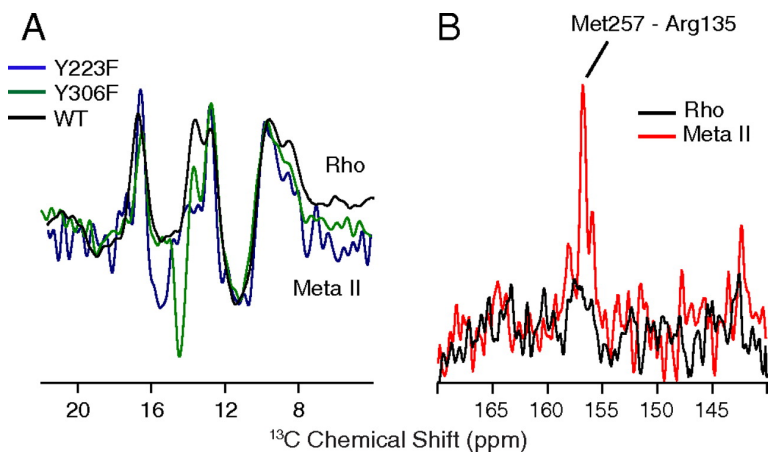

Fig. 3.3. Arg135$^{3.50}$-Met257$^{6.40}$ contacts in Meta II. *(A) ^{13}C NMR difference spectra between rhodopsin and Meta II in the region of ^{13}Cε-Met for the wild-type receptor (black line) and the Y223F (blue line) and Y306F (green line) mutants. The ^{13}Cε-Met257 resonance at 14.7 ppm exhibits a cross peak with ^{13}Cζ-Arg135$^{3.50}$ in Meta II (see B). Mutation of either Tyr223$^{5.58}$ or Tyr306$^{7.53}$ leads to slight shifts in the ^{13}Cε-Met257$^{6.40}$ resonance. (B) Rows through the Met-Cε diagonal resonance are shown from 2D ^{13}C DARR NMR spectra of rhodopsin (black line) and Meta II (red line) labeled with ^{13}Cε-methionine and ^{13}Cζ-arginine. A strong cross peak is observed in Meta II at the ^{13}Cε-Met chemical shift of 14.7 ppm and the ^{13}Cζ-Arg135$^{3.50}$ chemical shift of 156.8 ppm. The cross peak is assigned to a close through-space contact between Arg135$^{3.50}$ and Met257$^{6.40}$. Arg-Met cross peaks are not observed in the spectrum of dark rhodopsin (black line).*

In contrast, to the lack of chemical shift changes in arginines, there are substantial changes observed in the chemical shifts of methionines upon receptor activation. Fig. 3.3A presents the ^{13}C NMR difference spectrum between ^{13}Cε-Met-labeled rhodopsin and Meta II. The negative ^{13}C resonance at ~15 ppm can tentatively be assigned to Met257$^{6.40}$ in Meta II on the basis of its sensitivity to mutation of Tyr223$^{5.58}$ and Tyr306$^{7.53}$. To test for a direct Arg135$^{3.50}$ - Met257$^{6.40}$ interaction in Meta II, we labeled rhodopsin with both U-^{13}C,^{15}N arginine and ^{13}Cε-methionine and measured internuclear Arg-Met distances using 2D ^{13}C dipolar assisted rotational resonance (DARR) NMR. We do not observe Arg ^{13}Cζ - Met ^{13}Cε cross peaks in the 2D DARR NMR spectrum of rhodopsin (Fig. 3.3B, black) consistent with the rhodopsin crystal structure where no Arg Cζ - Met Cε carbon pairs are closer than ~6 Å. In contrast, an Arg Cζ - Met Cε cross peak is observed in Meta II (Fig. 3.3B, red) that we tentatively assign to Arg135$^{3.50}$ - Met257$^{6.40}$. In the opsin crystal structure, the Arg135$^{3.50}$ Cζ - Met257$^{6.40}$ Cε distance is 4.6 Å, within the range of the 2D DARR NMR experiment. The putative Arg135$^{3.50}$ - Met257$^{6.40}$ contact in Meta II

correlates with the position of these two residues in the opsin crystal structure. The next closest Arg - Met pair is Arg135$^{3.50}$ and Met253$^{6.36}$, whose Cζ - Cε distance is 6.5 Å.

To further characterize the local environment of Arg135$^{3.50}$ in Meta II, we targeted the two conserved tyrosines (Tyr223$^{5.58}$ and Tyr306$^{7.53}$) that appear to stabilize the ionic lock in an open conformation (Fig. 3.1B). The side chain hydroxyl groups of Tyr223$^{5.58}$ and Tyr306$^{7.53}$ may act in concert to preserve the dark state electrostatic environment of Arg135$^{3.50}$.

Fig. 3.4 presents difference spectra generated by subtraction of the spectrum of wild-type rhodopsin from the spectrum of one of three tyrosine mutants (Y136F, Y223F or Y306F). Only the region of the ^{13}Cζ tyrosine resonances is shown. These spectra allow us to directly assign the ^{13}Cζ tyrosine chemical shifts in rhodopsin and in Meta II. Both the Tyr223$^{5.58}$ and Tyr306$^{7.53}$ ^{13}Cζ resonances shift downfield slightly upon activation to 156.2 and 155.9 ppm, respectively, reflecting an increase in hydrogen bonding of the ^{13}Cζ-OH group and indicating that both tyrosines are in a similar environment in Meta II. The chemical shifts are consistent with protonated tyrosines. For comparison, the difference spectrum of Y136F is shown in Fig. 3.4A. The ^{13}Cζ-chemical shift of Tyr136$^{3.51}$ does not change upon activation.

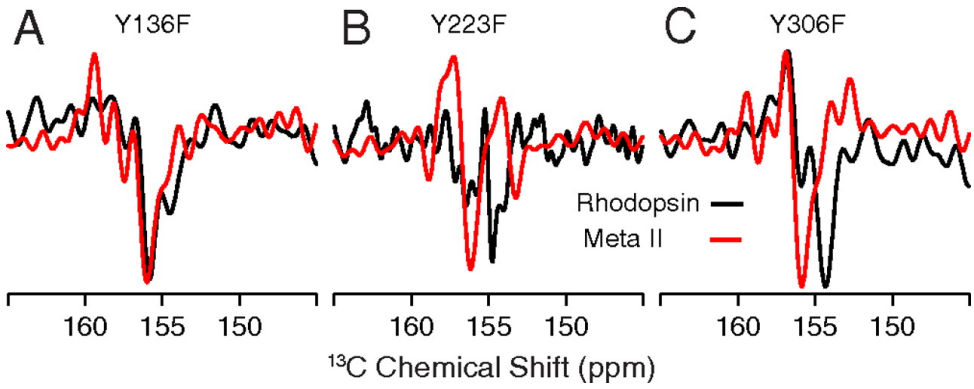

Fig. 3.4 . ^{13}Cζ chemical shifts of Tyr136$^{3.51}$, Tyr223$^{5.58}$, and Tyr306$^{7.53}$ in rhodopsin and Meta II. *Difference spectra obtained between rhodopsin (black line) and Meta II (red line) for the three tyrosine mutants: Y306F, Y223F, and Y136F. The difference spectra are taken between the wild-type protein and the mutant in order to reveal the frequency of the ^{13}Cζresonance. Tyr223$^{5.58}$ and Tyr306$^{7.53}$ both exhibit downfield changes in chemical shift between rhodopsin and Meta II. The ^{13}Cζ chemical shift of Tyr136$^{3.51}$ is not appreciably altered upon conversion to Meta II. Markus Eilers collected the NMR data for the Y136F mutant.*

To establish if direct Tyr223$^{5.58}$-Met257$^{6.40}$ and Tyr306$^{7.53}$-Met257$^{6.40}$ contacts occur in Meta II, we obtained 2D DARR NMR spectra of wild-type (black) and mutant (red) rhodopsin ^{13}C labeled at Cε-methionine and Cζ-tyrosine (Fig. 3.5). In rhodopsin, rows taken through the Met-Cε diagonal resonance of the DARR spectrum reveal cross peaks between Tyr191^{EL2}-Met288$^{7.35}$ at 159.4 ppm and Tyr268$^{6.51}$-Met288$^{7.35}$ at 156.7 ppm (*172*). In the dark, both Tyr191^{EL2} and Tyr268$^{6.51}$, participate in network of hydrogen bonding interactions that help to situate EL2 deep within the retinal-binding pocket. The observation that neither of these cross peaks change upon substitution of Tyr223$^{5.58}$ or Tyr306$^{7.53}$ is consistent with a native-like inactive conformation being adopted by both mutants.

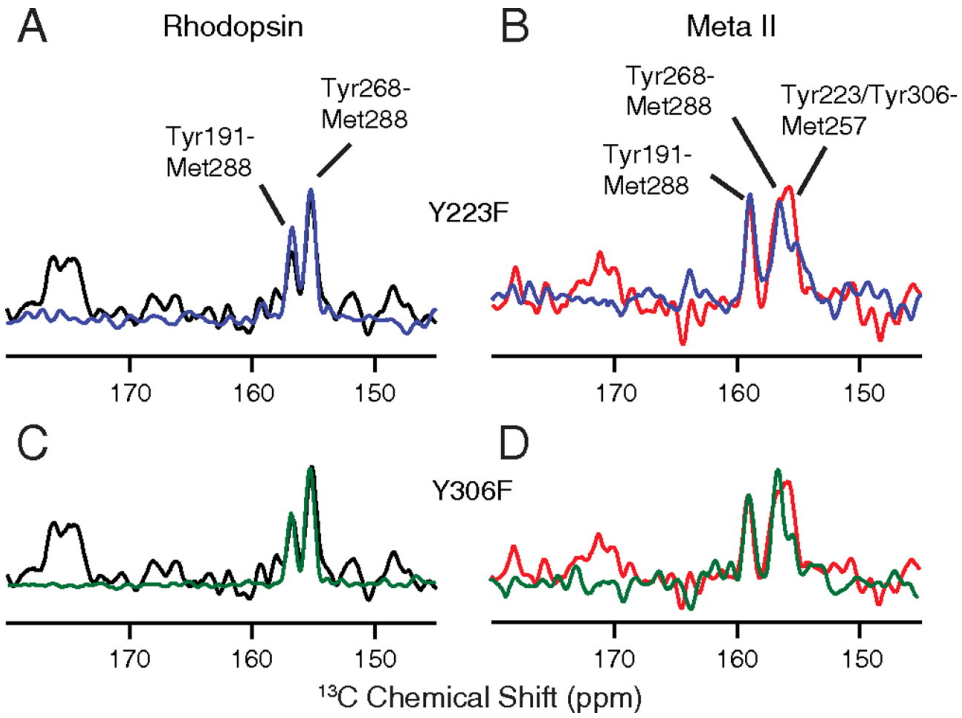

Fig. 3.5. Tyr223$^{5.58}$-Met257$^{6.40}$ and Tyr306$^{7.53}$-Met257$^{6.40}$ contacts in Meta II. *Rows through the Met-Cεdiagonal resonance are shown from 2D ^{13}C DARR NMR spectra of rhodopsin (black line) and Meta II (red line) labeled with ^{13}Cζ-tyrosine and ^{13}Cε-methionine. The rhodopsin and Meta II rows are overlaid with the corresponding rows obtained of the Y223F (blue line) and Y306F (green line) mutants in order to determine if either of these tyrosines contact Met257$^{6.40}$ in Meta II. Upon mutation of Tyr223$^{5.58}$ or Tyr306$^{7.53}$, there is loss of intensity of the cross peak at 156 ppm, consistent with these tyrosines having similar chemical shifts and interacting with Met257$^{6.40}$ in Meta II.*

In the rows corresponding to wild-type Meta II, a shoulder appears at ~156 ppm (Fig. 3.5B,D red), consistent with the chemical shifts of Tyr223$^{5.58}$ and Tyr306$^{7.53}$ observed in Fig. 3.4. This shoulder is lost upon mutation of either Tyr306$^{7.53}$ or Tyr223$^{5.58}$. These data confirm the

proximity of Met257$^{6.40}$ to both Tyr306$^{7.53}$ and Tyr223$^{5.58}$ in Meta II. In turn, these results place both tyrosine side chains in close proximity to the active state position of Arg135$^{3.50}$.

3.1.2. Tyr223$^{5.58}$ stabilizes the active Meta II intermediate.

The lack of chemical shift changes in the arginine ^{15}N and ^{13}C resonances (Fig. 3.2) suggests that the electrostatic environment around Arg135$^{3.50}$ does not change appreciably upon activation. This observation along with the NMR structural data on Meta II showing that Tyr223$^{5.58}$ and Tyr306$^{7.53}$ surround Arg135$^{3.50}$ suggests that these residues interact with one another and may contribute to the stabilization of the active Meta II conformation. To address the role of these tyrosine residues in Meta II stability, we monitored the decay of Meta II by fluorescence spectroscopy.

Fig. 3.6 presents fluorescence data on the decay of Meta II in wild-type rhodopsin and the Y223F mutant. For wild-type rhodopsin, fluorescence increases in the transition from Meta II to opsin. The fluorescence changes are associated with a loss of an interaction between Trp265$^{6.48}$ and the retinal chromophore that quenches tryptophan fluorescence in Meta II (*154*). When plotted as a function of time after illumination, the fluorescence increase can be fit to a single exponential function. For the Y223F mutant, the fluorescence intensity reaches a maximum after 400 s corresponding to a five-fold increase in the rate of Meta II decay relative to the wild-type receptor. For comparison, mutation of either Tyr136$^{3.51}$ or Tyr306$^{7.53}$ to phenylalanine increases Meta II decay by a factor of 2 (Table 3.1). These data suggest that Tyr223$^{5.58}$ has a greater contribution to Meta II stability than either Tyr136$^{3.51}$ or Tyr306$^{7.53}$.

We then tested the ability of the Y223F mutant to activate the G protein transducin. Table 3.1 compares transducin activity of the Y223F mutant with that of wild-type rhodopsin and the Y136F and Y306F mutants. For the Y223F mutant, there is a large decrease in both the initial rate of transducin activation, and the maximum level of activation as compared to wild-type rhodopsin, consistent with the rapid hydrolysis of the all-*trans* retinal SB in the formation of opsin.

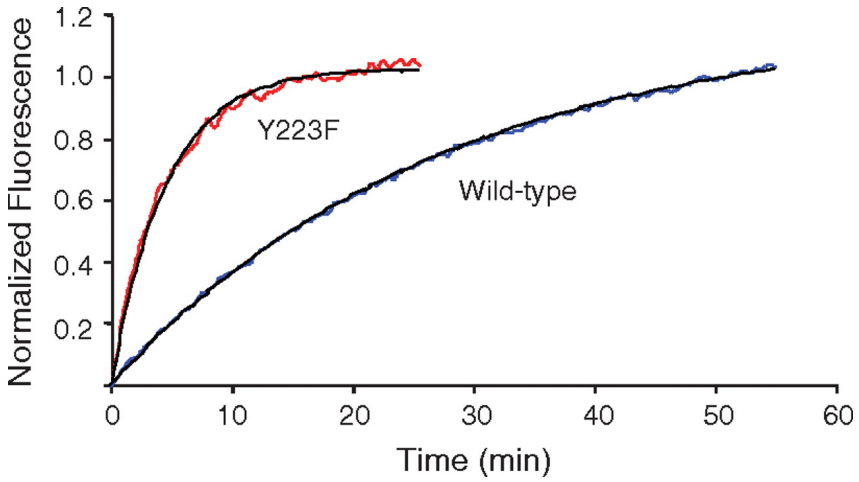

Fig. 3.6. Comparison of Meta II decay in wild-type and Y223F rhodopsin. *The fluorescence emission at 330 nm from wild-type rhodopsin and the Y223F mutant is plotted as a function of time after light activation. Normalized Meta II decay rates were calculated by fitting the data to a first-order decay function. There is a 4.7-fold increase in the rate of Meta II decay upon mutation of Tyr223$^{5.58}$ (Table 3.1). Kieron South from the laboratory of Phil Reeves provided the data that was used to generate this figure.*

	Meta II Decay		Rate Of Transducin Activation	
	Mean half-life (min)	Decay Rate (Normalized)	Initial	Overall
Wild Type	14.78	1.00	1.00	1.00
Y136F	12.53	1.18	1.49	1.06
Y223F	3.17	4.66	0.06	0.05
Y306F	10.52	1.40	0.84	0.72
A123L	3.83	3.86	0.69	0.34
A132S	9.30	1.59	0.31	0.63

Table 3.1. Rates of Meta II decay and transducin activation. *Metarhodopsin II decay and transducin activation were assayed by monitoring intrinsic changes in tryptophan fluorescence for rhodopsin and transducin respectively. Measurements are shown for both wild-type and mutant receptor. For comparison, rates were normalized to WT values and present alongside the raw measurements. Kieron South in the laboratory of Phil Reeves collected rates of Meta II decay and transducin activity.*

For Y136F, we observed that Meta II stability was similar to wild-type rhodopsin. However, the initial rate of transducin activity was significantly (1.5X) higher. In a previous study, it was found that a nearby rhodopsin retinitis pigmentosa mutant (V137M) also displayed significantly elevated (1.25X) initial rates of transducin activation (*194*). In the case of Y136F, we do not observe an associated increase in SB hydrolysis, suggesting that the structural consequences of this mutation are limited to the cytoplasmic side of the receptor. The analogous tyrosine has been the focus of several studies in other class A GPCRs, such as the vasopressin receptor (*195*) and CCR3 (*196*), where a conservative substitution blocks signaling while maintaining native-like ligand affinity.

Further support for the role of Tyr223$^{5.58}$ in stabilizing Meta II comes from FTIR measurements obtained at lower temperature (Fig. 3.7). Analysis of vibrational band intensities characteristic of Meta I and Meta II shows that the Meta I ⇔ Meta II equilibrium is strongly shifted to the Meta I state in the Y223F mutant.

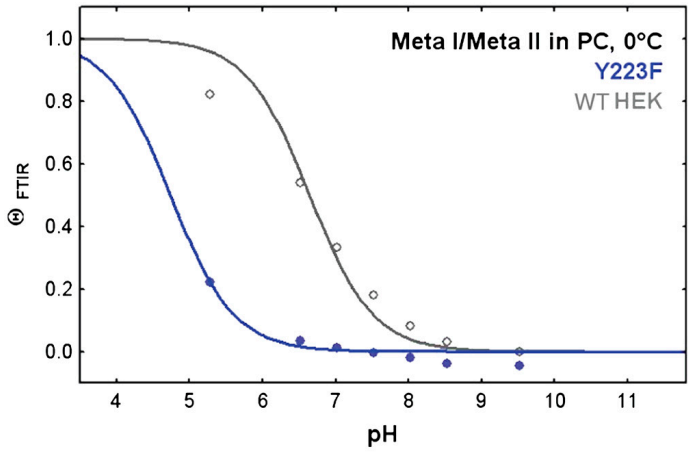

Fig. 3.7. FTIR studies of wild-type rhodopsin and the Y223F. *FTIR spectroscopy provides a complementary method to NMR and absorption spectroscopy for characterizing the activation of rhodopsin. The FTIR-based titration curves (ΘFTIR) of the Meta I to Meta II equilibrium are shown on the basis of monitoring the vibrational bands characteristic of Meta I and Meta II as a function of pH (1). It has previously been shown that coupling of the two protonation switches that control receptor activation at 10 °C and below reestablishes the classical two-state equilibrium between Meta I and protonated Meta IIbH+ (1). Here, we use FTIR to probe how the Y223F mutation influence this equilibrium. Mutation of Tyr223 to phenylalanine causes a strong shift in the equilibrium toward the Meta I conformation. The observation of a shift of the equilibrium toward Meta I in the Y223F mutant highlights the role of this tyrosine in stabilizing the active state of rhodopsin. FTIR spectroscopy was performed with a Bruker Vertex 70 spectrometer with a mercury-cadmium-telluride detector. Spectra were recorded at 4 cm−1 using 200–400 pmol membrane-reconstituted pigment and the sandwich sample type with 200 mM 1,3-bis[tris(hydroxymethyl)methylamino]propane (at pH 6.0 and higher) or MES buffer (at pH 5.0) (1). Photoactivation was achieved by a 1-s photolysis using an array of six light-emitting diodes at 530 nm (1). Spectra were normalized by using the fingerprint bands of the chromophore between 1,200 and 1;300*

cm^{-1}. Membrane reconstitution of n-dodecyl maltoside (DDM)-purified pigments was achieved by mixing pigment and phosphatidylcholine lipids from egg yolk (from a 6.3 mM stock in 1% DDM) at a protein:lipid molar ratio of 1:200. The mixture was incubated for 2 h on ice. Detergent was extracted by incubation with small polystyrene beads (Biobeads SM-2; BioRad), which were washed extensively with water to remove glycerol and floating beads. DDM extraction was performed in two rounds of incubation of 4 h and a last round of 12 h at 4 °C on a rotator. For each milligram of DDM present (prior to the first round of extraction), 20 mg of washed biobeads were used in each round, ensuring complete removal of the detergent. After each round, biobeads were allowed to settle to recover the supernatant. After the last round of extraction, all biobeads were carefully removed and proteoliposomes were collected by centrifugation for 4 h at 100;000 × g. THe FTIR data were collected by Katrina Zaitseva in the laboratory of Reiner Vogel at the University of Freiburg.

3.1.3. Ala132$^{3.47}$ orients Tyr223$^{5.58}$ in Meta II.

One helix turn from Arg135$^{3.50}$, toward the receptor core, is the group conserved Ala132$^{3.47}$. As mentioned in Chapter 1, group conserved residues generally have low conservation when considered individually, but are highly conserved when considered as a group consisting of amino acids with small or weakly polar side chains, namely Ala, Gly, Ser, Thr, Cys. These residues have a high propensity to mediate TM helix interactions (*197*) and have been shown to allow interaction of the signature residues in the class A GPCRs (*77*). Position 3.47 has the highest level of group conservation within this group (99%). In the crystal structure of opsin, the large rotation of Tyr223$^{5.58}$ places its aromatic side chain in van der Waals contact with Ala132$^{3.47}$. The rapid decay of Meta II upon mutation of Tyr223$^{5.58}$ is similar to that previously observed for mutation of Glu122$^{3.37}$ (*198*). Glu122$^{3.37}$ hydrogen bonds with His211$^{5.46}$ on the extracellular side of the receptor in Meta II and is thought to hold H5 in an active orientation (*99*). The His211$^{5.46}$-Glu122$^{3.37}$ pair is conserved in the high sensitivity rod cell pigments and distinguishes them from the lower sensitivity cone pigments. The question arises as to whether there is a similar pair-wise stabilizing interaction between Tyr223$^{5.58}$ and Ala132$^{3.47}$ on the intracellular side of the receptor.

To test this hypothesis, we mutated Ala132$^{3.47}$ to leucine and serine, and measured Meta II decay by tryptophan fluorescence. These data reveal an increased rate of Meta II decay (Table 3.1) suggesting that a larger side chain at position 132$^{3.47}$ does not allow Tyr223$^{5.58}$ to form a stabilizing interaction with Arg135$^{3.50}$. The observed increase in the rate of Meta II decay in the A132L mutant is consistent with a lower activity of the Meta II state with respect to transducin binding.

The group-conserved amino acids (G, A, S, T, C) were originally identified as those residues that have the highest propensity for mediating helix interactions in membrane proteins (*197*). In the class A GPCRs, there are 13 group-conserved residues that are located mainly in helices H1-H4 (*126*). Analysis of the packing density of the seven TM helices indicates that H1-H4 are the most tightly packed helices in the crystal structure of rhodopsin and that the group-conserved amino acids are located in the interfaces between these helices. Importantly, Ala132$^{3.47}$ does not fit this pattern. Ala132$^{3.47}$ is located on H3, but oriented toward the H5-H6 interface. The results described above, in combination with the opsin structure, provide an explanation for the high conservation of this residue. Whereas the group conserved amino acids mainly mediate helix-helix interactions in the inactive state of rhodopsin, Ala132$^{3.47}$ acts a molecular notch to orient the Tyr223$^{5.58}$ side chain efficiently toward Arg135$^{3.50}$ and stabilize the active Meta II intermediate (Fig. 1).

Alanine is highly conserved (68% identity) at position 3.47 in the rhodopsin subfamily of class A GPCRs. Position 3.47 is also conserved as an alanine in the melanocortin receptors (98%), and as a threonine in the chemokine receptors (55%). In the amine subfamily this site is predominantly a serine (68% identity). In the β_2AR, we previously studied the influence of substitution of the group-conserved amino acids in the TM helix core with larger hydrophobic residues (*80*). Substitution of the wild-type alanine at position 3.47 with leucine or valine dramatically lowered receptor activity, whereas serine at position 3.47 exhibited wild-type activity, suggesting that the role of Ala132$^{3.47}$ in rhodopsin is likely the same across the class A GPCRs. In this regard, the recent crystal structures of both the β_2AR and the A_{2A} receptors show that Tyr$^{5.58}$ has rotated toward Ala$^{3.47}$, as in opsin. This active state orientation for Tyr$^{5.58}$ may be due to the T4L insert between H5 and H6 used to crystallize both receptors (see below). Comparison with the wild-type receptors shows that the T4L insert results in significantly higher affinity for subtype-selective agonists, which the authors suggest may reflect a shift toward the active state (*114, 199*). In the β_1AR, which was not crystallized with the T4L insert, Tyr$^{5.58}$ was mutated to alanine as part of a suite of mutations engineered to stabilize the inactive conformation of the receptor (*200*).

3.1.4. The Y223F mutation causes structural changes in EL2.

The shift in the Meta I ⇔ Meta II equilibrium and faster Meta II decay of the Y223F mutant suggest that the changes introduced by this mutation are allosterically coupled to the extracellular side of the receptor. This hypothesis is also in agreement with the coupling of EL2 and H5 motion during activation (*172*). Meta II decay is defined by hydrolysis of the SB. There are several amino acids on or near EL2 on the extracellular side of rhodopsin that can modulate SB hydrolysis (*201, 202*). These include Glu113$^{3.28}$, the counterion to the Schiff base (*81*). We propose that the position of EL2 is linked to the position of Glu113$^{3.28}$ and SB hydrolysis.

To characterize whether the mutation of Tyr223$^{5.58}$ (and Tyr306$^{7.53}$) is coupled to structural changes in EL2, we expressed the Y223F and Y306F mutants with ^{13}Cβ-labeled cysteine. The cystine Cβ spectrum provides a probe for changes in the highly conserved Cys110$^{3.25}$ and Cys187^{EL2} disulfide bond. The β-carbon resonances in cystines are observed in a unique chemical shift window (34-50 ppm) and are sensitive to the secondary structure with a range of 34 to 43 ppm for α helices and 36 to 50 ppm for β sheets (*203*). We previously observed strong cross peaks between the Cys110$^{3.25}$-Cys187^{EL2} β-carbon resonances at 36.4 ppm and 46.8 ppm in the dark, respectively (*172*). These resonances do not change position in the Y223F or Y306F rhodopsin spectra.

Figure 3.8 presents rows from the 2D DARR NMR spectra of Meta II of the Y223F (blue) and Y306F (green) mutants labeled with ^{13}Cβ-cysteine as compared to wild-type Meta II (red). In contrast to the comparison with dark rhodopsin, there is a shift of the Cys187^{EL2} resonance in the Meta II spectrum of the Y223F mutant compared to wild-type Meta II. In wild-type Meta II, the ^{13}Cβ-Cys187^{EL2} resonance shifts to 50.1 ppm due to a change in the conformation of EL2, while the chemical shift of Cys110$^{3.25}$ on TM helix H3 does not change (*172*). In the Y223F mutant, the Cys187^{EL2} resonance moves upfield to 48.2 ppm (Fig. 3.8A). Fig. 6C shows the cross peak associated with Cys110$^{3.25}$. This cross peak does not shift in the Y223F mutant confirming that the influence of the mutation is localized to EL2. In the Y306F mutant (Figs. 3.8B,D), the cross peaks associated with Cys110$^{3.25}$ and Cys187^{EL2} are at the same position as in wild-type Meta II indicating that there is no coupling between the NPxxY sequence and the conserved cysteine disulfide.

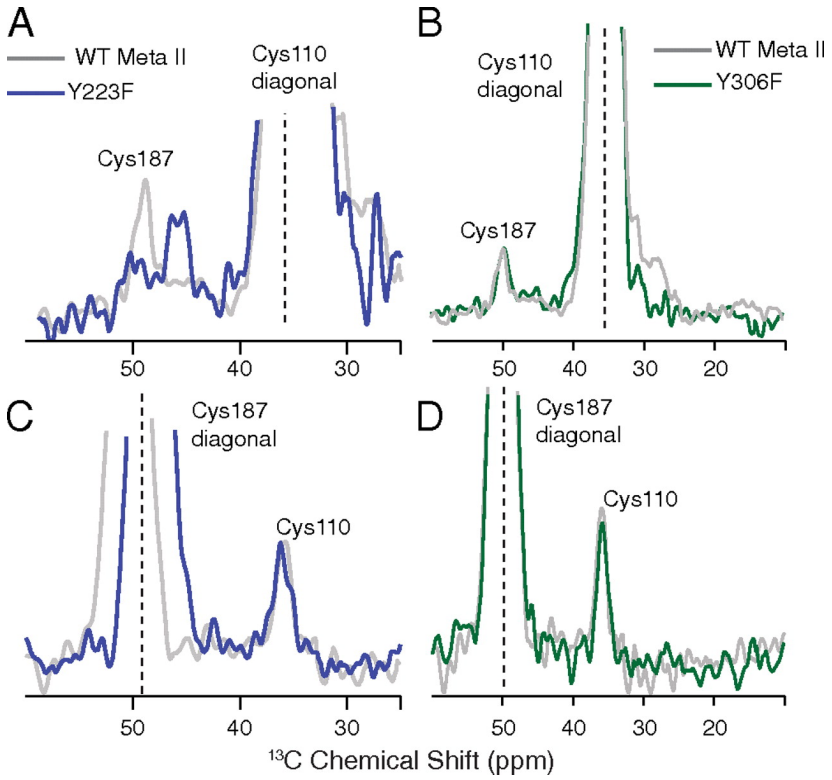

Fig. 3.8. Coupling of H5 to EL2 motion in the Y223F mutant of Meta II. *Rows extracted from 2D ^{13}C DARR NMR spectra acquired of the activated Meta II state of wild-type rhodopsin (gray line) and the Y223F (blue line) and Y306F (green line) mutants. The rows show the Cβ region of Cys110$^{3.25}$ and Cys187^{EL2} and were taken through the diagonal resonances of Cys110$^{3.25}$ (A and B) and Cys187^{EL2} (C and D). Mutation of Tyr223$^{5.58}$ alters the chemical shift of Cys187^{EL2} with respect to wild-type rhodopsin (gray line). However, a mutation of Tyr306$^{7.53}$ does not influence the wild-type chemical shift for the Cβ of Cys187^{EL2}.*

3.1.5. Defining the open and closed states of the Glu134$^{3.49}$-Arg135$^{3.50}$-Glu247$^{6.30}$ ionic lock.

The current study addresses several open questions regarding how retinal isomerization on the extracellular side of rhodopsin is coupled to the cytoplasmic ionic lock. We show that the interactions of Arg135$^{3.50}$ with Met257$^{6.40}$, Tyr223$^{5.58}$ and Tyr306$^{7.53}$ observed in opsin are also present in the active Meta II intermediate, consistent with the outward rotation of H6 upon activation (*95, 107*). Mutational studies indicate that the Arg135$^{3.50}$ - Tyr223$^{5.58}$ interaction, which is facilitated by group-conserved Ala132$^{3.47}$, has a strong influence on the stability of the active state conformation.

The ionic lock was originally described as a conserved hydrophobic cage motif in the gonadotropin-releasing hormone receptor at the cytoplasmic end of transmembrane helix H3 involving Asp$^{3.49}$, Arg$^{3.50}$ and Ile$^{3.54}$ (*204*). Ballesteros *et al.* (*204*) proposed that a salt bridge

between Asp$^{3.49}$ and Arg$^{3.50}$ stabilizes the inactive receptor and that upon activation Asp$^{3.49}$ becomes protonated with the charged Arg$^{3.50}$ side chain being prevented from orienting toward the cytoplasmic surface by Ile$^{3.54}$. A more complex ionic lock involving the interaction of Arg$^{3.50}$ with both Asp$^{3.49}$ on H3 and Glu$^{6.30}$ on H6 was based on the observation that mutation of both D3.49N and E6.30Q in the β_2 adrenergic receptor resulted in increased in basal activity (*205*). In the past few years, however, the crystal structures of the adenosine A_{2A} (*199*), and β_1 (*200*) and β_2 (*114*) adrenergic receptors have been determined and, in contrast to the crystal structure of rhodopsin, show no direct interaction between Arg$^{3.50}$ and Glu$^{6.30}$, although the Asp$^{3.49}$-Arg$^{3.50}$ salt bridge is retained.

Our current results on the interactions of Arg135$^{3.50}$ in Meta II, along with amino acid conservation, provide insights into the nature of the closed and open states of the ionic lock. Table 3.2 presents a summary of the conservation of the residues contributing to the ionic lock in inactive rhodopsin and active Meta II. There is a strong conservation of arginine (97%) at position 3.50 and Glu/Asp (90%) at position 3.49. Lysine (0.9%) and histidine (0.2%), and Asn (2.4%) and Gln (1.7%) only rarely occur at positions 3.50 and 3.49, respectively. In contrast, Glu247$^{6.30}$ is not well conserved across the class A GPCRs, implying that there are various mechanisms for stabilizing the inactive conformations of GPCRs in the region of the ionic lock. In the β_1 and β_2 receptors, the position of Arg$^{3.50}$ is stabilized by a tyrosine on CL2, whose conservation in the amine subfamily (85%) is as high as the conservation of Glu$^{6.30}$ (83%). The conservation of two different residues that may stabilize Arg$^{3.50}$ in the amine receptors suggests that there may be multiple inactive states or that these residues have other functions in the regulation of receptor activity (*206*).

Table 3.2 also summarizes the conservation of residues stabilizing the active conformation of Arg135$^{3.50}$. The conservation of Tyr223$^{5.58}$ (86%) is particularly striking since the tyrosine side chain is oriented toward the lipid in the dark-state crystal structure of rhodopsin, implying that this residue only has protein contacts in the active state conformation. In contrast, methionine at position 6.40 is not conserved in the class A GPCRs, yet plays an important role in stabilizing the inactive conformation of rhodopsin (see below). Together, these observations support the view that the Glu134$^{3.49}$-Arg135$^{3.50}$ salt bridge is the essential interaction for stabilizing the inactive state of class A GPCRs (*59*). Neutralization of Glu134$^{3.49}$, rather than breaking of the

Arg135$^{3.50}$ - Glu247$^{6.30}$ salt-bridge, is key to shifting the receptor to its active conformation where the conserved interactions are between Arg$^{3.50}$, Tyr$^{5.58}$ and Tyr$^{7.53}$, as observed in Meta II and the crystal structure of opsin.

						Percent occurrence*				
Class A		Rhodopsin		β_2-AR		Identity	Small	Polar	Aromatic	Hydrophobic
3.47	Ala	132	Ala	128	Ala	35.5 (56)	99.0	0.7	0.1	0.3
3.49	Asp	134	Glu	130	Asp	65.0 (82)	1.8	95.9	1.2	1.5
3.50	Arg	135	Arg	131	Arg	97.2 (97)	0.8	98.6	0.1	0.5
3.51	Tyr	136	Tyr	132	Tyr	69.3 (74)	8.1	4.9	85.9	10
3.54	Ile	139	Val	135	Ile	54.2 (72)	2.9	0.4	0.4	96.6
5.58	Tyr	223	Tyr	219	Tyr	86.0 (92)	5.6	6.2	86.6	2.0
6.30	Glu	247	Glu	268	Glu	33.3 (17)	13.3	78.9	1.2	5.8
6.40	Ile	257	Met	278	Ile	29.1 (15)	8.8	1.2	1.8	89.4
7.53	Tyr	306	Tyr	326	Tyr	93.5 (96)	1.5	0.6	96.1	4.3

Table 3.2. Conservation of Ala132$^{3.47}$, Glu134$^{3.49}$, Arg135$^{3.50}$, Tyr136$^{3.51}$, Val139$^{3.54}$, Tyr223 , Glu247$^{6.30}$, Met257$^{6.40}$, and Tyr306$^{7.53}$. The data is this table was extracted from the protein databank by Sina Erfani.

3.1.6. Met257$^{6.40}$ stabilizes rhodopsin in the inactive state.

We had previously observed that most site-directed mutants of Met257$^{6.40}$ allow opsin activation by the addition of all-*trans* retinal as a diffusible ligand (*207*). The observation that Met257$^{6.40}$ shifts into contact with Arg135$^{3.50}$ in the H3-H6 interface provides an explanation for the phenotypes of the Met257$^{6.40}$ mutations and the role of Met257$^{6.40}$ in the activation mechanism. The Met257$^{6.40}$ mutants with the highest constitutive activity are M257Y, M257N, and M257S. The polar side chains at position 6.40 in these mutants will interact more strongly with Arg135$^{3.50}$ than the hydrophobic methionine side chain, and consequently stabilize the active state. In other class A GPCRs (Table 3.2), the β-branched amino acids, threonine, isoleucine and valine, are the most common residues observed at position 6.40. When substituted into rhodopsin (*207*), these residues do not confer appreciable constitutive receptor activity (4.4-9.6%), but do allow almost full activation (62-83%) upon the addition of all-*trans* retinal. These results indicate that rather than stabilizing the active state, Met257$^{6.40}$ stabilizes the inactive state of the receptor.

If Met257$^{6.40}$ is not stabilizing the Meta II structure, the question arises as to the relative stabilizing effects of Tyr223$^{5.58}$ and Tyr306$^{7.53}$. When these two tyrosines are mutated to phenylalanine, our measurements of transducin activation and Meta II decay indicate that Tyr223$^{5.58}$ plays a much greater role in stabilizing Meta II than Tyr306$^{7.53}$. With a sequence identity of 86% (Table 3.2), Tyr223$^{5.58}$ is the most highly conserved amino acid on H5.

Asparagine and serine are the two next most common residues. Strikingly, phenylalanine and tryptophan are not found at this position, nor are glutamate or aspartate. The absence of aromatic amino acids at this position indicates that the preference is for a polar residue, while the lack of negatively charged amino acids indicates that in class A GPCRs the open conformation of the ionic lock is not stabilized by a salt bridge involving Arg135$^{3.50}$.

3.1.7. Allosteric coupling across the transmembrane core of rhodopsin.

Solid-state NMR measurements have previously suggested that the displacement of EL2 upon activation is coupled to a rotation of H5 (*172*). The coupled motion of EL2 and H5 was based on mutational experiments where substitutions in EL2 resulted in structural changes in H5 (*172*). In the current study, we show that mutations in H5 (i.e. Y223F) result in structural changes in EL2 (i.e. Cys187^{EL2}). In agreement with previous studies on Cys187^{EL2} (*208*), mutation of Tyr223$^{5.58}$ does not affect the wild-type properties of rhodopsin in the dark, but leads to a less stable Meta II intermediate upon activation. In wild-type rhodopsin at neutral pH, hydrolysis of the all-*trans* retinal SB and loss of the retinal chromophore in the Meta II to opsin transition shifts the receptor to an inactive conformation (*189*). Inactive opsin is stabilized, at least in part, by electrostatic interactions involving Glu113$^{3.28}$ and Lys296$^{7.43}$ since mutation of either residue to a neutral amino acid increases constitutive receptor activity (*209*). Interestingly, in opsin (*95*), these residues do not interact directly, but rather interact most closely with Cys187^{EL2} and Glu181^{EL2}, respectively, on EL2. Coupling of the position of EL2 to the orientation of H5 in the Meta II to opsin transition would suggest there is a role for Tyr223$^{5.58}$ in both the opening and closing of the Arg135$^{3.50}$-Glu134$^{3.49}$ ionic lock.

In summary, the current study highlights the roles of several residues mediating the opening and closing of the ionic lock in rhodopsin activation. The observed active state contacts of Arg135$^{3.50}$ with Met257$^{6.40}$, Tyr223$^{5.58}$ and Tyr306$^{7.53}$ allow us to define the open conformation of the ionic lock. In particular, we show that a novel interaction between Tyr223$^{5.58}$ and Ala132$^{3.47}$ in the active Meta intermediate can explain both the high sequence identity of Tyr223$^{5.58}$ and the high group conservation of Ala132$^{3.47}$ across the class A GPCRs.

3.2. β_2 Adrenergic receptor.

β_2AR is arguably the best characterized ligand-activated G protein-coupled receptor (*210*). The gene for β_2AR was first cloned from the genome of *Mesocricetus auratus* (*211*) and found to share sequence similarity with rhodopsin. Subsequent functional studies of site-directed β_2AR mutants mapped the ligand-binding pocket to the transmembrane core in a region similar to what is occupied by 11-*cis* retinal in rhodopsin (*212*).

In the vertebrate visual system, a single heterotrimeric G protein (transducin) is present in both rod and cone cells to accommodate signal transduction via photoactivated visual pigments, including rhodopsin (*213-215*). In contrast, activated β_2AR has been found to interact with both Gi and Gs (Fig. 3.9). It has also been shown that the insulin receptor tyrosine kinase phosphorylates several tyrosine residues on the intracellular surface of β_2AR (*206*). Furthermore, signal transduction through the MAP kinase pathway is stimulated via β_2AR in complex with β-arrestin (*216, 217*). Certain ligands previously classified as inhibitors of β_2AR signaling have actually been found to stimulate signal transduction through G protein-independent pathways (collateral efficacy) (*218*). Therefore, a detailed description of receptor activation requires comparison between multiple ligand-bound receptor states.

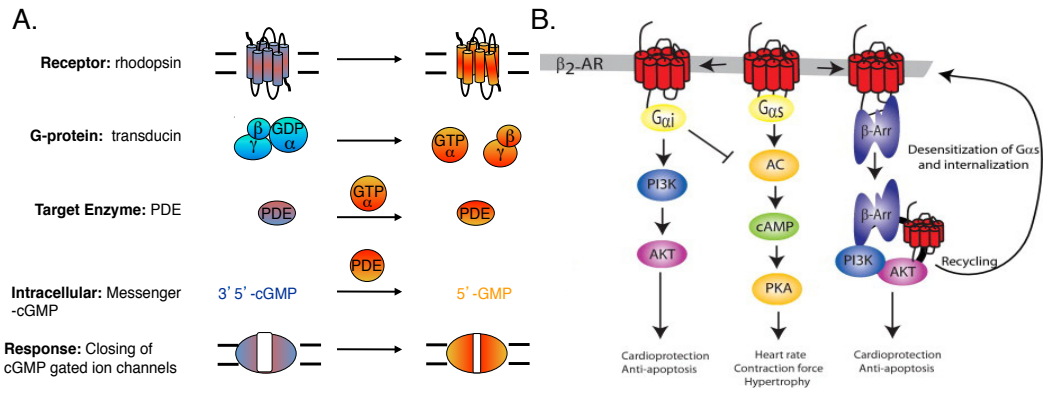

Fig. 3.9. β_2AR and rhodopsin signaling cascades. *Retinal isomerization fully converts the dark state of rhodopsin into its active Meta II state, this two-state model of receptor activation is unique to the visual pigments (A). β_2AR receptor exists a continuum of transiently populated intermediates whose conformations are stabilized by specific ligands (B). The conformational heterogeneity of activated β_2AR coincides with the various downstream signaling targets with which it interacts. In contrast, rhodopsin signalling involves a signal pathway and a heterotrimeric G protein that is dedicated to signal transduction in the visual pigments.*

During the last five years, several crystal structures have been presented that capture β_2AR in various ligand-bound states (*86, 87, 112, 219, 220*). The first series of crystal structures captured inactive conformations bound to a potent inverse agonist (carazolol) and various antagonists (*87, 219*). When bound to carazolol, the basal activity of β_2AR is significantly reduced (*87*). Therefore, a comparison between these crystal structures can potentially reveal the conformational changes that are associated with a reduction in basal activity. However, the differences between these structures are minimal.

Subsequently, three crystal structures of β_2AR were presented for the active conformation (*86, 112, 220*). In one structure, a synthetic agonist was covalently bound to the ligand-binding pocket (*220*). When compared to carazolol-bound state, the agonist-bound crystal structure suggests that the structural changes associated with receptor activation are minimal. Concurrently, the structure of agonist-bound β_2AR was presented in complex with an exogenous G protein mimetic peptide (Nb80) (*86*) and a full heterotrimeric G protein (Gs) (*112*). The resulting structure showed a significant rearrangement of the transmembrane helices and is thought to represent the canonical ternary complex (*33*). The extensive structural differences between agonist-bound structures in the presence and absence of down stream effectors have left open the question of how agonist binding induces cell signaling.

One of the more puzzling aspects that comes from the recent crystallographic data of β2AR (*86, 87, 112, 219, 220*) is the remarkable overlap between the structures of active and inactive conformations. In each case, the only significant change is the position cytosolic moiety of transmembrane helix H6, which is consistent with EPR measurements conducted on rhodopsin almost 20 years ago (*154*). Moreover, these structures represent snapshots in a dynamic process that likely involves a number of conformational intermediates (*37, 102, 221, 222*). As a result, other biophysical studies are required if one hopes to understand the mechanism by which agonist binding at the extracellular surface allows the receptor to interact with signaling targets in the cytosol.

Several computational studies have been conducted to describe the interconversion between active and inactive receptor conformations of β_2AR (*223-225*). In those studies, the authors appear to have conquered the technical challenges associated with molecular dynamic

simulations that span hundreds of microseconds. However, the simulations suggest that prior to G protein binding, the agonist-bound conformation of β_2AR is identical to that of the inactive state. As such, it is difficult to couple ligand binding to G protein activation.

In rhodopsin, one of the key components of the ligand (i.e. retinal) binding pocket is EL2. Crystal structures of rhodopsin reveal substantial contacts between the 11-*cis* retinal chromophore and various residues of EL2 (*98, 181, 226*). Previous NMR measurements have been used to suggest that rhodopsin activation involves a significant change in the conformation of EL2 (*171, 172*). However, inactive crystal structures of β_2AR reveal that EL2 extends out into the extracellular space (*219*). The unique position of EL2 in the inactive conformation of β_2AR serves to increase the accessibility of the ligand-binding pocket to the bulk solvent and may provide an explanation for the increase in basal activity. Agonist-bound crystal structures of β_2AR do not reflect an activation-induced change in the conformation of EL2.

In 2010, Bokoch *et al.* (*227*) presented solution NMR studies of β_2AR that revealed distinct conformations of EL2 associated with specific ligand-bound states. The study marked the first high-resolution structural data that described activation-induced conformational changes in and around the ligand-binding pocket of β_2AR. Specifically, the authors collected ^{13}C chemical shift measurements to monitor a conserved salt bridge (Asp192 and Lys305), which restricts the position of EL2 in the inactive conformation. In the presence of a high affinity agonist, the NMR data report a weakening of Asp192-Lys305 interaction consistent with agonist-induced motion of EL2. In rhodopsin, EL2 motion is associated with a change in the rotational orientation of transmembrane helix H5 (*172*). A question that still remains to be addressed is whether or not a similar allosteric coupling is involved in the activation mechanism of β_2AR.

Understanding the dynamic processes of β_2AR activation requires comparison between several receptor conformations whose temporal and thermal stability are not amenable to most biophysical methods. Solid-state NMR spectroscopy affords the opportunity to investigate unstable receptor conformations at low temperature. In addition, measurements can be carried out using the native sequence without a requirement for non-native binding partners or large protein insertions. In the following subsections, we use solid-state NMR spectroscopy to probe structural changes as a function of bound ligand species.

3.2.1. Trapping homogenous populations of various receptor conformations.

In order to investigate the structural differences between two receptor states using NMR spectroscopy, there are several factors that need to be addressed. First, the states being compared must correspond to a single receptor conformation. The second issue is one of sensitivity. The chemical shift of a particular nucleus is strongly influenced by the electrostatic environment, making it a suitable probe for detecting changes in local secondary and tertiary structure. However, there are a number of line-broadening components in the solid state arising from orientation-dependent nuclear spin interactions that are insufficiently averaged out (Chapter 2.2). As a result, there is often considerable spectral overlap. Therefore, the conformational differences between compared states must be large enough to induce a chemical shift change that exceeds the line-widths. In order to address the issues mentioned above, we compare ^{13}C chemical shift measurements between two ligand-bound receptor preparations.

Figure 3.10 presents a series of ^{13}C NMR difference spectra. For the left panel, spectra were calculated by subtracting 1D ^{13}C CPMAS spectra collected on BI167,107-bound from carazolol-bound β_2AR samples (~6 mg) that were isotope-enriched at various positions ($^{13}C\beta$-Ser, $^{13}C\beta$-Cys, and $^{13}C\varepsilon$-Met, respectively). For comparison the right panel depicts the corresponding regions of rhodopsin *minus* Meta II difference spectra. In both cases positive peaks correspond to resonances that are unique to the inactive, inverse agonist-bound state, while negative intensity represents chemical shift assignments for nuclei in the active, agonist-bound state.

For rhodopsin, difference spectra were calculated from active and inactive spectra that were collected using a single sample. For difference spectra of β_2AR, two samples with the same isotope-enrichment were required. Isotope-enriched β_2AR was heterologously expressed in HEK293S cells in a manner analogous to that used to generate samples of rhodopsin (see Chapter 2.1). For carazolol-bound β_2AR samples, growth media was supplemented with 100 nM carazolol during induction and subsequently purified from the cell membranes as described in chapter 2.1. The same strategy cannot be used for BI167107-bound samples since activated receptors are quickly internalized and processed by endogenous degradation machinery in the HEK293S cells. As such, expression was induced in the presence of 5 uM alprenolol. The receptor was first extracted in DDM micelles and bound to immunoaffinity resin. After immunoprecipitation, alprenolol was replaced with BI167107 via slowly (0.3 ml/min) washing

with 20 mM HEPES pH7.5, 100mM NaCl with 10 uM BI167107. The approach is predicated on the dramatic difference in Kd between BI167107 and alprenolol (84 pM and 1 nM, respectively).

For each receptor, difference bands are on the order of 1-2 ppm. In rhodopsin, photoisomerization converts the covalently bound retinal chromophore from an inverse to a full agonist allowing the receptor to fully populate the active Meta II state as assayed by UV/Vis spectroscopy. On the basis of similar line widths, we conclude that β_2AR difference spectra were also calculated from samples with conformational homogeneity.

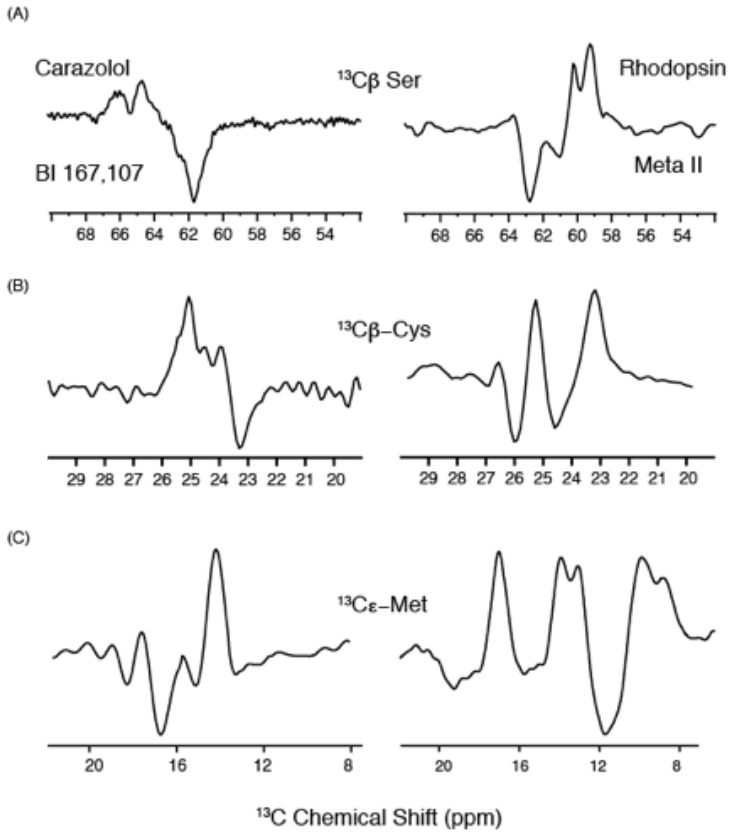

Fig. 3.10. ^{13}C Difference spectroscopy of β_2AR and rhodopsin. *^{13}C chemical shift measurements were made on β_2AR in the presence of either BI167107 or carazolol. Carazolol minus BI167107-bound difference spectra are shown in the regions of ^{13}Cβ-Ser (A), ^{13}Cβ-Cys (B), and ^{13}Cε-Met (C) in the left-hand panel. For comparison, the analogous regions from dark (inactive) minus Meta II (active) difference spectra of rhodopsin are shown in the right-hand panel.*

Despite having similar line-widths, difference spectra of β_2AR show a marked reduction in the number of difference bands compared to those seen for rhodopsin. One interpretation of these data is that the degree to which the two states being subtracted differ from one another are not

equivalent for both receptors. In rhodopsin, the 11-*cis* isomer of retinal acts as an inverse agonist to virtually eliminate all basal activity. In contrast, carazolol only reduces the basal activity of β_2AR by 50%. As such, the differences between the BI167107- and carazolol-bound β_2AR conformations may not be as pronounced as those seen in the transition to metarhodopsin II from rhodopsin.

3.2.2. T4-lysozyme induces conformational changes at the intracellular surface.

As mentioned earlier, one of the more productive strategies used to crystallize β_2AR has been to express the receptor as a chimeric species with T4-lysozyme. An obvious draw back of the chimera strategy is the fact that the receptor is missing the third intracellular loop (IL3) (Fig. 3.11). In addition to serving as a site of interaction for heterotrimeric G proteins, IL3 bridge two helices that have been shown to undergo significant conformational changes upon activation for a number of GPCRs (*43, 111, 228*). The current understand is that activation induces structural changes in H5 and H6. In turn, helical motion is coupled to a conformational change in IL3 to reveal the site of G protein interaction. It stands to reason that inserting a large protein adduct would significantly alter both the structure and function.

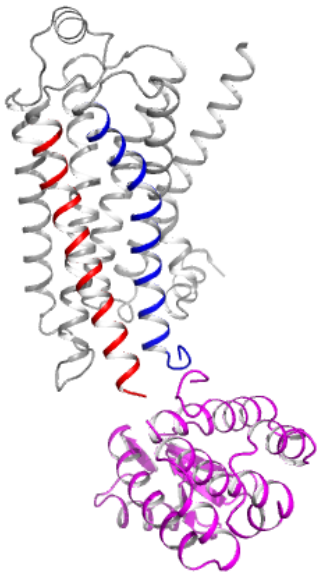

Fig. 3.11. T4 lysozyme. *The high-resolution crystal structure for the inactive conformation of the β_2AR was solved using a β_2AR-T4L chimera. The chimera has a large non-native sequence (magenta) in place of the third intracellular loop. Loop replacement may perturb the structure of H5 (red) and H6 (blue) and has been shown to eliminate G protein binding.*

In chapter 3.1, NMR measurements were described that show a disruption of the ionic lock between Arg135$^{3.50}$ on H3 and Glu247$^{6.40}$ on H6 upon activation of rhodopsin. As a result, H6 is displaced and the side chain of a highly conserved tyrosine residue (Tyr223$^{5.58}$) rotates towards the helical bundle to interact with Arg135$^{3.50}$ and stabilize the active state orientation of H5 (Fig.

3.12, right). In 2001, work from the Javitch group revealed that a similar event occurs upon activation of β_2AR (*205*). However, high-resolution crystal structures of the β_2AR do not reveal an ionic lock between H3 and H6. Moreover, the sidechain of Tyr219$^{5.58}$ is oriented towards Arg131$^{3.50}$ in a manner that is intermediate between its position in rhodopsin and metarhodopsin II (Fig. 3.10).

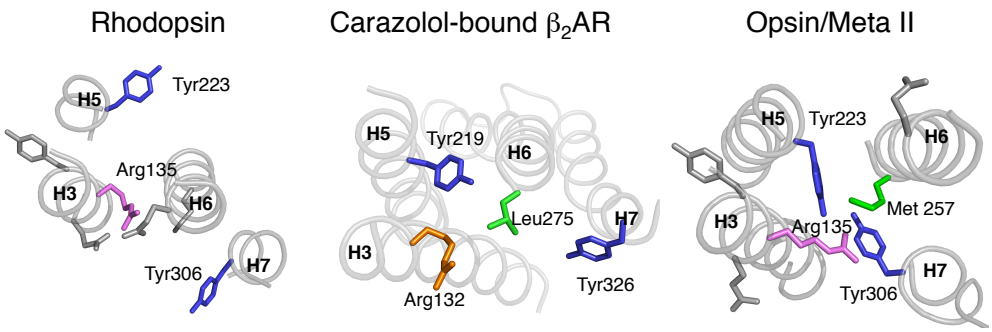

Fig. 3.12. Rhodopsin versus β_2AR. *A comparison of the rhodopsin, Meta II, and the inactive β_2AR crystal structures reveals that the orientation of Tyr223 in the inactive β_2AR structure is reminiscent of its position in Meta II, the active photointermediate.*

In order to address whether the addition of T4-lysozyme induces an active state orientation of H5, we monitored its position relative to the stable H1-H4 core. Specifically, ^{13}C labels were incorporated into carazolol-bound β_2AR to measure the distance between Met215$^{5.54}$ and Cys125$^{3.44}$ using 2D ^{13}C DARR experiments. The internuclear distance between Cε-Met215$^{5.54}$ and Cβ-Cys125$^{3.44}$ is within the detection limit of DARR as measured in the carazolol-bound crystal structure. However, the NMR data fail to reveal such a contact (Fig. 3.13A). We interpret the lack of a Cε-Met215$^{5.54}$ - Cβ-Cys125$^{3.44}$ contact to suggest that the addition of T4-lysozyme has disrupted the ionic lock and allowed H5 to adopt an active state orientation. Our interpretation is consistent with MD simulations that reveal an intact ionic lock in the inactive conformation when T4-lysozyme is removed and IL3 is rebuilt. (*225, 229, 230*).

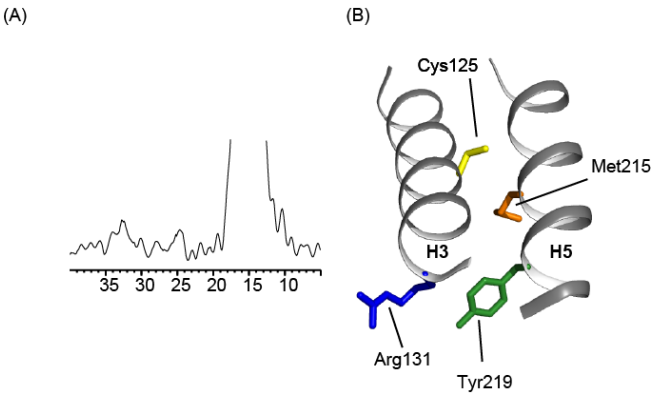

Fig. 3.13. T4-Lysozyme induces a rotation of H5 in the β_2AR. *(A) rows extracted through the ^{13}Cε-Methionine resonance of a 2D DARR spectrum collected on carazolol-bound, isotope-enriched β_2AR. The displayed region is expanded to show and polarization transfer between ^{13}Cε-Met and ^{13}Cβ-Cys and no such contact is observed. The data are inconsistent with the internuclear distance between Cε- Cε-Met215$^{5.54}$ and Cβ-Cys125$^{3.44}$.*

3.2.3. Changes in serine hydrogen bonding upon receptor activation.

From Figure 3.10, we see that the most pronounced differences between carazolol-bound and BI167107-bound β_2AR are observed in the region of ^{13}Cβ-Ser. Figure 3.14 shows the ^{13}Cβ-Ser chemical shift dispersion of β_2AR in the presence of BI167107 and carazolol. There is a significant overlap between the ^{13}Cβ-Ser chemical shift dispersion of carazolol and alprenolol-bound receptor conformations (data not shown). In contrast, the BI16707-bound spectrum reveals a peak at 61.9 ppm, which is consistent with a change in the hydrogen bonding character for the side chain of at least one serine residue.

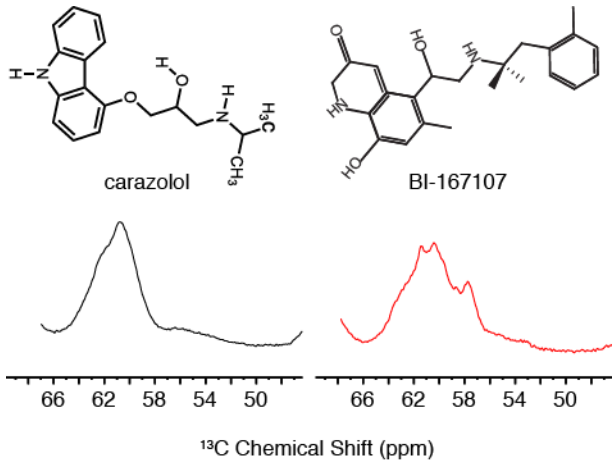

Fig. 3.14. Distinct ^{13}Cβ-serine chemical shifts in activated β_2AR. *^{13}C chemical shift measurements were collected on β_2AR in the presence of either carazolol (left) or BI167107 (right). The ^{13}Cβ-Ser chemical shift dispersion is shown for carazolol and BI167107-bound states. For the spectrum on the left, carazolol (5 μM) was added to the culture media concurrent with induction of expression. For the spectrum on the right, receptor expression was induced in the presence of 5 μM alprenolol. BI-167107 was subsequently introduced via on-column ligand exchange. In the crystal structure of β_2AR with BI-*

167107 bound, Ser203 and Ser207 form hydrogen bonds with the ligand. One can speculate that the serine NMR resonances observed in the spectrum with bound BI-167107 correspond to Ser203, Ser204, and Ser207.

The aromatic moieties of these three ligands (BI167107, alprenolol, and carazolol) are thought to occupy a similar region of the binding pocket. BI167107 contains two hydrogen bonding partners that are able to interact with the sidechain hydroxyl groups of the Ser203 and Ser207. These two residues are part of a triad of serine residues conserved throughout the amine subfamily of class A GPCRs (the SSXXS motif). In contrast, no hydrogen bonds are formed between these conserved serine residues and either carazolol or alprenolol (*219*). These data strongly suggest that the ^{13}Cβ-Ser chemical shift perturbations seen in the BI167107-bound spectrum reflect hydrogen bond formation with Ser203 and Ser207.

Within the SSXXS motif, Ser203 and Ser207 show strict conservation while Ser204 does so to a lesser degree (*104*). It was initially put forth that Ser204 and Ser207 were thought to be the most probable catechol docking sites (*231*). As such, the sidechains of Ser204 and Ser207 are thought to interact with the hydroxyl substituents of the catechol ring moiety in catecholaminergic ligands such as epinephrine and norepinephrine. These interactions would allow the catechol ring moiety to interact with aromatic residues of H6 (i.e. Phe290 and Trp286) (*49*) as a part of the "rotamer toggle switch" (*111*). This context provides a framework for how agonist binding leads to a rearrangement of the transmembrane helices.

Moreover, it is been shown that the reduced binding affinities of ligands to mutants of Ser203, 204 and 207 can, to a certain degree, be rescued by adding additional interacting groups in the non-catecholic part of the catecholamine molecule (*232*). All such evidence along with an increased understanding of the role of SSXXS motifs in transmembrane helix orientation (*233, 234*) and interactions (*235*) indicate that the serine triad in H5 may play a vital role in the conformational motion of β_2AR.

3.2.4. The rotational orientation of H5 correlates with receptor activation.

In section 3.2.2, it was introduced that the internuclear distances between Cε-Met215$^{5.54}$ and Cβ-Cys125$^{3.44}$ serves as a marker for the interhelical interface between H3 and H5. As described earlier, there are a number of group-conserved residues throughout H1-H4 that mediate close packing to form a stable transmembrane core during receptor activation. Therefore, H1-H4

serves as a static frame of reference by which helix motion can be measured for H5-H7. In rhodopsin, H5 rotation is thought to be induced by steric clashes between Met207 of H5 and the β-ionone ring of retinal upon isomerization (*171*). Figure 3.15 (panel A) shows rows extracted through the ^{13}Cβ-Cys region of 2D DARR solid-state NMR spectra collected on isotope-enriched rhodopsin in both the dark (black) and active metarhodopsin II state (red). In the dark, crosspeaks are absent between the ^{13}Cε-Met and ^{13}Cβ-Cys resonances. In contrast, conversion to metarhodopsin II results in the emergence of a strong ^{13}Cε-Met-^{13}Cβ-Cys cross peak that has previously been assigned to Cε-Met207$^{5.45}$ and Cβ-Cys167$^{4.56}$, whose sidechains come closer together upon an activation-induced rotation of H5 (*171*). Similarly, one can use the Cε-Met215$^{5.54}$ and Cβ-Cys125$^{3.44}$ internuclear distance to monitor the rotation of H5 with respect to the stable core in β_2AR.

Figure 3.15 (panel B) presents rows extracted through the ^{13}Cβ-Cys region of 2D DARR solid-state NMR spectra collected on isotope-enriched β_2AR in the presence of an inverse agonist (carazolol, black) as well as agonist (BI167107, red). In the inverse agonist-bound conformation, crosspeaks are absent between ^{13}Cε-Met and ^{13}Cβ-Cys resonance. However, a strong ^{13}Cε-Met-^{13}Cβ-Cys cross peak is observed in the agonist-bound conformation. We have tentatively assigned the active state ^{13}Cε-Met - ^{13}Cβ-Cys cross peak to Cε-Met215$^{5.54}$ - Cβ-Cys125$^{3.44}$ on the basis of internuclear distances measured from X-ray crystal structures (*112, 113*). Together, the NMR data presented in Figure 3.15 suggest that a rotation of H5 with respect to the stable transmembrane core is a feature of activation of both β_2AR and rhodopsin.

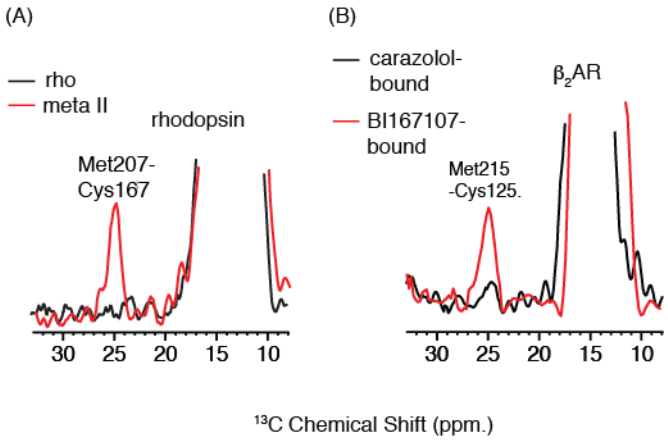

Fig. 3.15. H5 Rotation is a conserved feature of GPCR activation. *(A)Rows extracted from 2D ^{13}C correlation spectra collected active(red) and inactive (black) rhodopsin are shown. The extracted rows reveal an active state dipolar coupling between ^{13}Cε-Met207$^{5.42}$ on H5 and ^{13}Cβ-Cys167$^{3.56}$ of the H1-H4 core. (B) Rows are shown from 2D ^{13}C correlation spectra collected on β_2AR in the presence of an inverse agonist (carazolol) and a full synthetic agonist (BI167107). The extracted row reveals dipolar couplings between ^{13}Cε-Met and ^{13}Cβ-Cys.*

Based on analysis of the interaction between catecholaminergic ligands and fluorophore-labeled receptor, it has been proposed that β_2AR activation occurs in a multiple steps. The progression from one intermediate to another is dependent on the number of hydroxyl groups present in the catecholamine molecule (*222*). The idea that specific interactions between the receptor and hydrogen bonding partners of cateholaminergic ligands force a stepwise conversion of β_2AR into its active conformation is consistent with the ability of functional groups in the catecholamine molecule to synergistically contribute to both ligand binding and receptor activation (*102*).

In order to investigate the proposed heterogeneity associated with active conformations of β_2AR, we look at the rotational orientation of H5 using the internuclear distance between Cys125 and Met215 as a function of bound ligand species. Figure 3.16 presents rows extracted through the ^{13}Cε-Met resonance of a 2D DARR spectrum collected on ^{13}C-enriched β_2AR bound to either carazolol, alprenolol or BI167107. The displayed region is expanded to show polarization transfer between Cε-Met and Cβ-Cys. As described in Chapter 2, polarization transfer occurs through the dipolar interaction and has strong distance dependence. When the dipolar coupling strength is compared across the three ligand-bound receptor conformations, a correlation with ligand efficacy is revealed. The internuclear Cβ-Cε distance between Met215 and Cys125 measured from the crystal structures of the β_2AR reflect a decreased distance between these two residues that correlates with activity (i.e. carazolol<alprenolol<BI167107). The NMR data are consistent with the same statement. (D,E, and F, respectively).

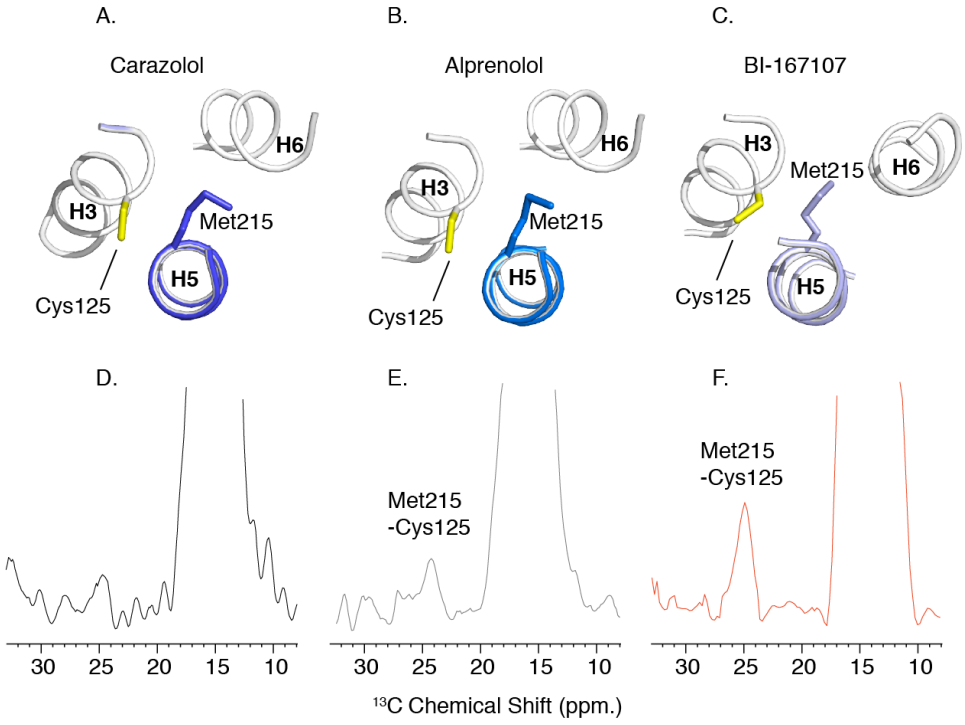

F***ig. 3.16. The rotational orientation of H5 correlates with activity in the β_2AR activation.*** *Views from the cytosolic surface of the β_2AR in the presence of an inverse agonist (carazolol). antagonist (alprenolol) and a full synthetic agonist (BI167107) are shown in panels A, B and C respectively. The side chains of Met215$^{5.54}$ and Cys125$^{3.44}$ are displayed. The Cβ-Cε internuclear distance between Cys125 and Met215, in the presence of carazolol, is 5.7 Å. The same two nuclei in the alprenolol- and BI167107-bound receptor conformations are separated by 5.5 Å and 4.1 Å respectively. As such, the internuclear distance between these two nuclei serves as a marker for the rotational orientation of transmembrane helix H5. Rows extracted from 2D ^{13}C correlation spectra collected on the β_2AR in the presence carazolol (D), alprenolol (E), and BI16707 (F) are shown. The extracted row reveals dipolar couplings between ^{13}Cε-Met and ^{13}Cβ-Cys.*

We interpret these data in this subsection to suggest that H5 undergoes a graded response to receptor activation. In addition, we propose that hydrogen bond formation between polar moieties on the catechol ring of aminergic ligands provides the driving force for a rotation of H5. In the context of interactions with downstream signaling targets, the degree to which H5 has rotated may have consequences for how effectively IL3 can interact with G protein.

3.3 CHAPTER CONCLUSION AND FUTURE DIRECTIONS

The work on Rhodopsin was subsequently extended to the ligand activated β_2AR, where structural studies are presented to suggest that H5 rotation is a common element of GPCR activation. The NMR results track the rotational orientation of transmembrane helix H5 with

respect to the stable H1-H4 core and establish an activation-induced rotation of transmembrane helix H5. The most marked difference was seen when comparing data collected in the presence of BI167107, a full agonist, with that of carazolol, an inverse agonist. That the rotation orientation of H5 in the presence of Alprenolol, an antagonist, was unique, suggested a graded response to receptor action. The implication is that these changes in rotational orientation for H5 correlate with the hydrogen bonding status of signature conserved Tyr219$^{5.58}$. In addition, the rotational orientation of transmembrane helix H5 correlates with changes in the electrostatic environment of several serine residues. We interpret the data in terms of hydrogen bond formation between the polar constituents on the catechol ring moiety of bound ligand and the hydroxyl side chains of the SSXXS motif on H5, which is conserved through the amine subfamily. We draw a parallel between ligands hydrogen-bonding to the SSXXS motif in the β_2AR and steric clashes between the β-ionone ring and side chains of H5 in rhodopsin. Both mechanisms serve to couple the presence of agonist in the binding pocket with a rotation of H5. In fact, the residues in rhodopsin that correspond to the position of the SSXXS motif consist of hydrophobic sidechains (i.e. Met207$^{5.43}$, Phe208$^{5.44}$) that form steric contact with all-*trans* retinal in Meta II. Since all-*trans* retinal is such a potent agonist in rhodopsin, a future experiment would be to introduce large residues in place of the small side chains of the SSXXS motif in the β_2AR. The expectation is that H5 rotation would occur in a manner that is insensitive to the hydrogen bonding abilities of the activating ligand.

As with other ligand activated GPCRs, there are a number of ligands that modulate receptor function in the β_2AR. The β_2AR work in this thesis provides evidence of how a particular set of interactions between the receptor and ligands can generate ligand-specific conformational changes. The idea is that GPCR signaling has evolved to trigger permutations of individual structural change in order to elicit the desired physiological response. The challenge is now to probe a set of specific structural changes (i.e. H5 rotation) in order to establish which conformational triggers confer activation.

CHAPTER 4: STRUCTURAL CHANGES IN TRANSMEMBRANE HELIX 6 UPON GPCR ACTIVATION.

It has been known since the pioneering EPR studies of Hubbell and coworkers using site-directed spin labeling that activation of rhodopsin involves the outward rotation of transmembrane helix H6 (*43*). However, a mechanistic understanding of how retinal isomerization is coupled to H6 motion has been lacking. The first high-resolution crystal structure of rhodopsin was obtained in 2000 of the inactive, dark state of the receptor (Figure 4.1) (*98*). This structure revealed the position of highly conserved residues within the large family of class A GPCRs, but provided few clues about the mechanism of receptor activation. The crystal structure of opsin, which captures the outward rotation of H6, revealed several key elements of the activation mechanism (*95, 107*). In the dark state of the rhodopsin, Arg135$^{3.50}$ forms a salt bridge with Glu247$^{6.30}$ on H6. In opsin, the rotation of H6 moves Glu247$^{6.30}$ toward H5 where it forms a new electrostatic interaction with Lys231$^{5.66}$. H6 motion also places Met257$^{6.40}$ in contact with Arg135$^{3.50}$ on transmembrane helix H3. However, this latter interaction appears to require the outward tilt of H6, which displaces the intracellular end of H6 by ~5 Å relative to H3 (*47*). That is, the interface between H3 and H6 is tightly packed and the outward motion of H6 allows the side chain of Arg135$^{3.50}$ to extend toward Met257$^{6.40}$ and make contact (see Figure 4.1C). In addition, the opsin crystal structure showed that the intracellular ends of both helices H5 and H7 undergo rotation to allow two highly conserved tyrosine residues to hydrogen bond with Arg135$^{3.50}$. Tyr223$^{5.58}$ on H5 and Tyr306$^{7.53}$ on H7 rotate toward Arg135$^{3.50}$ in the active receptor and contribute to breaking of the Arg135$^{3.50}$-Glu247$^{6.30}$ salt bridge (*95, 107*). The combined effect of these structural changes is to open up a cavity on the intracellular side of the receptor that serves as the binding site for the C terminal tail of the Gα subunit of transducin, the heterotrimeric G protein that associates with light-activated rhodopsin.

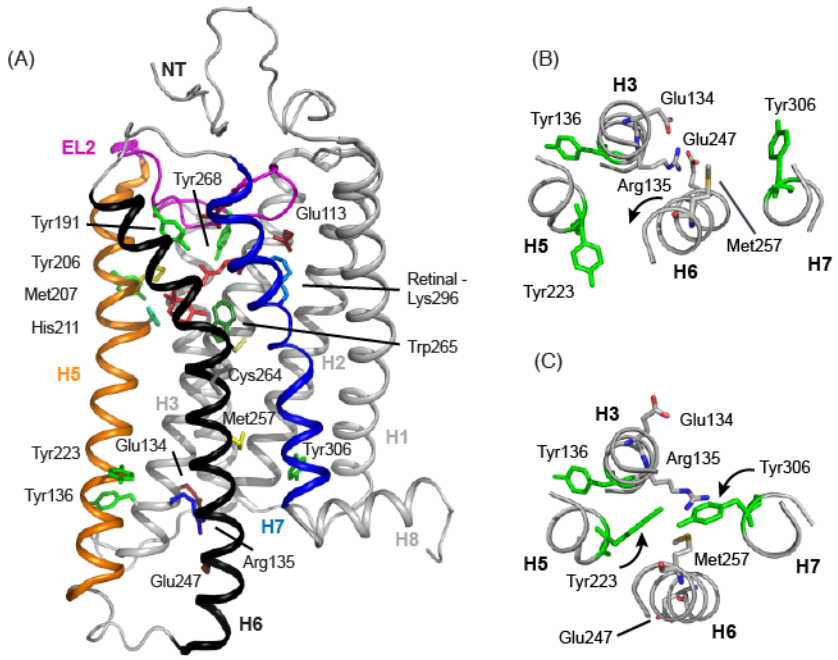

Fig. 4.1. Crystal structures of rhodopsin (PDB access code = 1GZM) and Meta II (PDB access code = 3PXO) highlighting key residues associated with photoactivation. *(A) The full receptor structure is shown. The retinal is buried between the transmembrane helices on the extracellular side of the protein with the second extracellular loop (EL2) forming a cap on the retinal binding site. Motion of helices H5, H6 and H7 during activation opens up the G-protein binding site on the intracellular side of the receptor, while helices H1–H4 form a tightly packed core. (B) Cross section of the intracellular side of rhodopsin in the region of the Arg135$^{3.50}$ - Glu247$^{6.30}$ salt bridge. Only selected helices are shown for clarity. (C) Structure of the intracellular side of Meta II in the region of the ionic lock. There are several differences between inactive rhodopsin (panel B) and Meta II (panel C). Rotation of H6 breaks the Arg135$^{3.50}$ - Glu247$^{6.30}$ contact and moves Met257$^{6.40}$ into the H3-H6 interface. The intracellular end of H6 tilts outward, allowing the side chain of Arg135$^{3.50}$ to extend and contact Met257$^{6.40}$. Rotation of H5 and H7 place Tyr223$^{5.58}$ and Tyr306$^{7.53}$ into contact with Arg135$^{3.50}$. Hydrogen bonds between these tyrosines and Arg135$^{3.50}$ stabilize the active state of the receptor.*

Several observations argue that the motions of helices H5, H6 and H7 are part of a common activation mechanism for Class A GPCRs. First, a number of the residues described above are highly conserved (*126*). Arg135$^{3.50}$ is part of the conserved ERY motif on helix H3 (i.e. residues Glu134$^{3.49}$-Arg135$^{3.50}$-Tyr136$^{3.51}$). Tyr223$^{5.58}$ is the most highly conserved residue on H5, while Tyr306$^{7.53}$ is part of a conserved NPxxY sequence on H7. Second, recent crystal structures of the β_2AR with bound agonists show an outward displacement of H6 and confirm that this signature structural change for rhodopsin activation is present in a ligand-activated GPCR (*86, 112*). Nevertheless, the large changes in H6 in these crystal structures are only observed when the receptor is in complex with an antibody mimicking the G protein. The structures of the β_2AR (*220*) and other ligand-activated GPCRs (*236, 237*) without stabilizing antibodies exhibit structural changes that are much smaller than those observed in the active state of rhodopsin. One possible explanation for the differences between rhodopsin and the ligand-activated

receptors is that rhodopsin has evolved several mechanisms to reduce basal activity, including the salt bridge between Arg135$^{3.50}$ and Glu247$^{6.30}$, which are essential for a visual receptor. In contrast, ligand-activated receptors typically exhibit high levels of basal activity. These receptors are inherently dynamic molecules that interconvert between transiently populated conformational states (*221*). As a result, if the visual receptors and ligand-activated receptors share a common activation mechanism, there are likely interactions that restrict H6 motion in rhodopsin that are released following photo-isomerization, but prior to the conformational change that ultimately generates the active receptor.

Figure 4.2 presents the photoreaction pathway leading from dark, inactive rhodopsin to the active Metarhodopsin II (Meta II) intermediate. In the dark state, the retinal chromophore is bound as a protonated Schiff base to Lys296$^{7.43}$ on transmembrane helix H7. Absorption of light triggers the rapid isomerization of the retinal from the 11-*cis* to the all-*trans* configuration. The early intermediates contain a conformationally distorted all-*trans* retinal chromophore (*238*). Calorimetric studies have shown that ~30 kcal/mol of the absorbed light energy is stored in Bathorhodopsin, the first relatively long-lived intermediate (*239*). The trapped energy is released as the retinal relaxes (*240-243*). and the surrounding amino acids reorient in the transitions to the Blue-shifted Intermediate, Lumirhodopsin and Metarhodopsin I (Meta I). Meta I immediately precedes the activated Meta II state. The current study focuses on the orientation and interactions involving helix H6 in Meta I in order to establish whether conformational changes occur in this helix leading up to the active Meta II state.

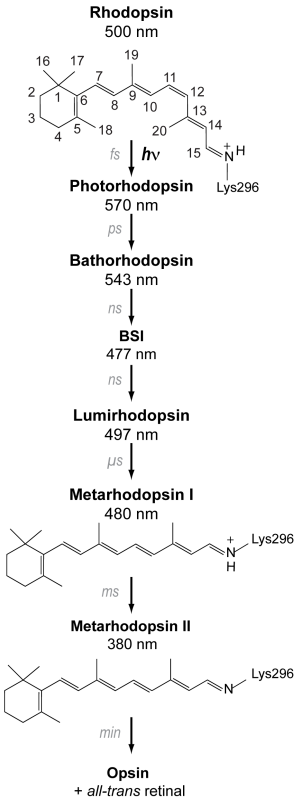

Fig. 4.2. Photoreaction of rhodopsin. *Structures of the 11-cis and all-trans retinal chromophores and the photoreaction intermediates of rhodopsin are shown. Absorption of light results in 11-cis to all-trans isomerization of the retinal. The retinal-protein complex subsequently relaxes thermally through a series of spectrally well-defined intermediates: Photorhodopsin, Bathorhodopsin, the Blue Shifted Intermediate (BSI), Lumirhodopsin, and Meta I. Deprotonation of the retinal Schiff base nitrogen occurs in the formation of the Meta II intermediate. Meta I exists in a pH- and temperature-dependent equilibrium with the active Meta II intermediate.(244) High pH and low temperature favor Meta I. Evidence for substantial structural changes in Meta I comes from time resolved absorbance measurements showing that the transition to Lumirhodopsin is the last step in the photoreaction sequence that does not exhibit differences between lipid and detergent environments. In addition, Meta I is the first intermediate that cannot be fully photo-converted back to rhodopsin.*

The retinal chromophore in the Meta I intermediate has an all-*trans* configuration and exhibits an absorption maximum (λ_{max}) at 480 nm. There are no high-resolution crystal structures of Meta I. However, a 5.5 Å resolution structure of Meta I obtained by electron cryo-microscopy of 2D crystals showed no significant displacements of the transmembrane helices as compared to the dark state of rhodopsin (*117*). The largest change in Meta I relative to rhodopsin was in the region of Trp265$^{6.48}$ on helix H6 (*117*), which suggested a local change either in the conformation of the Trp265$^{6.48}$ side chain or in the rotational orientation of the H6 helix.

In contrast to the low-resolution structure of Meta I, a number of biophysical studies have revealed conformational changes that stretch from the retinal binding site on the extracellular side of the receptor to the G-protein binding site on the intracellular surface in Meta I. On the extracellular side of rhodopsin, Fourier transform infrared (FTIR) spectroscopy shows that Glu122$^{3.37}$ becomes more strongly hydrogen bonded in the transition to Meta I (*245*). Glu122$^{3.37}$ is located on helix H3 near the retinal β-ionone ring, and its side chain is hydrogen bonded to the backbone carbonyl of His211$^{5.46}$ on H5. These residues are part of a hydrogen bonding network that extends to the second extracellular loop (EL2). Coupled motion of the retinal and H5 has been implicated in the transition to the active Meta II state (*172*).

On the intracellular side, FTIR measurements of rhodopsin containing *p*-azido-L-phenylalanine, an engineered non-native amino acid, show that there are strong changes in polarity at the ends of helices H5 and H6 in the formation of Meta I. These changes are consistent with a rotation of H6 and movement of its intracellular end of H5 away from H3 (*228*). Furthermore, Meta I is the first substrate for rhodopsin kinase (*246*), which binds to Meta I and Meta II with equal affinity (*247*), and has been reported to be able to bind the G protein transducin (*248, 249*). Together these results imply that a conformational change on the extracellular side of the receptor, induced by retinal isomerization, modulates the intracellular surface of Meta I.

Solid-state NMR spectroscopy provides a complementary approach for probing the structure of Meta I and defining the structural changes that occur as light energy is channeled into rhodopsin. Previous solid-state NMR studies on Meta I were restricted to the chromophore and showed that the retinal polyene chain is in a relaxed conformation in contrast to the distorted conformation adopted in the dark state (*241, 242, 250, 251*). In following subsections, we describe ^{13}C and ^{15}N solid-state MAS NMR measurements on Meta I trapped in digitonin that target structural changes in the protein centered on helix H6. Digitonin is unusual compared to other detergents as the hydrophobic end of the digitonin is composed of a rigid spirostan steroid tail rather than flexible fatty acyl chains. It has been used extensively to stabilize the Meta I intermediate (*63, 213, 252*), since it was first shown to be effective in blocking the transition from Meta I to Meta II (*253*). The ability of digitonin to trap Meta I is comparable to that of cholesterol, which was previously used to trap Meta I in 2D crystals of rhodopsin (*117*). Both digitonin and cholesterol have a rigid steroidal structure that prevents the Meta I to Meta II transition. In contrast, the transition to the Meta II intermediate is facilitated by solubilization of rhodopsin in DDM detergent, which creates a fluid environment. Our structural measurements on Meta I can be compared with previous measurements of rhodopsin and Meta II. The comparison with rhodopsin allows us to infer what structural changes occur between the dark state and Meta I. The comparison with Meta II allows us to infer what structural changes are directly associated with receptor activation. Two dimensional ^{13}C DARR NMR measurements reveal an interhelical contact between $^{13}C\zeta$-labeled Arg135$^{3.50}$ and $^{13}C\varepsilon$-labeled Met257$^{6.40}$ indicating that transmembrane helix H6 rotates in the formation of Meta I. However, the NMR data show that EL2 and H5 have not shifted into their active state conformations. Our results help to define the

sequential structural changes occurring between rhodopsin and Meta I that prime the receptor for transition to the active Meta II state.

4.1. Trapping of the Metarhodopsin I intermediate.

The Meta I intermediate is characterized by a visible absorption maximum at 480 nm. Figure 4.3A presents absorption spectra showing the conversion of rhodopsin (λ_{max} = 500 nm, black line) to Meta I (λ_{max} = 480 nm, blue line) following illumination by light with wavelengths longer than 495 nm. The stability of Meta I in digitonin is temperature dependent. At 4°C, rhodopsin is fully converted to the Meta I intermediate and is stable for over 30 min (light blue line). When rhodopsin in digitonin is illuminated at 20°C, a mixture of Meta I and Meta II (λ_{max} = 380 nm) is formed (red line). This mixture is stable for over 30 min (orange line). The temperature dependence of the transition to Meta II has previously been characterized (*57, 213, 254*). The Meta II substate that is obtained at 20°C in digitonin likely corresponds to Meta IIa on the basis of EPR measurements showing that digitonin effectively blocks the large increase in the mobility of a spin label at residue $250^{6.33}$ near the intracellular end of H6 (*254*). As such, the outward tilt of H6 is associated with the Meta IIa to Meta IIb transition (*254*).

A second characteristic feature of the Meta I state is that the retinal chromophore has an all-*trans* configuration and is attached to $Lys296^{7.43}$ as a protonated Schiff base. To address the protonation state of the retinal Schiff base linkage, Figure 4.3B presents the ^{15}N MAS NMR spectra of rhodopsin (black) and Meta I (orange) containing $^{15}N\zeta$-labeled lysine. The $^{15}N\zeta$-$Lys296^{7.43}$ resonance in rhodopsin (black) is observed at 156.8 ppm. In Meta I, the $^{15}N\zeta$-$Lys296^{7.43}$ resonance broadens and shifts slightly to 155.7 ppm. The similar ^{15}N chemical shifts between rhodopsin and Meta I demonstrate that the Schiff base nitrogen is protonated. Deprotonation of the Schiff base has a dramatic effect on the $^{15}N\zeta$-$Lys296^{7.43}$ chemical shift, which is observed at 282.2 ppm in Meta II (*170*).

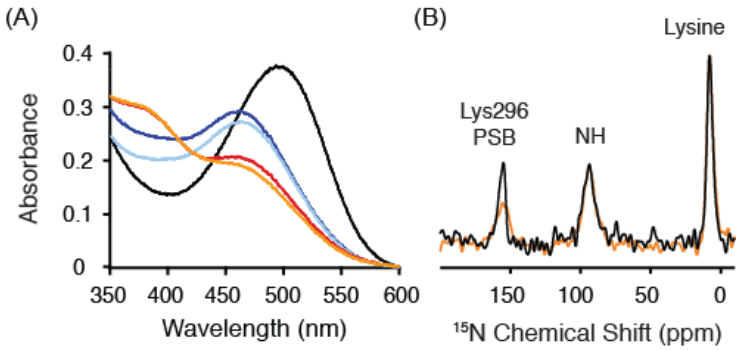

Fig. 4.3. Trapping of the Meta I intermediate in digitonin. *(A) UV-Vis spectra provide a means to follow the conversion of rhodopsin (λ_{max} = 500 nm, black line) to Meta I (λ_{max} = 480 nm, blue line) after illumination by light (> 495 nm) at 4°C. Meta I remains stable in digitonin for over 30 min at 4°C (light blue line). Conversion at 20°C leads to a mixture of Meta I and Meta II (red line), which does not change appreciably over 30 min (orange line). (B) One dimensional ^{15}N spectra of rhodopsin (black) and Meta I (orange) labeled at $^{15}N\zeta$-lysine are shown that were obtained using ^{1}H-^{15}N cross polarization. The $^{15}N\zeta$-Lys296$^{7.43}$ chemical shift is observed as a distinct narrow peak at 156.8 ppm in rhodopsin (black). In Meta I, the resonance shifts slightly and broadens. The $^{15}N\zeta$ resonances for the other $^{15}N\zeta$-labeled lysines in rhodopsin are observed as a broad peak ~8.0 ppm. The UV/vis data in panel A was collected by Markus Eilers and the NMR data in panel B was collected by Shivani Ahuja.*

We also measured the ^{13}C chemical shifts of Meta I regenerated with several selectively ^{13}C-labeled retinals (Figure 4.4). There is a good correspondence of the NMR frequencies with other studies on Meta I (*241, 242, 250*). For example, the $^{13}C10$, $^{13}C11$ retinal resonances in Meta I at 130.6 ppm and 139.2 ppm, respectively, are in agreement with previous measurements of Meta I trapped in lipids (*241*). Although both saturated lipids and digitonin result in an observable broadening of the ^{13}C resonances of the polyene chain(*250*), we can show in Figure 4.4 that, in digitonin, there is good conversion from rhodopsin to Meta I with <15% formation of Meta II. The ability to photo-convert rhodopsin to Meta I may be associated with the reduction in light scattering from detergent micelles, as compared to lipid multilayers.

4.2 Structural changes in the region of EL2 in Meta I.

The second extracellular loop (EL2) of rhodopsin is part of the retinal-binding pocket (*98*). NMR measurements on Meta II have revealed activation-induced structural changes in EL2 (*172*) and in the vicinity of the retinal chromophore (*171*). We compare our previous results on rhodopsin and Meta II with NMR measurements of the Meta I intermediate in the region of EL2.

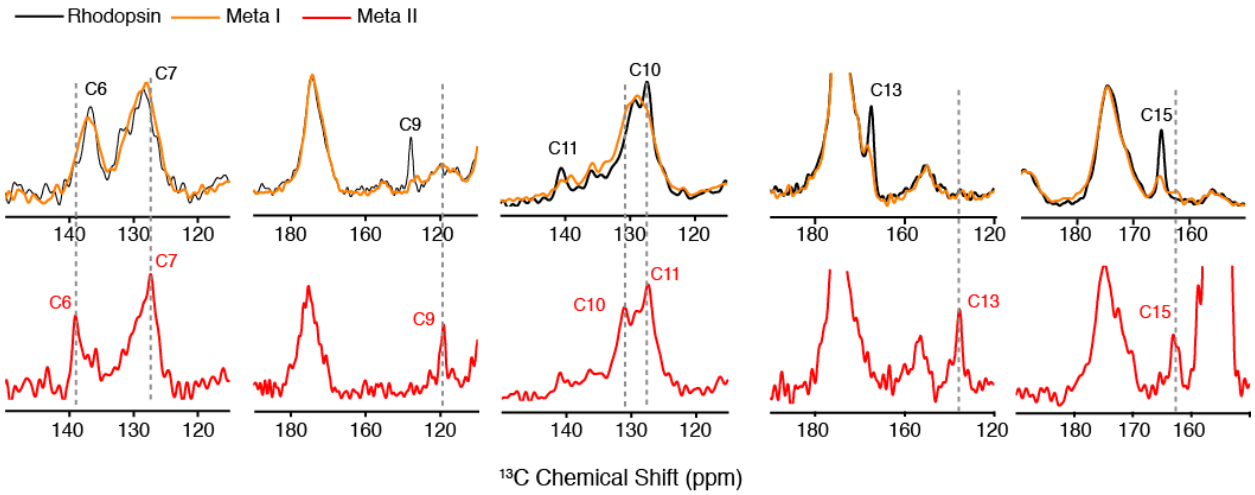

\

Fig. 4.4. One-dimensional ^{13}C MAS NMR spectra of rhodopsin and Meta I. *Rhodopsin was regenerated with 11-cis retinal selectively ^{13}C labeled at different carbons along the polyene chain and the β-ionone ring. Overlap of the ^{13}C MAS NMR spectra of rhodopsin (black) and Meta I (orange) shows that most of the retinal resonances broaden considerably in Meta I as compared to the sharp narrow resonances observed in rhodopsin and Meta II (red). There is nearly complete conversion to Meta I from rhodopsin. For example, the ^{13}C9 retinal resonance in rhodopsin falls in an uncrowded region of the spectrum. The residual intensity of the ^{13}C9 resonance in the Meta I spectrum is <15% of its original intensity in rhodopsin. Also, there is <15% conversion of rhodopsin to Meta II. For example, the spectra with ^{13}C13 retinal show a complete absence of a resonance associated with Meta II. All of the NMR data presented in this figure was collected by Shivani Ahuja.*

Characteristic changes in ^{13}C chemical shifts have been observed previously in NMR difference spectra between rhodopsin and Meta II for tyrosine, methionine, glycine and cysteine residues on EL2 and EL3 (*171, 172*). Figure 4.5A shows the difference spectra for ^{13}Cζ-tyrosine between rhodopsin and Meta I (orange) and between rhodopsin and Meta II (black). Positive peaks correspond to rhodopsin and negative peaks correspond to Meta I or Meta II. The ^{13}Cζ-tyrosine chemical shift is sensitive to hydrogen bonding of the side chain Cζ-OH group (*174*). There are two distinct resonances that appear upon the formation of Meta II (*172*). The

downfield resonance at 158.9 ppm corresponds to Tyr191 on EL2 (i.e. Tyr191^{EL2}), which becomes more strongly hydrogen bonded in Meta II. The upfield resonance at 153.1 ppm corresponds to Tyr206$^{5.41}$, which becomes more weakly hydrogen bonded in Meta II. These two resonances are not observed in Meta I indicating that EL2 and H5 have not shifted into the conformation characteristic of the active state.

Figure 4.5B presents difference spectra for ^{13}Cε-methionine between rhodopsin and Meta I (orange) and between rhodopsin and Meta II (black). In the rhodopsin - Meta II difference spectrum, we have assigned the positive resonance at 17.2 ppm (rhodopsin) and the negative resonance at 12.8 ppm (Meta II) to Met288$^{7.35}$ based on its disappearance in the M288L mutant (see Chapter 5). Met288$^{7.35}$ is located on H7 and is at the interface between EL2 and the extracellular end of H7. The rhodopsin - Meta I difference spectrum indicates that Met288 in Meta I has moved into an environment characteristic of the active state, suggesting local structural changes in H6, H7 or EL2.

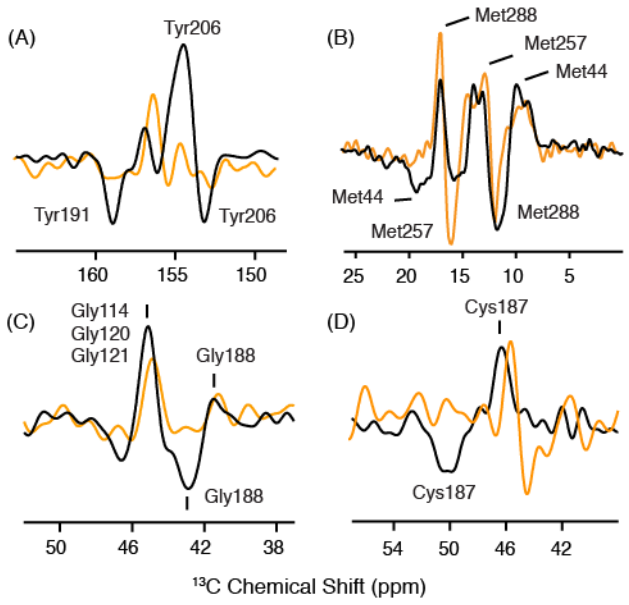

Fig. 4.5. ^{13}C MAS difference spectra of rhodopsin, Meta I and Meta II. *Difference spectra are shown for rhodopsin - Meta I (orange) and rhodopsin - Meta II (black) using rhodopsin isotopically labeled with ^{13}Cζ-tyrosine, ^{13}Cε-methionine, ^{13}Cα-glycine and ^{13}Cβ-cysteine. Positive peaks correspond to rhodopsin and negative peaks correspond to Meta I or Meta II. (A) The tyrosine ^{13}Cζ difference spectrum between rhodopsin and Meta II exhibits two positive and two negative resonances. The two Meta II resonances at 158.9 and 153.1 ppm, and have been assigned to Tyr191^{EL2} and Tyr206$^{5.41}$, respectively (172). These resonances are not observed in the rhodopsin - Meta I difference spectrum. (B) The methionine ^{13}Cε difference spectrum between rhodopsin and Meta II exhibits three distinct positive*

and two negative resonances. (C) The glycine $^{13}C\alpha$ difference spectrum shows two positive and two negative resonances. The upfield resonances in rhodopsin at 41.5 ppm and in Meta II at 42.9 ppm have been assigned to Gly188^{EL2} (172). The appearance of a negative resonance at the position of Gly188^{EL2} is not observed in the rhodopsin - Meta I difference spectrum. (D) In the cysteine $^{13}C\beta$ difference spectrum between rhodopsin and Meta II, the chemical shift of Cys187^{EL2} changes from 46.8 ppm to 50.1 ppm.(172) The disulfide bridge between Cys187^{EL2} and Cys110$^{3.25}$ tethers EL2 to the helical bundle. The NMR data is this figure was collected by Shivani Ahuja.

The chemical shift for Met257$^{6.40}$ in Meta II was assigned at 14.7 ppm based on a cross peak with Arg135$^{3.50}$ (*96*). A corresponding negative resonance is not observed in the rhodopsin - Meta II difference spectrum because the resonance does not change between rhodopsin and Meta II. Despite significant structural changes at the cytoplasmic end of H6, the summation of partial charges surrounding the side chain of Met257 in both rhodopsin (i.e. proximity to Asn302) and Meta II (i.e. proximity to Tyr306 and Tyr223) are similar. As a result, the $^{13}C\varepsilon$-Met257 chemical shifts are similar in rhodopsin and Meta II. In contrast, a strong negative cross peak is observed at 15.8 ppm in Meta I (discussed below).

In the rhodopsin - Meta II difference spectrum, we have also assigned the positive resonance at 10.5 ppm (rhodopsin) and negative resonance at 19.2 ppm (Meta II) to Met44$^{1.39}$ (*171*). Met44$^{1.39}$ is located near the retinal Schiff base. The positive resonance at 10.5 ppm is observed in the rhodopsin - Meta I difference spectrum. However, the negative resonance at 19.2 ppm is not observed in Meta I. These results suggest that the environment of Met44$^{1.39}$ near the protonated Schiff base in Meta I is different from rhodopsin, but does not yet correspond to the active Meta II state.

Figure 4.5C presents the rhodopsin - Meta II difference spectrum (black) for $^{13}C\alpha$-glycine. We have assigned the positive resonance at 41.5 ppm and the negative resonance at 42.9 ppm to Gly188^{EL2} based on its disappearance in the G188A mutant (*172*). The appearance of the positive peak at ~42 ppm in the rhodopsin - Meta I spectrum (orange) indicates that Gly188^{EL2}, located in EL2, is influenced by the conversion to Meta I. However, the absence of the negative peak at 42.9 ppm argues that the EL2 has not yet adopted the final conformation observed in the Meta II state (*172*). The large positive peak at 45.5 ppm in Meta II is associated with several glycines on H3 (Gly114$^{3.29}$, Gly120$^{3.35}$ and Gly121$^{3.36}$) (*171, 172*). The observation of a positive peak at this position in the rhodopsin - Meta I difference spectrum suggests a possible structural change in H3 in the transition to Meta I. Gly114$^{3.29}$ on H3 is adjacent to Glu113$^{3.28}$ and one helical turn

from Cys110$^{3.25}$. Changes in the interactions of the protonated Schiff base with its counterion are likely to induce structural changes in the helix backbone in this region. For example, the largest changes in the crystal structure of lumirhodopsin, relative to rhodopsin, were observed in two helical turns of H3 centered on Gly120$^{3.35}$ and Gly121$^{3.36}$ (*255*)

Figure 4.5D shows the changes in the ^{13}Cβ resonances of the highly conserved Cys110$^{3.25}$-Cys187^{EL2} disulfide group. Cys110$^{3.25}$ is at the extracellular end of H3 and Cys187^{EL2} is part of the β4 strand of EL2. In DDM, the ^{13}Cβ resonance of Cys187^{EL2} shifts from 46.8 ppm to 50.1 ppm upon conversion of rhodopsin to Meta II (*172*). In digitonin, the dark state ^{13}Cβ resonance of Cys187^{EL2} is at 45.5 ppm and shifts to 44.4 ppm in Meta I. The change in chemical shift of Cys187^{EL2} suggests a conformation or environment distinct from either the dark state or Meta II.

2D MAS NMR dipolar recoupling experiments provide support for the conclusion that EL2 has not yet shifted into its active state conformation. Figure 4.6A presents slices through the ^{13}Cζ-tyrosine diagonal resonance from 2D DARR NMR spectra of rhodopsin (black) and Meta I (orange). In rhodopsin, at least four (of five possible) ^{13}Cζ Tyr - ^{13}Cα Gly cross-peaks are detected. The cross-peaks at 42.0 ppm and 45.5 ppm are assigned to contacts between Tyr268$^{6.48}$ and Gly188^{EL2}, and between Tyr178^{EL2} and Gly114$^{3.29}$, respectively (*172*). In Meta I, these contacts are observed. The most substantial change between rhodopsin and Meta I is broadening of the Tyr178^{EL2} -Gly114$^{3.29}$ cross-peak. In Meta II (Figure 4.6B, red), the Gly188^{EL2}-Tyr191^{EL2} cross-peaks are absent. The loss of this cross peaks is attributed to a reorganization of the EL2 hydrogen bonding network upon activation, respectively (*172*).

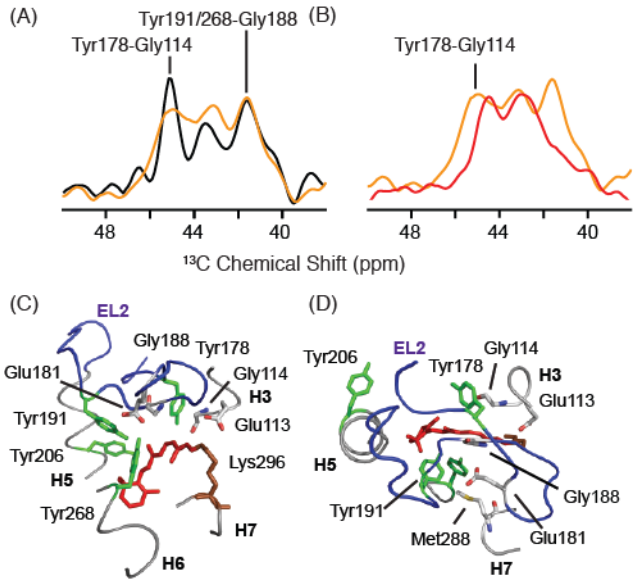

Fig. 4.6. Two-dimensional DARR NMR spectra of ^{13}Cζ-tyrosine, ^{13}Cα-glycine-labeled rhodopsin. *Slices through the diagonal resonances of ^{13}Cζ-tyrosine showing through space ^{13}C...^{13}C contacts with ^{13}Cα-glycine are shown for rhodopsin (black) and Meta I (orange) in panel (A) and for Meta I (orange) and Meta II (red) in panel (B). Cross peaks between ^{13}Cζ-tyrosine and ^{13}Cα-glycine provide a way to monitor changes on the extracellular side of the rhodopsin. In the rhodopsin crystal structure (1U19), there are six ^{13}Cζ-tyrosine - ^{13}Cα-glycine contacts located in the extracellular region of rhodopsin involving 5 tyrosines and 5 glycines: Tyr10^{NT}-Gly3^{NT}, 3.9 Å; Tyr10^{NT} -Gly280^{EL3}, 4.4 Å; Tyr29^{NT} -Gly101^{EL1}, 4.0 Å; Tyr178^{EL2} -Gly114$^{3.29}$, 4.5 Å; Tyr191^{EL2} -Gly188^{EL2}, 5.2 Å; Tyr268$^{6.51}$ -Gly188 ^{EL2}, 5.3 Å. The slices shown in (A) reveal that the Tyr-Gly contacts are similar between rhodopsin and Meta I. However, the same comparison between Meta I and Meta II in (B) shows that the Tyr178 ^{EL2} -Gly114$^{3.29}$ contact is lost in Meta II. (C, D) Structure of the extracellular side of rhodopsin (PDB access code = 1GZM) viewed from the side (C) and from the extracellular surface. The structure highlights the position of EL2 over the retinal binding site and the positions of several of the amino acids discussed. The NMR data is this figure was collected by Shivani Ahuja.*

In rhodopsin, EL2 folds into two β-strands (β3 and β4) that form a plug over the retinal-binding site and prevent access of hydroxylamine to the protonated Schiff base linkage. Both β-strands are constrained in the dark state by a conserved disulfide bond between Cys110$^{3.25}$ (H3) and Cys187^{EL2} (β4) and a network of hydrogen bonding interactions. NMR chemical shift measurements of Meta II indicate a rearrangement of hydrogen bonding interactions between EL2 and amino acids on transmembrane helices H5 and H6 (*172*). These changes in EL2, relative to rhodopsin, have suggested that EL2 adopts an active conformation that is coupled to the motion of transmembrane helices H5, H6 and H7 (*172*).

Several observations in the current study suggest that EL2 has not adopted an active conformation in Meta I. First, the characteristic Meta II chemical shifts of Cys187^{EL2}, Gly188^{EL2}

and Tyr191^{EL2} on the β4 strand of EL2 are not observed in Meta I. Second, a contact between Gly188^{EL2} on EL2 and Tyr268$^{6.48}$ at the extracellular end of H6, which is present in rhodopsin, is still observed in Meta I, but absent in Meta II (*172*). Third, the Met288$^{7.35}$-Tyr268$^{6.48}$ and Met288$^{7.35}$-Tyr191^{EL2} cross-peaks have similar intensities in rhodopsin and Meta I indicating that EL2 has not markedly changed its position relative to the extracellular ends of H6 and H7. The only indication of substantial change in the vicinity of EL2 is the chemical shift change of Met288, which may reflect changes in the position of H6 and H7 (see below) rather than changes in the position of EL2.

The NMR measurements indicating that EL2 has not changed conformation are consistent with recent studies on the accessibility of the retinal Schiff base to hydroxylamine (*256*). In Meta II, hydroxylamine is able to hydrolyze the Schiff base linkage between the retinal chromophore and the side chain of Lys296$^{7.43}$. However, in both rhodopsin and Meta I, the protonated Schiff base is not accessible to hydroxylamine (*256*). (This conclusion disagrees with an earlier study (*257*), where hydroxylamine was shown to react at 275 K with a metarhodopsin intermediate, presumably Meta I, in a pH independent fashion. Later experiments on Meta I trapped at 240 K were not able to confirm this result (*256*), which opened up the possibility that in the earlier experiments the reactive metarhodopsin intermediate was Meta III. Meta III is known to react with hydroxylamine (*57*)). As a result, the increased accessibility of the Schiff base to hydroxylamine in Meta II is likely due to change in the packing interactions of EL2 with the retinal. In this regard, Meta I with EL2 tightly packed against the retinal may serve as a model for Class A GPCRs where the main function of EL2 seems to be as an agonist diffusion barrier as in the angiotensin II type 1 receptor (*258*)

Although EL2 does not appear to have reached the structure adopted in Meta II, there are marked changes in the NMR linewidths associated with the retinal chromophore. In rhodopsin and Meta II, narrow, distinct NMR resonances are observed, implying that there are well-defined conformations associated with the active and inactive states of rhodopsin. In contrast, we observe substantial broadening of the ^{15}N and ^{13}C resonances of the Schiff base and retinal in Meta I. The broadening of the ^{13}C resonances was previously interpreted in terms of heterogeneity in the conformation of the polyene chain of the retinal chromophore (*250*). Alternatively, broadening of the ^{15}Nζ-Lys296$^{7.43}$ and ^{13}C-retinal resonances may reflect the loss a single well-defined

hydrogen bonding contact with Glu113$^{3.28}$ and water in the binding pocket. As such, the broadening may be associated with the formation of a complex counterion involving Glu113$^{3.28}$, Glu181^{EL2} and structural water molecules (*63*).

The concept of a complex counterion has previously been discussed. Yan *et al.* (*63*) proposed that there is a switch in the Schiff base counterion from Glu113$^{3.28}$ to Glu181^{EL2} in the formation of Meta I. In the dark state of rhodopsin, Glu113$^{3.28}$ is part of a hydrogen bonding network stretching to Glu181^{EL2} via the backbone carbonyl of Cys187^{EL2} and a structural water molecule (*259*). Yan *et al.* (*63*) observed a dramatic shift in the pKa of the protonated Schiff base upon mutation of Glu181^{EL2} in EL2 and have suggested that Glu181^{EL2} is the predominant counterion in the Meta I state. Lüdeke *et al.* (*260*). have found that Glu181^{EL2} is unprotonated in both rhodopsin and Meta I, and have argued that together Glu113$^{3.28}$ and Glu181^{EL2} form a complex counterion.

4.3. Structural changes in H6 in Meta I.

The difference spectra of ^{13}Cζ-tyrosine and ^{13}Cε-methionine in Figures 4.5A and B also provide insights into the structural changes occurring in the transmembrane helices H5 and H6. Tyr206$^{5.41}$ on H5 does not adopt its active state conformation in Meta I (Figure 4.5A). This tyrosine is part of a hydrogen bonding network with His211$^{5.46}$ (H5), Glu122$^{3.37}$ (H3), Trp126$^{3.41}$ (H3) and Ala166$^{4.55}$ (H4). The conversion to Meta II is associated with a rearrangement of this network such that the side chain of His211 hydrogen bonds directly with the side chain of Glu122$^{3.37}$ (*99, 108*). This rearrangement appears to be driven by direct contact of the retinal β-ionone ring with H5 (*171, 172*). ^{13}C dipolar couplings reveal close contacts between Met207$^{5.42}$ and the retinal C6 and C7 carbons upon conversion to Meta II (*171, 172*).

The rhodopsin - Meta I difference spectrum of ^{13}Cε-methionine (Figure 4.5B) reveals a large negative resonance at 15.8 ppm. This frequency is close to that of Met257$^{6.40}$ in Meta II (*96*). The tentative assignment of the 15.8 ppm resonance in Meta I to ^{13}Cε-Met257$^{6.40}$ raises the possibility that H6 has rotated in Meta I to place the Met257$^{6.40}$ side chain in an environment similar to that in Meta II.

Figure 4.7A presents difference spectra between rhodopsin and Meta I (orange) and between rhodopsin and Meta II (black) for rhodopsin containing ^{13}Cζ-labeled arginine. As above, the

positive peaks correspond to rhodopsin and negative peaks correspond to Meta I or Meta II. The rhodopsin - Meta II difference spectrum in the region of the ^{13}Cζ arginine chemical shift does not reveal any substantial changes indicating the chemical shift of Arg135$^{3.50}$ is similar in rhodopsin and Meta II.

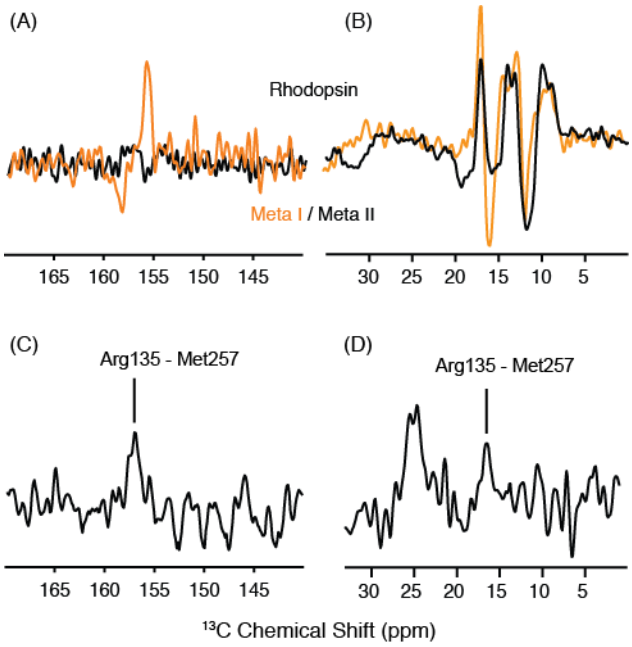

Fig. 4.7. ^{13}Cζ-arginine and ^{13}Cε-methionine changes in the transition to Meta I. *(A) Rhodopsin - Meta I (orange) and rhodopsin - Meta II (black) difference spectra are shown in the region of ^{13}Cζ -arginine. The ^{13}Cζ -arginine chemical shifts do not appear to differ between rhodopsin and Meta II, as indicated by the flat baseline in the corresponding region of the difference spectrum. In contrast, the rhodopsin - Meta I difference spectrum reveals a single ^{13}Cζ -arginine has changed in the transition to Meta I. (B) Rhodopsin - Meta I (orange) and rhodopsin - Meta II (black) difference spectra are shown in the region of ^{13}Cε-methionine. A strong negative peak at 15.7 ppm corresponds to a new ^{13}Cε-methionine resonance in Meta I. (C,D) Slices extracted from a 2D DARR NMR spectrum reveal a cross peak between ^{13}Cζ -Arg135$^{3.50}$ and ^{13}Cε-Met257$^{6.40}$ in Meta I.*

In contrast to the absence of changes in the rhodopsin - Meta II difference spectrum, the rhodopsin - Meta I difference spectrum reveals a change in chemical shift of a single arginine ^{13}Cζ resonance from 155.7 ppm in rhodopsin to 157.3 ppm in Meta I. To confirm that this arginine is Arg135$^{3.50}$, we obtained 2D DARR NMR spectra of rhodopsin labeled with both ^{13}Cζ-arginine and ^{13}Cε-methionine. Figures 7C and 7D present slices from the 2D DARR NMR spectrum of Meta I extracted at the diagonal resonances of ^{13}Cε-methionine and ^{13}Cζ-arginine, respectively. Figure 4.7C reveals a ^{13}Cζ-Arg135$^{3.50}$ - ^{13}Cε-Met257$^{6.40}$ cross-peak at 156.9 ppm in the slice taken through the ^{13}Cε-methionine diagonal resonance, while Figure 4.7D reveals a

^{13}Cε-methionine - ^{13}Cζ-arginine cross-peak at 16.2 ppm in the slice taken through the ^{13}Cζ-arginine diagonal resonance. The intensities of the ^{13}Cε-methionine - ^{13}Cζ-arginine cross-peaks in Meta I relative to the diagonal resonances are roughly the same intensity as in Meta II (*96*), where the internuclear distance is 4.5 - 5 Å. We attribute the appearance of a ^{13}Cζ-Arg135$^{3.50}$ - ^{13}Cε-Met257$^{6.40}$ cross-peak to rotation of H6.

In both active opsin and Meta II, the rotation of H6 that places Met257$^{6.40}$ in contact with Arg135$^{3.50}$ is accompanied by the rotation of H5 and H7 (*96*). This rotation has implications for two salt bridges formed by Arg135$^{3.50}$ in the dark state of rhodopsin. The first salt bridge between Arg135$^{3.50}$ and Glu247$^{6.30}$, often referred to as the ionic lock, must be broken upon rotation of H6. The second salt bridge between Arg135$^{3.50}$ and Glu134$^{3.49}$ is disrupted with the rotation of Tyr223$^{5.58}$ on H5 and Tyr306$^{7.53}$ on H7. Tyr223$^{5.58}$ and Tyr306$^{7.53}$ form hydrogen bonds with the arginine guanidinium side chain to stabilize Arg135$^{3.50}$ in a protonated state (*96*).

To test whether there are parallel changes in Meta I, 2D DARR NMR spectra were obtained of rhodopsin, Meta I and Meta II using rhodopsin labeled with ^{13}Cε-methionine and ^{13}Cζ-tyrosine. Figure 4.8 presents slices through the ^{13}Cε-methionine diagonal resonance corresponding to Met288$^{7.35}$ in the ^{13}Cζ-tyrosine region of rhodopsin (Figure 4.8A; black) at 17.2 ppm and Meta I (Figure 4.8A,B; orange) at 12.8 ppm. In Figure 4.8A, we observe two cross-peaks that we assign to the two tyrosines closest to Met288$^{7.35}$ (i.e. Tyr268$^{6.48}$ at 3.9 Å and Tyr191^{EL2} at 5.2 Å) (*96*). Upon conversion to Meta I, these cross-peaks do not change position or intensity. However, in Meta II the Met288$^{7.35}$ - Tyr191^{EL2} and Met288$^{7.35}$-Tyr268$^{6.48}$ cross-peaks shift downfield, and two overlapping cross-peaks assigned to Met257$^{6.40}$ - Tyr223$^{5.58}$ and Met257$^{6.40}$ - Tyr306$^{7.53}$ appear at 155.7 ppm (*96*)

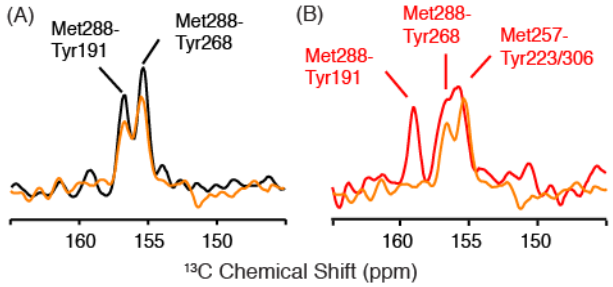

Fig. 4.8. Two-dimensional 2D DARR NMR spectra of ^{13}Cζ tyrosine, ^{13}Cε methionine-labeled rhodopsin. *(A) Slices through the ^{13}Cζ tyrosine diagonal resonance from 2D DARR NMR spectra of*

rhodopsin (black) and Meta I (orange) labeled with $^{13}C\zeta$-tyrosine and $^{13}C\varepsilon$-methionine highlight the region of Tyr-Met cross-peaks. In rhodopsin, we observe cross-peaks between Met288$^{7.35}$ -Tyr191^{EL2} and Met288$^{7.35}$ -Tyr268$^{6.51}$. Upon conversion to Meta I, the intensity of the cross-peaks does not change appreciably. (B) Slices through the $^{13}C\zeta$-tyrosine diagonal resonance from 2D DARR NMR spectra of Meta I (orange) and Meta II (red) are shown using the same labeling strategy as in (A). The NMR data in this figure was collected by Shivani Ahuja.

A hallmark of rhodopsin activation is the outward displacement of helix H6 from the helical bundle (*43, 46, 47*). Cross-linking of the intracellular ends of H3 and H6 blocks this motion and prevents receptor activation (*43, 106*). Hubbell and coworkers have demonstrated that the outward motion of H6 occurs following the internal proton transfer from the retinal protonated Schiff base to Glu113$^{3.28}$ (*46*).

In the cryo-EM structure of Meta I, Schertler and coworkers found that there was increased electron density on the side of H6 facing the β-ionone ring at the level of Trp265$^{6.48}$ (*117*). However, there was no change observed in the position of the intracellular end of H6, as seen in opsin, indicating that H6 does not tilt outward in Meta I. One way to reconcile the cryo-EM structure of Meta I showing a displacement of Trp265$^{6.48}$ with the NMR results showing a contact between Met257$^{6.40}$ and Arg135$^{3.50}$ is to propose that H6 rotates in Meta I without an outward displacement.

The displacement of the Trp265$^{6.48}$ side chain may also be reflected in recent deuterium NMR studies of Brown and coworkers (*261*). In rhodopsin, the Trp265$^{6.48}$ side chain is packed against the C18 and C20 methyl groups. These methyl groups exhibit a much more restricted rotational motion than the C19 methyl group in the 6-*s*-*trans*, 12-*s*-*trans*, 11-*cis* retinal chromophore in rhodopsin because of steric clashes within the retinal molecule (i.e. the C18 methyl group clashes with the C8H proton in a twisted 6-*s*-*cis* geometry and the C20 methyl group clashes with the C10H proton in a twisted 12-*s*-*trans* geometry). However, differences in the activation energy (E_a) for rotational motion of these methyl groups between rhodopsin and Meta I and between Meta I and Meta II may have contributions from steric clashes with the protein (*261*). The E_a of the C19 methyl group increases in the transition from rhodopsin to Meta I and from Meta I to Meta II, and is in fact greater than the E_a for C20 methyl group in Meta II. These observations are consistent with $^{13}C...^{13}C$ distance measurements showing that the Trp265$^{6.48}$ side chain moves from a position in contact with the C20 methyl group to a position in contact with the C19 methyl group upon receptor activation (*173, 262*)

The proposed rotation of H6 in Meta I is in agreement with recent azido labeling studies on rhodopsin where *p*-azido-L-phenylalanine is incorporated into positions at the intracellular end of H6 (*228*). These studies show that there are large changes in the vibrational frequencies of the azido label at position $250^{6.33}$ between lumirhodopsin and Meta I. However, no further changes in the azido vibrations are observed in the formation of Meta II suggesting that structural changes in this region of the receptor are complete in Meta I. These results on azido-labeled rhodopsin were interpreted in terms of a rotation of H6 to break the $Arg135^{3.50}$-$Glu247^{6.30}$ salt bridge in Meta I.

Figure 4.9 shows the residues in the interface between H3 and H6. The distance between the labeled ^{13}Cε-$Met257^{6.40}$ - ^{13}Cζ-$Arg135^{3.50}$ carbons is ~11 Å in dark rhodopsin (dashed line in Figure 4.10A). The conversion to Meta I brings the labeled ^{13}C sites to within ~6 Å. Rotation of H6 alone does not reduce the distance between these sites, arguing that the side chains of both $Arg135^{3.50}$ and $Met257^{6.40}$ reorient in Meta I. MD simulations guided by NMR restraints suggest that the side chain of $Met257^{6.40}$ ratchets past $Leu128^{3.43}$ (Figure 4.10B). The rotation of H6 changes the packing interactions in the H3 and H6 interface in several ways that facilitate side chain motion. The proposed rotation of H6 moves $Val254^{6.37}$ away from $Arg135^{3.50}$, which otherwise blocks the motion of the arginine side chain toward $Met257^{6.40}$, and also moves $Met257^{6.40}$ toward $Ala132^{3.47}$. In the previous section (Chapter 3.1) we described that $Ala132^{3.47}$ is a group conserved residue in class A GPCRs. In Meta II, Ala132 serves as a molecular notch for Tyr223. The small side chain of $Ala132^{3.47}$ also provides space for bending of the $Met257^{6.40}$ side chain toward $Arg135^{3.50}$ in the transition to Meta I. As a result the H3-H6 ionic lock between $Arg135^{3.50}$ and $Glu247^{6.30}$ is broken while the $Lys231^{5.66}$ and $Glu247^{6.30}$ interaction seen in the active form of opsin is not formed in Meta I despite a movement of these residues towards each other. The loss of the $Glu247^{6.30}$ salt bridge in Meta I can explain the observed increased hydration specific for this intermediate (*263*)

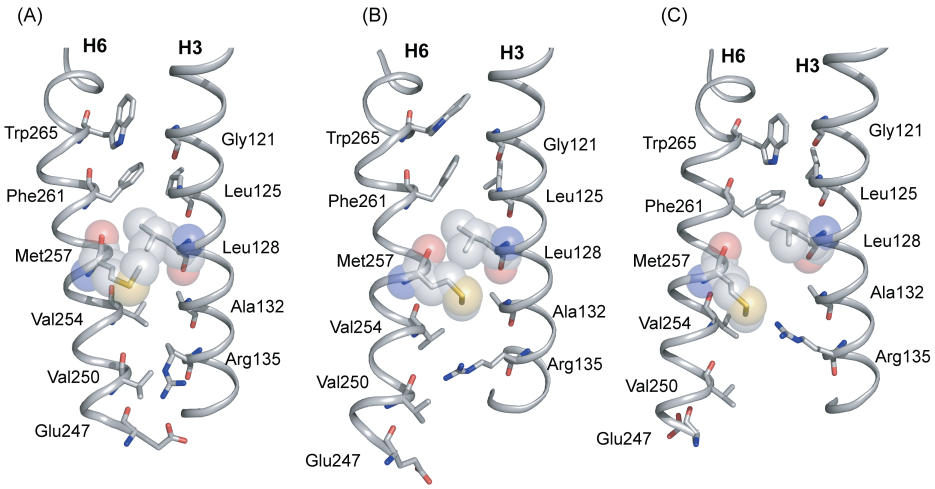

Fig. 4.9. Structural changes in H3 and H6 upon rhodopsin activation. *Packing interactions are shown between H3 and H6 in the crystal structure of rhodopsin (PDB access code = 1GZM) (A), Meta I (B) and in the crystal structure of Meta II (PDB access code = 3PXO) (C). The Meta I structure is based on MD simulations guided by NMR constraints. NMR measurements between Arg135$^{3.50}$ and Met257$^{6.40}$, in combination with azido labeling studies (228) and EPR (43) measurements of Meta I and Meta II, are consistent with rotation of H6. Trp265$^{6.48}$ in the conserved CWxP motif on H6 is locked in place in dark rhodopsin by the 11-cis retinal chromophore. Retinal isomerization releases the packing constraints on the Trp265$^{6.48}$ indole ring. Gly121$^{3.36}$ on H3 is strictly conserved in the visual receptors (126). The small side chain facilitates packing of the Trp265$^{6.48}$ side chain in dark rhodopsin, but does not hinder H6 rotation. Leu128$^{3.43}$ and Met257$^{6.40}$ are closely packed in dark rhodopsin. Leu128$^{3.43}$ is highly conserved (78%) in GPCRs and is part of a tightly packed transmembrane core (126). The rotation of H6 is facilitated by the small side chain at position 132$^{3.48}$. This position is highly conserved in the GPCRs as either an alanine (36%) or a serine (50%) (96). The Arg135$^{3.50}$ side chain interacts with Glu247$^{6.30}$ in the dark and is prevented from moving toward the Met257$^{6.40}$ by Val254$^{6.37}$. Val254$^{6.37}$ is conserved (63%) as a β-branched amino acid across the Class A GPCRs. Rotation of H6 breaks the Arg135$^{3.50}$- Glu247$^{6.30}$ interaction and removes the steric interaction with Val254$^{6.37}$. The side chain of Glu247$^{6.30}$ is in an intermediate position between Arg135$^{3.50}$ and Lys231$^{5.66}$. These figures were generated from a MD simulation that was conducted by Colleen Kirkup from the laboratory of Carlos Simmerling.*

4.4. Structural changes on H5 in Meta I.

We interpret the results in Figures 4.7 and 4.8 in terms of rotation of H6 in Meta I without the corresponding rotation of Tyr223$^{5.58}$ on H5 and Tyr306$^{7.53}$ on H7. This interpretation is consistent with several observations. First, while we observe an Arg135$^{3.50}$ - Met257$^{6.40}$ cross-peak in both Meta I and Meta II, we only observe the Met257$^{6.40}$ - Tyr223$^{5.58}$ and Met257$^{6.40}$ - Tyr306$^{7.53}$ cross-peaks in Meta II. Second, the rhodopsin - Meta I difference spectrum for ^{13}Cε-methionine of wild-type rhodopsin in Figure 4.7A is remarkably similar to the rhodopsin - Meta II difference spectrum for ^{13}Cε-methionine of the Y223F mutant (*96*). Additionally, in the Y223F mutant, there is a rapid decay of the Meta II state to opsin and an upfield shift of the ^{13}Cβ resonance of Cys187^{EL2} close to its position in rhodopsin. The rapid Meta II decay observed in

the Y223F mutant suggests that in wild-type Meta II the Tyr223$^{5.58}$ - Arg135$^{3.50}$ interaction is holding H5 in an active orientation, whereas in Meta II of the Y223F mutant, H5 has rotated back to an inactive orientation and this change is coupled to motion of EL2. FTIR measurements of the Y223F mutant show a shift in the pH-dependent equilibrium between Meta I and Meta II back toward Meta I (*96*).

Although we do not observe rotation of Tyr223$^{5.58}$ on H5 in Meta I, ^{13}C difference and DARR NMR spectra of Meta I and Meta II labeled with ^{13}Cβ-cysteine show there is a change in the H4-H5 interface. In the 1D ^{13}C difference spectra of ^{13}Cβ-cysteine-labeled rhodopsin, the Cβ carbons exhibit considerable changes in both Meta I and in Meta II (Figure 4.10A). We can assign the positive peaks at 23.2 ppm and 25.8 ppm to Cys167$^{4.56}$ and Cys264$^{6.47}$, respectively. These assignments were made based on the interhelical cross peaks to His211$^{5.46}$ and Tyr301$^{7.48}$ respectively (*172*). In Meta II, these resonances shift to 24.4 ppm and 26.2 ppm, respectively.

Met207$^{5.42}$ can serve as a probe for the motion of H5. In the formation of Meta II, a strong cross peak is observed between ^{13}Cε-Met207$^{5.42}$ on H5 and ^{13}Cβ-Cys167$^{4.56}$ on H4 (Figure 4.10B) (*171*). The side chain of Met207$^{5.42}$ rotates from its original position towards H4 to give space for the β-ionone ring of the retinal to pack against H5 in Meta II. In contrast, only a weak cross-peak is observed between Met207$^{5.42}$ and Cys167$^{4.56}$ in Meta I (Figure 4.10B). These data show that although the ligand-binding pocket in the region of H5 has responded to retinal isomerization, the motion is not as large as that observed in Meta II.

\

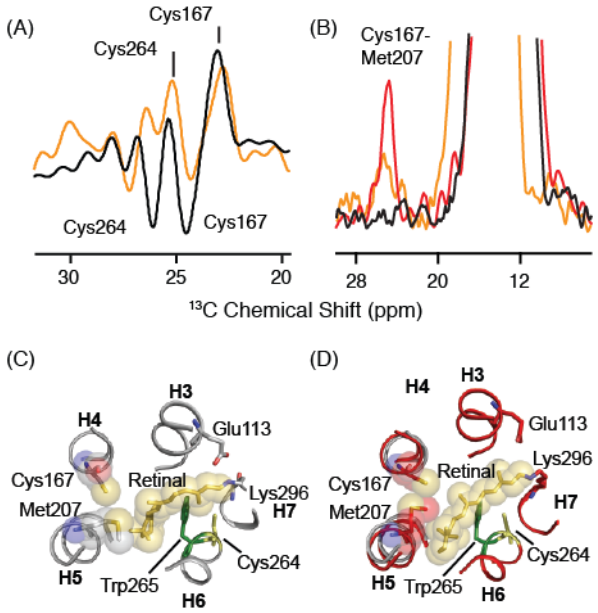

Fig. 4.10. Chemical shift changes in ^{13}Cβ-cysteine in the transition from rhodopsin to Meta I. *(A) Rhodopsin - Meta I (orange) and rhodopsin - Meta II (black) difference spectra in the region of reduced ^{13}Cβ-cysteine resonances. (B) Slices taken through 2D ^{13}C DARR NMR spectra of rhodopsin (black), Meta I (orange) and Meta II (red) exhibit a cross peak between Met207$^{5.42}$ and Cys167$^{4.56}$. (C) Structure of rhodopsin (PDB access code = 1GZM) in the region of the retinal binding site. The structure highlights the positions of Cys167$^{4.56}$ and Met207$^{5.42}$. (D) Structure of Meta II (PDB access code = 3PXO) showing displacement of H5 and closer interaction of Cys167$^{4.56}$ and Met207$^{5.42}$. The NMR data is this figure was collected by Shivani Ahuja.*

One of the triggers for activation of rhodopsin is the steric interaction between the β-ionone ring of the retinal and transmembrane helix H5 in the region of Met207$^{5.42}$ and Phe212$^{5.47}$. Contact of the β-ionone ring with H5 leads to rearrangement of hydrogen bonds between H3 and H5 on both the extracellular and intracellular sides of the receptor. On the extracellular end of H5, Tyr206$^{5.41}$ and His211$^{5.46}$ form hydrogen bonds with Trp126$^{3.41}$ and Glu122$^{3.37}$ on H3 in the dark state of rhodopsin. These hydrogen bonds are disrupted upon activation. On the intracellular end of H5, Tyr223$^{5.58}$ is oriented toward the surrounding lipid membrane in the dark state of rhodopsin, but rotates upon activation into the helical bundle to form a hydrogen bond with Arg135$^{3.50}$ of the conserved ERY sequence. The question is whether these changes occur in concert with rotation of H6 in Meta I or with the outward displacement of H6 in Meta II.

Ye *et al.* (*228*) observed only small changes in the azido vibrations between rhodopsin and Meta I when the azido label was incorporated at position 227$^{5.62}$ on H5, whereas much larger changes were observed upon formation of Meta II. These results differ from those using the azido probes on H6 (discussed above) and were interpreted in terms of a small movement of H5

in response to rotation of H6. In agreement with these studies, we observe a small increase in intensity of the Cys167$^{4.56}$-Met207$^{5.42}$ cross-peak in the formation of Meta I, but a much larger increase in the formation of Meta II (Figure 4.10B). We interpret the change of the Cys167$^{4.56}$ - Met207$^{5.42}$ contact in terms of displacement of H5 relative to H4 and rearrangement of the position of the Met207$^{5.42}$ side chain (Figures 9C and D), but conclude that the H5 helix has not completely shifted into its active state orientation.

Support for the conclusion that H5 has not adopted an active conformation in Meta I comes from both NMR and FTIR spectroscopy. The NMR chemical shift of Tyr206$^{5.41}$ provides a probe of the hydrogen bonding network centered on His211$^{5.46}$, where a distinctive upfield chemical shift of Tyr206$^{5.41}$ is observed in the rhodopsin - Meta II difference spectrum. We do not observe this chemical shift change for Tyr206 in the rhodopsin - Meta I difference spectrum (Figure 4.5A). In addition, we do not observe the contact between Tyr223$^{5.58}$ and Met257$^{6.40}$ in Meta I that is associated with the rotation of Tyr223$^{5.58}$ toward Arg135$^{3.50}$ observed in Meta II (see Figure 4.1C). In the ^{2}H NMR studies cited above (*261*), the E_a for rotation of the C18 methyl group increases in Meta I and then decreases in Meta II. These changes were interpreted in terms of a steric clash of the β-ionone ring with H5 in Meta I, and then displacement of H5 (to lessen the steric clash with the β-ionone ring) in Meta II.

In FTIR studies on Meta I and Meta II, the vibrational frequency at 1734 cm^{-1} associated with the Glu122$^{3.37}$ carboxyl group has provided an excellent probe of the hydrogen bonding interactions between H3 and H5. Siebert and coworkers found that the 1734 cm^{-1} vibration shifts to 1701 cm^{-1} in the transition from rhodopsin to Meta I indicating that Glu122$^{3.37}$ becomes more strongly hydrogen bonded (*53, 245*). However, in the transition to Meta II, the Glu122$^{3.37}$ vibration shifts to 1745 cm^{-1}, a signature of weaker hydrogen bonding. These results agree with both the NMR and azido-labeling studies described above showing that the position or orientation of H5 changes between rhodopsin and Meta I, and then undergoes further changes between Meta I and Meta II.

4.5. Sequence of events in the formation of the active Meta II State.

In this study, solid-state ^{13}C and ^{15}N NMR measurements of the Meta I intermediate are used to address the structural changes that precede receptor activation in rhodopsin. We find that the

largest conformational change in Meta I is rotation of transmembrane helix H6. The chemical shift changes associated with EL2 and the rotations of Tyr223$^{5.58}$ on H5 and Tyr306$^{7.53}$ on H7, which are observed in Meta II, have not occurred in Meta I. We discuss these observations in connection with the sequence of events that occur in the transition from rhodopsin to Meta I and from Meta I to the active Meta II conformation.

One of the challenges for understanding how light activates the visual receptor rhodopsin has been to delineate the chain of molecular events leading to the fully active Meta II conformation. The pioneering work of Hubbell and coworkers revealed that the defining motion is the outward tilting of H6 (*43*). However, the crystal structures of dark rhodopsin and its early photointermediates have provided few clues as to the sequence of the events that drive this motion. The crystal structures of Bathorhodopsin (*264*), Lumirhodopsin (*255*) and Meta I (*117*) showed only subtle changes from the structure of the dark state of rhodopsin. The picture that has emerged over the past decade is that the structural changes in the receptor leading up to Meta II only involve slight rearrangements of the side chains in the binding site to accommodate the all-*trans* chromophore. In contrast, the more recent structures of active opsin (*95, 107*) and Meta II (*94, 108*) capture substantial structural changes on the intracellular side of the receptor.

The two hallmarks of Meta II formation are the proton transfer from the protonated Schiff base to Glu113$^{3.28}$ and the outward motion of H6. Both steps are set up in Meta I. The observed Schiff base ^{15}N chemical shift in Meta I, along with vibrational spectroscopy studies (*63, 243, 260*), favor a slightly stronger protonated Schiff base – counterion interaction. The interaction may involve both Glu113$^{3.28}$ and Glu181^{EL2} as part of a complex counterion. As a consequence of a rearrangement in the electrostatic interactions near the protonated Schiff base, Glu113$^{3.28}$ may move into a more hydrophobic environment in Meta I and become the driving force for Schiff base deprotonation. Deprotonation of the Schiff base is the first of two protonation switches that must be triggered for rhodopsin activation (*60*).

The NMR evidence for rotation of H6 in the Meta I intermediate supports the conclusions drawn from previous azido labeling measurements (*228, 265*). Both studies suggest that H6 rotation disrupts the intracellular salt bridge between Arg135$^{3.50}$ and Glu247$^{6.30}$. In contrast, the electrostatic interaction between Arg135$^{3.50}$ and Glu134$^{3.49}$, both highly conserved residues, remains intact in Meta I and is arguably more important for stabilizing the inactive state of the

receptor. Protonation of Glu134$^{3.49}$ in Meta II has been described as the second protonation step required for rhodopsin activation (*60*). The NMR studies presented above indicate that the inward rotation of Tyr223$^{5.58}$ on H5 and Tyr306$^{7.53}$ on H7 have not occurred in Meta I and consequently must be associated with the outward motion of H6 upon activation.

Finally, the observed structural transitions in the formation of Meta I provide insights into the conservation of residues in the ligand-activated GPCRs and common elements of receptor activation. The ionic lock between Arg135$^{3.50}$ and Glu247$^{6.30}$ is not highly conserved. Even in those receptor subfamilies where these complementary charged residues are conserved, crystal structures often do not reveal a direct interaction (*199, 200, 219, 266*). For example, Schertler and coworkers have recently reported crystal structures of two inactive forms of the β1AR, one with an ionic lock between Arg$^{3.50}$-Glu$^{6.30}$ and the other without (*267*). The two forms were found with several inverse agonists bound. The lack of a stabilizing electrostatic interaction between H3 and H6 in the diffusible ligand-activated receptors may be associated with their levels of basal activity relative to the dark state of rhodopsin. In contrast, Arg135$^{3.50}$ and Glu134$^{3.49}$ are part of the highly conserved D/ERY sequence on H3, and their interaction appears to have a much more dramatic effect in modulating receptor activity. The observation of a direct interaction in Meta I between Arg135$^{3.50}$ and Met257$^{6.40}$, a non-conserved, but highly important residue in the visual receptors, suggests that in the ligand-activated receptors there are subfamily specific interactions that regulate receptor activation.

The work presented here describes solid-state NMR studies on the Metarhodopsin I intermediate in the photoreaction of the visual receptor rhodopsin. Metarhodopsin I is the intermediate immediately preceding Metarhodopsin II, the active state of the receptor. By comparing our current results with previous NMR measurements on Metarhodopsin II, we are able to define the structural changes that result in receptor activation. The major conclusion of the chapter is that transmembrane helix H6 has rotated in the formation of Meta I to break the intracellular ionic lock between Arg135$^{3.50}$ and Glu247$^{6.30}$. This motion, along with several additional smaller changes in structure, appears to prime the receptor for the transition to an active conformation.

CHAPTER 5: MECHANISM OF RHODOPSIN ACTIVATION: OPEN QUESTIONS AND PERSPECTIVES.

Rhodopsin activity is modulated exclusively by a change in the isomeric state of retinal rather than by binding of a ligand. In addition, the potency of 11-*cis* retinal as an inverse agonist is high, resulting in a dormant receptor conformation that is essentially devoid of basal activity. In contrast, the all-*trans* isomer of retinal acts as a full agonist. As such, rhodopsin activation represents a binary – its either full on or fully off – which is unique among class A GPCRs. Delineating the structural changes that are associated with rhodopsin activation is essential to understanding the mechanism by which class A GPCRs are activated. Despite the breadth of biophysical and biochemical data that has been collected on rhodopsin, there are a number of outstanding questions that prohibit a detailed understanding of receptor activation. Below are four of key questions.

What is the role of Schiff base deprotonation? The retinal is covalently bound to the side chain of Lys296$^{7.43}$ through a Schiff base linkage. In the dark, the carboxylate side chain of Glu113$^{3.28}$ stabilizes the Schiff base in its protonated state (*81*). In the transition from Meta I to Meta II, the retinal Schiff base is deprotonated via an internal proton transfer to Glu113$^{3.28}$. This protonation switch is essential for receptor function (*268*). The requirement for Schiff base deprotonation is not well understood, but there are several implications for neutralizing the Glu113$^{3.28}$ - Lys296$^{7.43}$ linkage. Specifically, H3 is free to rotate and cause structural changes at the cytosolic surface that may be associated with repositioning Arg135$^{3.50}$ in Meta II. Similarly, Schiff base deprotonation may allow the rotation of H7 with a concomitant change in the side chain orientation of Tyr306$^{7.53}$, which participates in a hydrogen bonding network with Tyr223$^{5.58}$ and Arg135$^{3.50}$ to stabilize Meta II.

Is Trp265$^{6.48}$ a part of a rotamer toggle switch? Trp265$^{6.48}$ is part of a conserved aromatic cluster on transmembrane helix H6. In the dark, the β-ionone ring of 11-*cis* retinal is packed against the side chain of Trp265$^{6.48}$. A conservative mutation, W265F, shows a marked reduction in rate of pigment formation and an increased rate of retinal hydrolysis. Computational studies based on site-directed mutagenesis have also suggested that, in the β_2AR, the analogous tryptophan undergoes a rotation about its χ_1 torsion angle upon receptor activation (*111*). Moreover, UV/vis studies of rhodopsin and site directed mutants show that

Trp265$^{6.48}$ undergoes a change in absorbance upon rhodopsin activation (*52*). However, crystal structures of agonist-bound GPCRs do not show a change in the side chain orientation of Trp265$^{6.48}$ with respect to its position in the inactive state. As a result, the issue of the rotamer toggle switch remains to be addressed.

Does retinal isomerization induce motion of EL2? In the dark, the β4-strand of EL2 is buried within the transmembrane core and packs against the retinal chromophore in its 11-*cis* conformation. Previously collected solid-state NMR measurements were interpreted in terms of a motion of EL2 away from the retinal upon rhodopsin activation (*172*). EL2 motion is consistent with an increased solvent accessibility of the retinal Schiff based in Meta II (*269*). However, the crystal structures of reversibly formed and constitutively active Meta II intermediates do not show a displacement of EL2 with respect to its position in the dark state. As such, the role of EL2 in rhodopsin activation remains an open question.

Does Pro267$^{6.50}$ serve as a flexible hinge for the motion of H6? Pro267$^{6.50}$ is part of a conserved CWxP motif on H6 and forms a 30° kink in the local secondary structure of H6. Computational studies have suggested that the conserved proline on H6 also serves as a flexible hinge for the helix motion upon activation in the β_2AR (*110, 270*) to allow G protein binding. However, crystal structures that capture GPCRs in their active conformations reveal a H6 kink that is similar to what is seen in the inactive conformation. A question that remains to be addressed is whether or not H6 motion occurs about Pro267$^{6.50}$.

The following subsections describe data that has been collected to address a number of the questions listed above. The data are put in the context of the existing literature and future directions are proposed.

5.1 Determining the location of the retinal chromophore in Meta II.

NMR measurements on the conformation of the 11-*cis* and all-*trans* isomers in dark rhodopsin and Meta II, respectively, have provided structural insights into how retinal functions as a light-activated ligand. Light induces a rapid and selective isomerization of the C11=C12 double bond. Deuterium NMR measurements on the retinal chromophore have shown that, in rhodopsin, the C20 methyl group is twisted out of the retinal plane and suggested that there is a small distortion or 'pre-twist' about the C11=C12 double bond (*251, 271*). The conformational

distortion "primes" the retinal for isomerization in a specific direction. Support for conformational distortions in the ground state structure of the retinal come from dipolar recoupling measurements. Measurements of the H-C10-C11-H torsion angle yield a value of 160 ± 10° in rhodopsin (*272*) and 180 ± 25° in the Meta I intermediate (*242*) indicating that this region has relaxed following isomerization.

We recently presented a model for Meta II that was generated *in silico* and guided by distance restraints from our NMR data (*262*). Upon activation, the β-ionone ring of the retinal translates across the binding pocket and the C20 methyl group rotates towards the extracellular surface. Changes in retinal-protein contacts are consistent with a displacement of EL2 from the binding pocket and a change in the side chain rotameric state of Trp265$^{6.48}$. However, three crystal structures recently determined offer competing models for the geometry of the retinal chromophore in Meta II. Figure 5.1 shows the comparison between the two competing retinal orientations. The NMR data suggest a retinal conformation that is similar to what is observed in the E113Q/N2C/D282C mutant (Panel A) (*94*). In contrast, the crystal structures of reversibly formed Meta II (*108*) and that of the M257Y/N2C/D282C constitutively active mutant (*93*) reveal a retinal conformation in which the β-ionone ring has rotated 180° about the axis of the membrane and the polyene chain is situated in a manner that orients both the C19 and C20 methyl groups towards the intracellular surface (Panel B).

The differences between the proposed conformations of all-*trans* retinal have profound implications for understanding how retinal isomerization activates rhodopsin. The C19 methyl group is quite distant from Trp265$^{6.48}$ in the dark state of rhodopsin, but in close contact with the C20. In Meta II the NMR data reveal a strong contact between Trp265$^{6.48}$ and the C19 methyl group of retinal and a loss of the C20 contact (*173*). There are two possible ways to explain these data. The first is that the Trp265$^{6.48}$ side chain moves in a manner consistent with the rotamer toggle switch (*111*). The second is that the retinal undergoes a large change in orientation in the binding site. In the crystal structure of reversibly formed Meta II, the orientation of the retinal has changed in a manner that satisfies the NMR data without motion of Trp265$^{6.48}$. Addressing the position of EL2 and the sidechain rotameric state of Trp265$^{6.48}$ in Meta II requires a detailed description for the orientation of the all-*trans* retinal.

We address the orientation of all-*trans* retinal in Meta II using solid-state NMR measurements. Specifically, we measured the internuclear distances between retinal methyl (C18, C20) groups and side chain atoms of residues within the binding pocket. NMR spectra of rhodopsin with $^{13}CH_3$-enriched retinal exhibit narrow linewidths for the retinal methyl groups (e.g. C18, 19 and 20). The narrow resonances are readily observed in the NMR spectra which facilitate peak assignment.

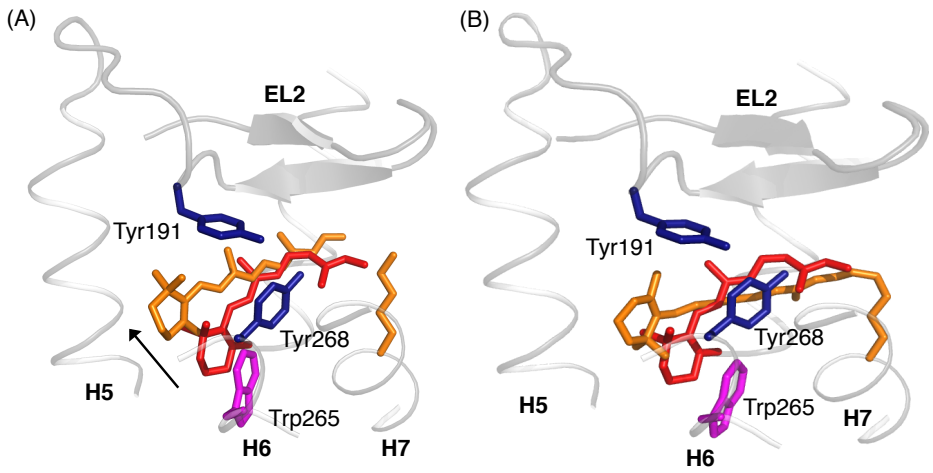

Fig. 5.1. Retinal conformation. *The conformation of all-trans retinal in Meta II is described by crystal structures of a constitutively active rhodopsin mutant (PDB ID: 2X72)(A) and a reversibly formed Meta II where all-trans retinal was added to low pH crystals of opsin (PDB ID: 1U19)(B). The two conformations offer opposing views for the orientation of polyene chain methyl groups as well as the β-ionone ring.*

5.1.1. Position of the C18 methyl group in Meta II.

As mentioned above, one of the major differences between the two competing models for the conformation of all-*trans* retinal in Meta II is the orientation of the β-ionone ring. In the dark state of rhodopsin, the β-ionone ring is packed between the indole side chain of Trp265$^{6.48}$ on H6 and Met207$^{5.42}$, Phe208$^{5.43}$ and Phe212$^{5.47}$ on H5. The close association between the β-ionone ring and residues on H5 and H6 provides a mechanism by which ring motion can induce helical movement.

In this subsection, solid-state NMR data are presented that define the local environment for the C18 methyl group of all-*trans* retinal in Meta II. The C18 methyl group is connected to the β-ionone ring and serves a marker for its location. In order to occupy the position shown in the

structure of reversibly formed Meta II, the β-ionone ring must rotate ~180° about the axis of the membrane.

Figure 5.2 presents rows extracted from an isotope-enriched rhodopsin sample that has been regenerated with ^{13}C5,18-labeled retinal in both the dark and Meta II states. In the dark, we observe a cross peak between the C18 methyl group and various aromatic carbons of a phenylalanine side chain. On the basis of internuclear distances measured from the dark state crystal structure of rhodopsin (*181*), there is only one phenylalanine residue (Phe261$^{6.44}$) within 7.5 Å of the C18 methyl group. Phe261$^{6.44}$ is part of the conserved aromatic cluster on H6, which includes Trp265$^{6.48}$.

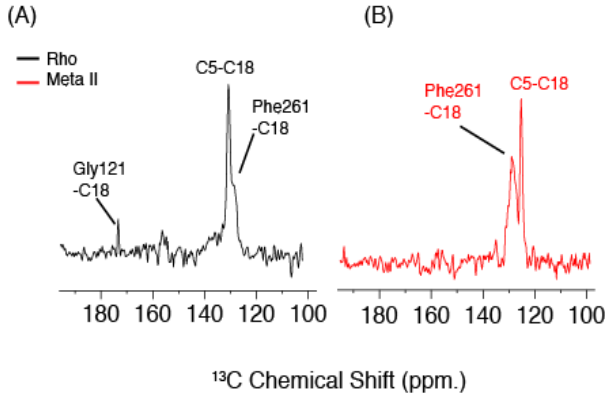

Fig. 5.2. Retinal C18 contacts. *Rows were extracted from 2D ^{13}C DARR NMR spectra collected on $^{13}C_{ring}$-Phe and ^{13}C1-Gly-labeled rhodopsin that had been regenerated with ^{13}C5,18 retinal. For comparison, the intermolecular cross peak between the C5 and C18 carbons of the retinal is shown in both states. In rhodopsin, crosspeaks are observed from C18 to both C1-Gly and C_{ring}-Phe (A). In Meta II, C18-Phe is the only retinal-protein crosspeak that is observed and its intensity is increased (B).*

If we are correct in assigning a dark state contact between C18 and Phe261$^{6.44}$, then the cross peak intensity reflects the aggregate sum of C18 contacts with several side chain carbons on Phe261$^{6.44}$, which range from 4.92 – 5.39 Å. In Meta II, the cross peak intensity for the C18-Phe contact is greater than what is observed in the dark (Fig. 5.2B). There are at least two possible interpretations for the increased intensity in C18-Phe contact upon activation. The reversibly formed crystal of Meta II (*108*) proposes a scenario in which the β-ionone ring has flipped towards the extracellular surface, where the internuclear distance between C18 and Phe261$^{6.44}$ has increased to over 12 Å. If the β-ionone ring has flipped in accordance with the crystal structure of reversibly formed Meta II (*108*), then the closest phenylalanine to C18 is at position

203. The internuclear distance between Phe203$^{5.38}$ and C18 is 6.00 Å, which is on the border of our detection limit and we would expect see a reduced intensity in the active state C18-Phe contact. Alternatively, if we interpret the NMR data as a decrease in internuclear distance between the C18 retinal methyl group and Phe261$^{6.44}$ upon activation, then this would imply that the β-ionone ring has translated across the retinal binding pocket towards H5. As a result, steric clashes between the β-ionone ring and the side chain of Met207$^{5.42}$ on H5 induce helical rotation. Translation of the retinal chromophore towards H5 is also consistent with the crystal structure of the E113Q/N2C/D282C Meta II intermediate (*94*).

Figure 5.2A also shows a cross peak between the retinal C18 methyl group and the carbonyl of a single glycine residue. In the inactive state crystal structure of rhodopsin, the C18 retinal methyl group is oriented towards transmembrane helix H3 in close proximity to Gly121$^{3.36}$. The internuclear distance between the retinal C18 methyl group and the carbonyl of Gly121$^{3.36}$ is 3.76 Å. There are no additional Gly-C18 contacts within 6 Å in the dark state crystal structure of rhodopsin. As a result, we assign the dark state Gly$^{3.36}$-C18 contact to Gly121$^{3.36}$. Upon receptor activation, the Gly121$^{3.36}$-C18 contact is lost. However, the increased distance between Gly121$^{3.36}$ and the retinal C18 methyl group does not distinguish between translation and rotation of the β-ionone ring.

Several studies have already suggested that GPCR activation involves a change in the rotational orientation of H5 at the cytosolic surface. The interaction between the β-ionone ring and H5 upon activation is consistent with NMR data and provides a mechanism by which retinal isomerization induces a rotation of H5.

5.1.2. Position of the C20 methyl group in Meta II.

Figure 5.3 presents rows extracted from an isotope-enriched rhodopsin sample that has been regenerated with ^{13}C12,20-labeled retinal in both the dark (black) and Meta II (red) states. The C20 methyl group is situation on the polyene chain. In rhodopsin, we observe cross peaks to a single ^{13}Cζ-Tyr from both C12 and C20 retinal carbons that are consistent with the crystal structures of the inactive conformation where the internuclear distances are 4.9 Å and 4.2 Å respectively. Upon conversion to Meta II, crosspeaks between C12,C20 and Tyr are observed.

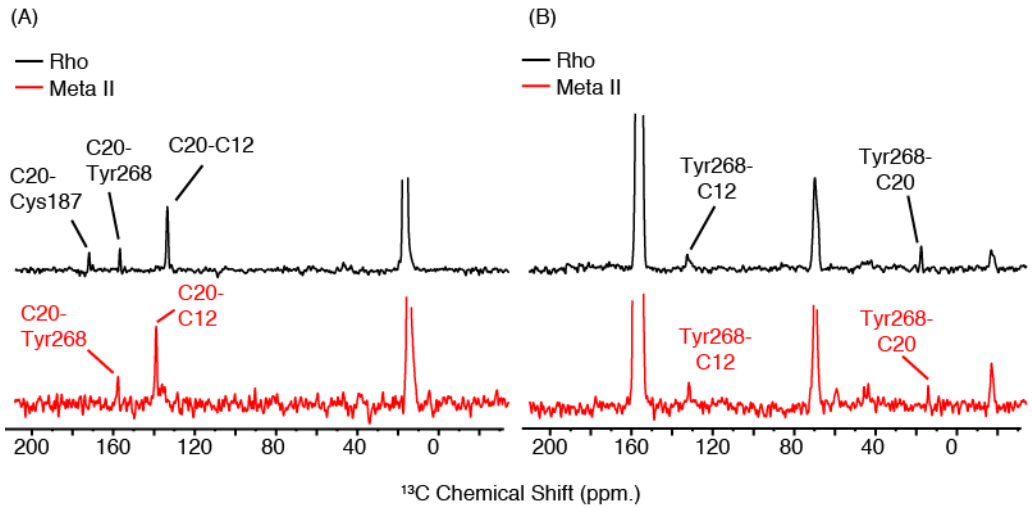

Fig. 5.3. Retinal C20-Tyr contacts. *Rows were extracted from 2D ^{13}C DARR NMR spectra collected on ^{13}Cζ-Tyr and ^{13}C1-Cys-labeled rhodopsin that have been regenerated with ^{13}C12,20 retinal. Panel A contains rows corresponding the ^{13}C20 chemical shift, while rows extracted through the ^{13}Cζ-Tyr region are shown in panel B. In rhodopsin (black), cross peaks are observed from Tyr268 to both C12 and C20 retinal carbons, these cross peaks remain in Meta II (red). For comparison, the intermolecular cross peak between C12 and C20 carbons of the retinal is shown in both states.*

The ^{13}Cζ-Tyr resonances corresponding to the C20-Tyr contacts in both rhodopsin and Meta II are 156.7 and 157.0 ppm, respectively. These resonances have previously been assigned to Tyr268 on the basis of comparing ^{13}Cζ-Tyr chemical shift measurements of Y268F mutant rhodopsin with those of the WT receptor (*172*). In addition, the dark state crystal structure of rhodopsin reveals that the closest tyrosine residue to the C20 methyl group of retinal is Tyr268$^{6.51}$ (4.18 Å), the next closest is Tyr191^{EL2} which is 7.96 Å away. The ^{13}Cζ-Tyr191^{EL2} chemical shift has previously been assigned to 154.9 ppm in rhodopsin and 159.3 ppm in Meta II on the basis of site-directed mutagenesis. Therefore, we assign the dark state C20-Tyr contact to Tyr268$^{6.51}$. In Meta II, the C20-Tyr cross peak is upfield from the ^{13}Cζ-Tyr191^{EL2} chemical shift and overlaps that of ^{13}Cζ-Tyr268$^{6.51}$ in Meta II. The only other tyrosine residue in the vicinity of C20 is Tyr178^{EL2} on the β3-strand of EL2. We cannot rule of the possibility of an active state contact between Tyr178^{EL2} and C20 based on chemical shift alone. However, previous NMR experiments have shown that the C20-Tyr cross peak remains present in Meta II spectra of Y178F mutant rhodopsin (*171*). As a result, we assign the active state Tyr-C20 contact to Tyr268$^{6.51}$ as well.

We use the Tyr268$^{6.51}$-C20 contact to help define the position of C20 and aid in the assignment of other retinal-protein contacts in Meta II. One such contact is between C20 and the

$^{13}C\alpha$ of a glycine that we observe in Meta II at a frequency of 45.2 ppm. In rhodopsin, the C20 methyl group is close to 2 glycine residues, $Gly114^{4.29}$ (7.0 Å) and $Gly188^{EL2}$ (6.3 Å); both of these internuclear distances are beyond the detection limits of dipolar recoupling experiments. The $^{13}C\alpha$-Gly chemical shift is sensitive to secondary structure, with average frequencies of 45.7 ppm and for glycines in an α-helix and 43.1 ppm for those in β-sheet structure (*273*). Gly188 is situated in the β4-strand of EL2 while $Gly114^{4.29}$ is on H3. The dark-state chemical shift of Gly188 has been assigned to 42.0 ppm on the basis of site-directed mutagenesis (*171*). The chemical shift of the dark state C20-Gly contact (45.2 ppm) is different from that of $Gly188^{EL2}$ and is consistent with a glycine in helical secondary structure, which is the case for $Gly114^{3.29}$. However, the $^{13}C\alpha$-$Gly188^{EL2}$ chemical shift moves into an unresolved region of the spectrum in Meta II.

In order to accurately assign the $^{13}C\alpha$-$Gly188^{EL2}$ chemical shift in Meta II, we used 2D ^{13}C dipolar recoupling experiments to correlate the $^{13}C\alpha$-$Gly188^{EL2}$ with the $^{13}C1$ of its neighboring residue, $Cys187^{EL2}$. In figure 5.4 2D, DARR plots are shown that contain cross peaks from $^{13}C\alpha$-Gly nuclei to both $^{13}C1$-Cys and $^{13}C\zeta$-Tyr (discussed below). There are several Cys-Gly pairs in the dark state crystal structures whose respective C1 and Cα nuclei are within 6 Å. Three of these contacts are within the flexible C-terminus where the inherent conformational plasticity results in broad linewidths that are indistinguishable from the level of spectral noise. The directly bonded Cys187-Gly188 pair has the shortest $^{13}C1$-$^{13}C\alpha$ distance (2.43 Å), while the remaining Cys-Gly pairs include $Gly114^{3.29}$ contacts to both Cys187 (3.93 Å) and Cys110 (4.82 Å), as well as a contact between Gly109 and Cys110 (4.43 Å). NMR spectra collected on rhodopsin in the dark reveal two strong cross peaks between $^{13}C1$-Cys and $^{13}C\alpha$-Gly that are centered at 45.3 ppm and 42.0 ppm. The peak at 45.3 ppm is likely a compound peak that reflects the Gly114 as well as the Gly109 contacts, since both glycine residues are situated on H3. The peak at 42.0 ppm is the most intense, falls in the region of $^{13}C\alpha$ chemical shift range for glycines in a β-sheet secondary structure, and overlaps our previous chemical shift assignment for $^{13}C\alpha$-$Gly188^{EL2}$. Moreover, we also observe a strong cross peak from a $^{13}C\zeta$-Tyr to a $^{13}C\alpha$-Gly at 42.0 ppm, which corresponds to a close contact between $Tyr268^{6.51}$ and $Gly188^{EL2}$ in Meta II.

In Meta II, we also observe two ^{13}C1-Cys and ^{13}Cα-Gly cross peaks. One of the active state ^{13}C1-Cys-^{13}Cα-Gly has a broad linewidth centered at ~45 ppm and likely represents a number of contacts involving glycines in an α-helical secondary structure (Gly224-Cys222 4.49 Å, Gly324-Cys322 4.13 Å, and Gly324-Cys323 2.41 Å). The second ^{13}C1-Cys-^{13}Cα-Gly contact has a narrow linewidth and is centered at 43.0 ppm, which is characteristic of a glycine residue in a β-sheet secondary structure. The intensity of the ^{13}C1-Cys-^{13}Cα-Gly cross peak at 43.0 ppm in Meta II is similar to that seen at 42.0 ppm in the dark, suggesting that polarization transfer between the two nuclei generating this cross peak is occurring over the same nuclear distance in both rhodopsin and Meta II. Cys187^{EL2} and Gly188 ^{EL2} are directly bonded backbone atoms whose internuclear distance is not subject to change upon receptor activation. On the basis of both the intensity and frequency of the ^{13}C1-Cys-^{13}Cα-Gly cross peaks in Meta II, we are comfortable in assigning the active state ^{13}Cα-Gly188 ^{EL2} resonance to 43.0 ppm. As such, no cross peak is observed between C20 and ^{13}Cα-Gly188 ^{EL2} in Meta II.

Therefore, we tentatively assign the active state ^{13}Cα-Gly-C20 contact to Gly114$^{3.29}$ for two reasons. First, Gly114$^{3.29}$ is in an H3 in a α-helix, which is consistent with a chemical shift of 45.2 ppm. Second, an active state ^{13}Cα-Gly114-C20 contact suggests that the C20 methyl group has rotated up towards the extracellular surface. A rotation of the C20 methyl group is consistent with computational studies (*274*) as well as the crystal structure of bathorhodopsin (*264, 275*), which reveals a clockwise rotation of the C20 methyl group (viewed from the Schiff base end of the retinal) within femtoseconds of isomerization. A clockwise rotation would place the C20 methyl group close to a number of residues on EL2. However, previous NMR spectra of Meta II reflect an increased distance between C20 and EL2. The lack of C20 contacts to EL2, in conjunction with the active state ^{13}Cα-Gly114-C20 contact, was a strong indicator that the position of the loop in Meta II was different from that of the dark state (*172*).

In the crystal structure of reversibly formed Meta II (*108*), the C20 methyl group is rotated ~90° counterclockwise. Such a rotation challenges the observations seen in bathorhodopsin (*264, 275*), and places the C20 methyl group close to a number of residues of H3. One residue in particular, Ala117, would have its sidechain within van der Waals contact of C20. It has previously been reported that site-directed mutations introducing aromatic side chains at position

117 dampen the transition to Meta II (*276*). The position of the C20 methyl group in the crystal structure of reversibly formed Meta II (*108*) would suggest the small side chain of Ala117 facilitates a counterclockwise rotation of C20 upon activation. In addition, the C20 methyl group is within 5.5 Å of Gly120$^{3.35}$ and Gly121$^{3.36}$, both of which are in a secondary structure similar to that of Gly114$^{3.29}$ and it is not inconceivable that there could be significant chemical shift overlap between the three residues. In order to unambiguously assign the active state ^{13}Cα-Gly–C20 contact, NMR experiments are required that measure active state retinal protein contacts in the G121A and G120A mutants. If either mutation reduces the intensity of the ^{13}Cα-Gly–C20 contact in Meta II, then it would strongly suggest a counterclockwise rotation of C20 and call into question the proposed motion of EL2.

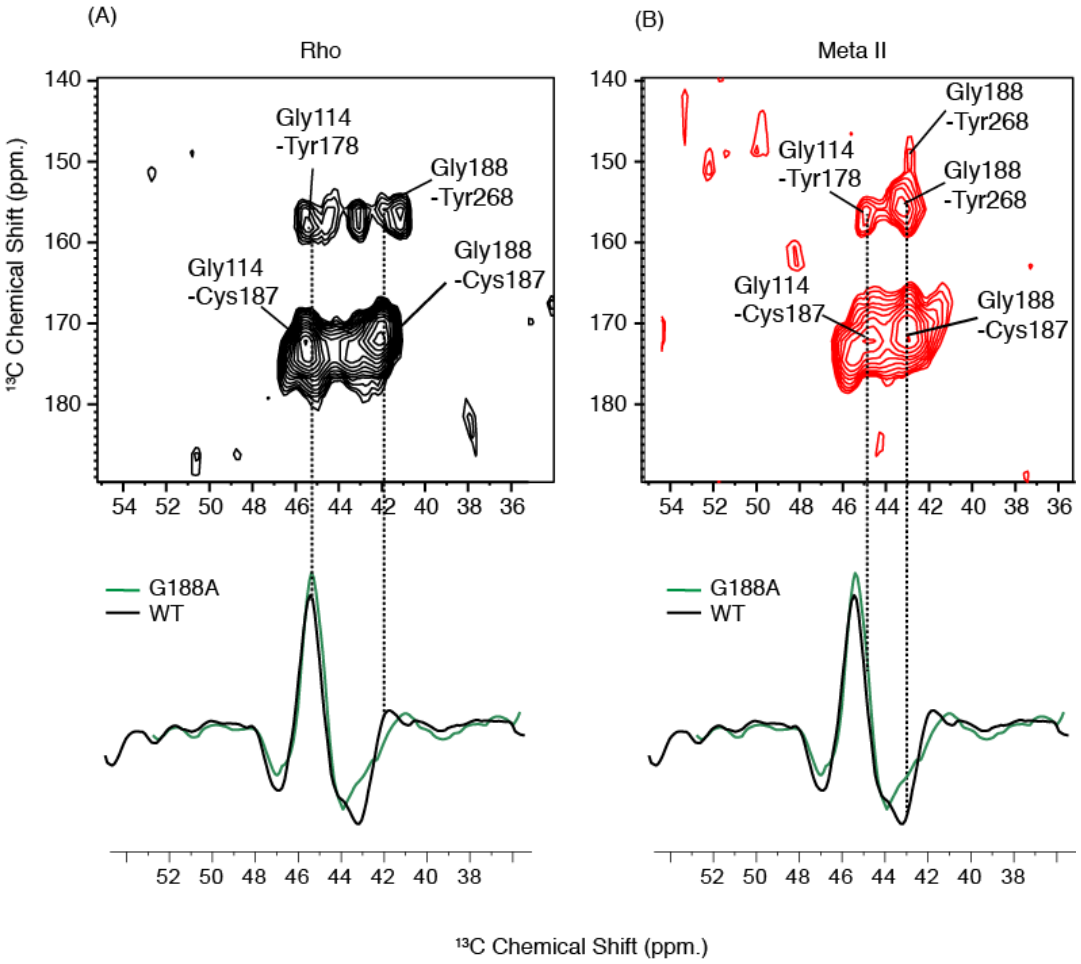

***Fig. 5.4. Glycine assignments**. 2D ^{13}C DARR NMR spectra were collected on $^{13}C\zeta$-Tyr- and $^{13}C1$-Cys-labeled rhodopsin. 2D plot of $^{13}C\alpha$-Gly cross peaks to both $^{13}C1$-Cys and $^{13}C\zeta$-Tyr are shown for both rhodopsin (black) and Meta II (red). The $^{13}C\alpha$-Gly resonances are correlated with difference bands in in rho minus Meta II spectra (bottom) collected on both WT (black) and the G188A mutant (green).*

5.2. Investigating the role of Pro267.

Proline residues are well known for their ability to serve as hinges points for motion of transmembrane helices (*270, 277, 278*). In Chapter 4, the motion of H6 upon rhodopsin activation was described. A question that remains to be addressed is whether or not the conserved Pro267$^{6.50}$ mediates H6 motion. In this section, we look at backbone ^{13}C chemical shift measurements of Ile263$^{6.56}$, whose carbonyl is freed from backbone hydrogen bonding by Pro267$^{6.50}$, to report local changes in secondary structure.

There are 22 Ile residues in rhodopsin and spectral overlap makes it difficult to interpret chemical shift changes by comparing standard ^{13}C MAS spectra. An alternative approach is to

use $^{13}C,^{15}N$ dipolar recoupling experiments (e.g. $^{13}C,^{15}N$ REDOR) to exchange magnetization and make resonance assignments based on heteronuclear correlations. By incorporating $^{13}C1$-Ile and ^{15}N-Cys into rhodopsin, we are able to exploit the heteronuclear ^{13}C-^{15}N dipolar coupling between Ile263$^{6.56}$ and Cys264$^{6.57}$. When we reduce the time allowed for the exchange of magnetization, we restrict polarization transfer to the directly bonded $^{13}C1$-^{15}N pairs that exist along the peptide backbone of sequential residues. As such, the $^{13}C1$-Ile, ^{15}N-Cys labeling scheme isolates the carbonyl of Ile residues that are followed by cysteines. In rhodopsin, Ile263-Cys264 is the only dipeptide sequence that fits the criteria.

Figure 5.5A shows a REDOR difference spectrum of $^{13}C1$-Ile, ^{15}N-Cys labeled rhodopsin two peaks are observed in the dark state. The observation of more than one peak in the S-S_0 spectrum is intriguing given the unique occurrence of the Ile-Cys dipeptide sequence in rhodopsin. The sharp peak at 169.34 ppm is consistent with non-helical secondary structure and a lack of hydrogen bonding interactions. We interpret these data and assign the peak at 169.34 ppm as the predominant non-hydrogen bonded carbonyl of Ile263. We also observe a broad peak centered at 173.49 ppm. The heterogeneous linebroadening of this downfield peak is consistent with multiple orientations of the carbonyl chemical shift tensor. In the dark state crystal structure, there is a water molecule whose proton is situated 5.9 Å from the carbonyl oxygen of Ile263$^{6.56}$. As such, a certain population of $^{13}C1$-Ile263$^{6.56}$ nuclei may be hydrogen bonding with a structural water molecule resulting in the broad peak at 173.49 ppm.

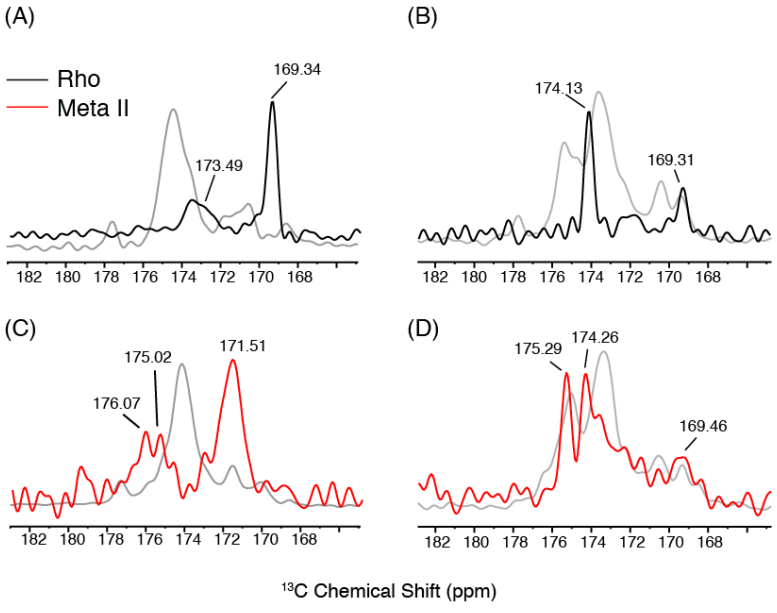

Fig. 5.5. Carbonyl chemical shift changes for Phe287 and Ile263. *^{13}C observed, ^{15}N dephased REDOR difference (S-S_0) spectra are shown for $^{13}C1$-Ile,^{15}N-Cys (A,C) and $^{13}C1$-Phe, ^{15}N-Met (B,D) labeled rhodopsin samples in the inactive dark (A,B, black) and the active Meta II (C,D red) conformation. REDOR spectra are superimposed with the corresponding $^{13}C1$ chemical shift dispersion from ^{13}C CPMAS spectra (grey).*

Figure 5.5A shows a REDOR difference spectrum of ^{13}C1-Ile, ^{15}N-Cys labeled rhodopsin. Again, two peaks are observed but at different frequencies than what were seen in the dark state. First, a broad peak centered at 171.51 ppm is observed with comparable intensity to that of the dark state peak at 169.32 ppm. In addition, two poorly resolved downfield peaks are observed indicating an increased conformational heterogeneity in Meta II with respect to the dark state. The observation that both peaks corresponding to the ^{13}C1-Ile263$^{6.56}$ chemical shift are modulated upon rhodopsin activation is indicative of either a change in hydrogen bonding interactions or backbone torsion angles. Neither of these two possibilities are in line with the crystal structures of Meta II (*93, 94, 108*). While the changes in backbone chemical shift of Ile263$^{6.46}$ are consistent with hinge motion about Pro267$^{6.50}$, more information is needed. Computational studies suggest a reorientation for the side chain of Cys$^{6.47}$ upon activation in the β_2AR (*111*), the analogous residue in rhodopsin is Cys264$^{6.47}$. One interpretation for the activation-induced changes in Ile263$^{6.46}$ backbone chemical shifts may be proximity to the free electron pairs on the sulfhydryl group of Cys264$^{6.47}$. Future directions may include collecting backbone ^{13}C-Ile263$^{6.46}$ measurements in the C267S mutant rhodopsin, which would magnify any potential interactions between the sidechain at position 267 and the carbonyl of Ile263$^{6.46}$.

Pro267$^{6.50}$ is adjacent to the sidechain of Pro291$^{7.38}$. The proximity of these two proline residues to the extracellular surface of rhodopsin provides a possible helix-loop-helix unit which couples the motion of H6 and H7 upon receptor activation. To address changes in the local secondary structure of Pro291$^{7.38}$, we used REDOR difference spectroscopy. Figure 5B shows and S-S_0 spectrum of ^{13}C1-Phe, ^{15}N-Met label rhodopsin where two peaks are observed at 169.31 ppm and 174.31 ppm. There are two Phe-Met bonds throughout the primary sequence of rhodopsin. The first is Phe287-Met288, which is the carbonyl of interest in terms of the H6-EL3-H7 helix loop helix unit. The other, Phe85-Met86, is located on H2 and its carbonyl group is hydrogen bonded to the amide proton of Gly89$^{2.56}$. The ^{13}C1-Phe resonance at 174.34 ppm falls within the characteristic region of carbonyls in α-helical secondary structure. Based on the lack

of breaks in secondary structure within H2, we assign the ^{13}C1-Phe resonance at 174.34 ppm to Phe85$^{2.52}$. Therefore, we assign the peak at 169.31 ppm to the ^{13}C1-Phe287$^{7.30}$ chemical shift.

Upon conversion to Meta II, the carbonyl chemical shifts filtered out by the ^{13}C1-Phe, ^{15}N-Met labeled sample result in three peaks. The broad upfield peak at 169.46 ppm is within the linewidth of the peak assigned to the ^{13}C1-Phe287$^{7.30}$ chemical shift in the dark, suggesting that this region of the receptor has not undergone a significant change in secondary structure upon activation. However, the linewidths have markedly increased, suggesting conformational heterogeneity. In addition, two downfield peaks are observed at 174.26 ppm and 175.29 ppm, the linewidths of which are similar to the dark state ^{13}C1-Phe resonance at 174.13 ppm. There are two possibilities for the apparent splitting of the upfield resonance in Meta II. One explanation is that one of the downfield peaks corresponds to a unique conformation for the backbone of Phe287$^{7.30}$. In that case, the broad peak at 169.46 may reflect anomalous conformational heterogeneity. Alternatively, Phe85$^{2.52}$ may have undergone a change in local environment. Phe85$^{2.52}$ is in close proximity to Gly120$^{3.35}$. The crystal structure of reversibly formed Meta II shows a decreased interhelical distance between H2 and H3 upon activation. It may be the case that the active state interface between H2 and H3 results in a peak splitting of the Phe85$^{2.52}$ carbonyl resonance. In order to differentiate between the two scenarios described above, ^{13}C backbone chemical shifts might be collected in Phe85$^{2.52}$ mutant rhodopsin.

Together, the changes in linewidth and/or chemical shift observed for both Phe283$^{7.30}$ and Ile263$^{6.46}$ upon rhodopsin activation are consistent with conformational plasticity. One interpretation of the results is that these regions serve as hinges for EL3.

5.3. Investigating structural changes at the extracellular surface of rhodopsin.

In Chapters 3 and 4 experimental data are presented that describe how retinal isomerization is coupled to structural changes on H5 and H6 that facilitate the binding of heterotrimeric G protein to active rhodopsin. The motion of H5 and H6 are features of a global activation mechanism that is conserved throughout family A GPCRs and facilitates the binding of heterotrimeric G protein. In contrast, the extracellular surface of rhodopsin is unique. In rhodopsin, EL2 penetrates into the transmembrane core to serve as part of the ligand binding pocket and its motion is restricted via steric clashes with EL3. In turn, EL3 is situated between EL2 and the flexible N terminus. It has

been proposed that EL2 is displaced from the retinal binding pocket upon retinal isomerization (*172*).

Due to a close association between the two extracellular loops, the displacement of EL2 suggests a concerted motion of EL3. How the interactions on the extracellular surface of rhodopsin differ from those of other GPCRs may provide insights into the unique biochemical features (i.e. thermostability and low basal activity) of the low light visual receptor. In the following subsections solid-state NMR experiments are described that target EL3. NMR data is provided that suggest EL3 motion occurs about two conserved proline residues on H6 and H7 in response to receptor activation. Next, NMR data are presented to examine the structural perturbations induced by a rhodopsin mutant that restricts motion of the extracellular surface. Finally, data are presented that targets the interface between EL3 and EL2 and discussed in the context of a concerted motion of EL2 and EL3.

5.3.1 EL2-EL3 (N2C, D282C) Structural changes on the extracellular surface.

In 2003, it was discovered that an engineered disulfide bridge between the N-terminus and the third extracellular loop (EL3) dramatically increases the thermal stability of rhodopsin, even in the absence of retinal (*279*). The double mutant that generates this non-native disulfide bridge (N2C, D282C) has been utilized to increase the thermal stability of constitutively active rhodopsin mutants that generally do not retain function when reconstituted in non-native membrane mimetics (*93, 94, 280*). In order to understand the nature of the enhanced stability imparted by the N2C, D282C double mutation at the molecular level, a detailed structural comparison with the wild type receptor conformation is required. However, crystallographic data on the N2C, D282C mutant do not reflect any significant structural deviations from that of the native sequence (*281*).

Solid-state NMR measurements were conducted to further probe the structure of the N2C, D282C mutant. First we looked at global structural features using ^{13}C difference spectroscopy. Figure 5.6 presents a comparison of ^{13}C difference spectra collected of WT rhodopsin (black) and the N2C, D282C mutant (blue). In panel A, positive bands centered at ~156 ppm and ~155 ppm correspond to the respective dark state $^{13}C\zeta$ chemical shifts of $Tyr192^{EL2}$ and $Tyr191^{EL2}$, which are modulated upon receptor activation. The dark state $^{13}C\zeta$ chemical shifts of $Tyr191^{EL2}$

and Tyr192^{EL2} are reproduced in the N2C, D282C mutant. In Meta II, the ^{13}Cζ chemical shift Tyr191^{EL2} and Tyr192^{EL2} are 159.4 ppm and 156.2 ppm respectively. In contrast, difference spectra of the N2C, D282C mutant do not contain negative peaks at the wild type ^{13}Cζ frequencies of Tyr191^{EL2} and Tyr192^{EL2}. Instead, a broad negative peak at ~157 ppm in the N2C, D282C, the intensity of which is likely to reflect the active state chemical shifts of both Tyr191^{EL2} and Tyr192^{EL2} in the mutant. In wild type, the ^{13}Cζ-Tyr191^{EL2} frequency undergoes an upfield shift by 5 ppm, which is consistent with a significant change in electrostatic environment. That such a drastic change in the ^{13}Cζ-Tyr191^{EL2} chemical shift is not observed upon activation of the N2C, D282 suggests that activation-induced structural changes in this region of the receptor are dampened by the non-native disulfide bridge.

The ^{13}Cζ-Tyr chemical shift is sensitive to the hydrogen bonding interactions of the phenol hydroxyl group. In the wild type receptor, chemical shift changes of Tyr191^{EL2} and Tyr192^{EL2} reflect a rearrangement of a hydrogen bonding interactions that tether EL2 to the retinal binding pocket (i.e. Tyr191^{EL2} and Tyr192^{EL2}). The dark state hydrogen bonding interactions of Tyr191^{EL2} and Tyr192^{EL2} are crucial for maintaining EL2 in its inactive conformation and preserving the integrity of the protonated Schiff base linkage (*282*). The observation that neither Tyr191^{EL2} nor Tyr192^{EL2} adopt their respective wild type Meta II chemical shifts upon activation of the N2C, D282C mutant suggests that EL2 motion has not occurred.

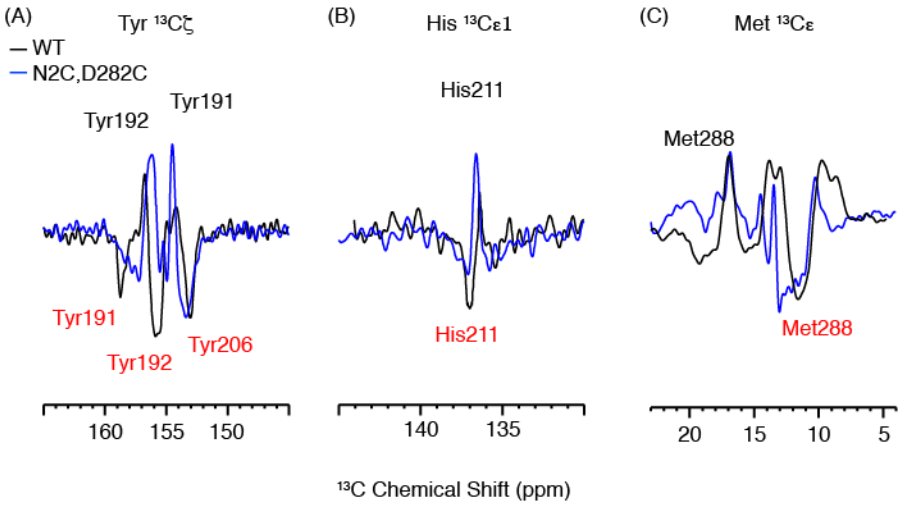

Fig. 5.6. ^{13}C chemical shift changes on the extracellular surface upon activation. *Rhodopsin minus Meta II difference spectra are presented for WT (black) and the N2C, D282C mutant (blue). Difference*

bands in the region of ^{13}Cζ-Tyr have been assigned to Tyr191, Tyr192, and Tyr206 (172); these chemical shift changes are associated with rearrangement of hydrogen bonding interactions between the retinal binding pocket and the EL2.

In wild type rhodopsin, one of the strongest pieces of NMR data that suggest a change in the conformation of EL2 upon activation is a change in the ^{13}Cβ chemical shift of Cys187. As described earlier (Chapter 3), Cys187^{EL2} is part of a disulfide bridge with Cys110$^{3.25}$, which tethers EL2 to H3. Upon activation, the ^{13}Cβ-Cys187^{EL2} frequency shifts from 46.8 ppm in rhodopsin to 50.1 ppm in Meta II. Figure 5.7 presents rows extracted from 2D ^{13}C DARR spectrum, collected on wild type (black) and N2C, D282C mutant Meta II, at the ^{13}Cβ-Cys110$^{3.25}$ chemical shift. In the wild type spectrum, we observe a single cross peak at 50.1 ppm, corresponding to the ^{13}Cβ-Cys187 chemical shift in the active state. In the N2C, D282C spectra, a single cross peak of comparable intensity is observed at 46.2 ppm. The implication is that the ^{13}Cβ-Cys187^{EL2} chemical shift has not significantly changed upon activation in the N2C, D282C mutant, which is consistent with a lack of EL2 motion. It is worth noting that we are not able to observe cross peaks between the ^{13}Cβ carbons of the non-native disulfide bond in the N2C, D282C mutant.

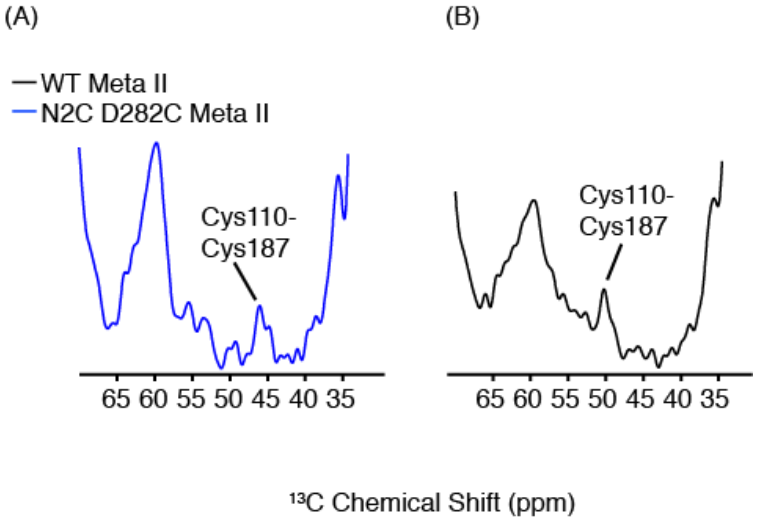

Fig. 5.7. Cys187. *Rows extracted from 2D ^{13}C DARR NMR spectra acquired of the activated Meta II state of wild-type rhodopsin (a) and the N2C, D282C mutant (b). The rows show the Cβ region of Cys110$^{3.25}$ and Cys187^{EL2} and were taken through the diagonal resonances of Cys110$^{3.25}$. In the N2C, D282C mutant, the chemical shift of Cys187^{EL2} is altered with respect to wild-type rhodopsin.*

The ^{13}Cζ-Tyr difference spectrum also shows a negative peak at 153.66 ppm that has been assigned to Tyr206 in Meta II (*99*). In the dark state of rhodopsin, Tyr206 participates in an

interhelical hydrogen bonding network involving His211$^{5.56}$, Glu122$^{3.27}$, and Trp126$^{3.41}$. A downfield shift in the ^{13}Cζ resonance of Tyr206$^{5.41}$ upon formation of Meta II is consistent with a decrease in hydrogen bonding character (*99*). We associate the weakened hydrogen bonding status of Tyr206$^{5.41}$ with a rotation of H5. The active state ^{13}Cζ chemical shift of Tyr206$^{5.41}$ is not affected by the N2C, D282C mutant, suggesting that H5 rotation still occurs.

To further investigate a rotation of H5 upon activation in the N2C, D282C mutant, we first look at the hydrogen bonding changes of His211$^{5.46}$. His211$^{5.46}$ is at the i-4 position of Pro215$^{5.50}$, which leaves its carbonyl oxygen freed from the backbone hydrogen bonding constraints dictated by its α-helical secondary structure. Instead, the backbone carbonyl is hydrogen bonded to the side chain of Glu122$^{3.37}$ in the dark and sidechain of His211$^{5.56}$ is hydrogen bonded to the phenol hydroxyl group of Tyr206$^{5.41}$. In Meta II, structural changes on H5 result in hydrogen bond formation between the sidechains of His211$^{5.46}$ and Glu122$^{3.37}$. His211$^{5.46}$ is the only neutral histidine residue in rhodopsin. As a result, its side chain ^{13}C chemical shifts are resolved from those of the remaining histidines. In rhodopsin, the ^{13}Cε$_1$-His211 chemical shift has previously been assigned to 136.9 ppm and shifts to 137.5 ppm upon activation (*99*). The new hydrogen bonding interaction between His211$^{5.46}$ and Glu122$^{3.37}$ in Meta II, modulates the ^{13}Cε$_1$-His211$^{5.46}$ chemical shift. In Figure 5.6B, ^{13}Cε$_1$-His difference spectra of wild type (black) are superimposed with N2C, D282C mutant. The pattern of difference bands in the ^{13}Cε$_1$-His are similar in both wild type and the N2C, D282C mutant suggesting that the activation-induced changes in sidechain hydrogen bonding of His211$^{5.46}$ are not perturbed.

In Chapter 3 we saw how rotation of H5 facilitates the formation of hydrogen bonding interactions between Arg135$^{3.50}$, Tyr223$^{5.58}$, and Tyr306$^{7.53}$ that help to stabilize the active Meta II state. In order to address whether a similar interaction exists in the active state of N2C, D282C mutant rhodopsin, 2D ^{13}C DARR spectra were collected and compared to those of the wild type. In Figure 5.8 rows are extracted at the ^{13}Cε-Met chemical shift that show polarization transfer to ^{13}Cζ-Tyr nuclei less than 6 Å away. In the wild type receptor, Tyr-Met contacts are observed at 155.9 ppm that correspond to cross peaks from Met257$^{6.40}$ to both Tyr223$^{5.58}$ and Tyr306$^{7.53}$ (*96*). The intensity of the cross peak at 155.9 ppm in Meta II spectra of the N2C, D282C mutant is markedly reduced with respect to that of the wild type. For comparison, an intrahelical cross

peak between Met207$^{5.42}$ and His211$^{5.46}$ in the wild type and mutant spectra is shown. The respective intensities of the Met207-His211 cross peaks are comparable between wild type and mutant spectra. As a result, the internuclear distance between Met257$^{6.40}$ and Tyr223/306 in Meta II is increased in the N2C, D282C mutant.

It is also worth noting that in wild type Meta II, we observe a strong cross peak between Met288$^{7.35}$ and Tyr191^{EL2} at 159.3 ppm (Fig. 5.8). In the N2C, D282C spectra, the ^{13}Cζ-Tyr191 resonance is shifted and broadens out. As result, we cannot comment on the internuclear distance between Tyr191^{EL2} and Met288$^{7.35}$ from the DARR spectrum of N2C, D282C.

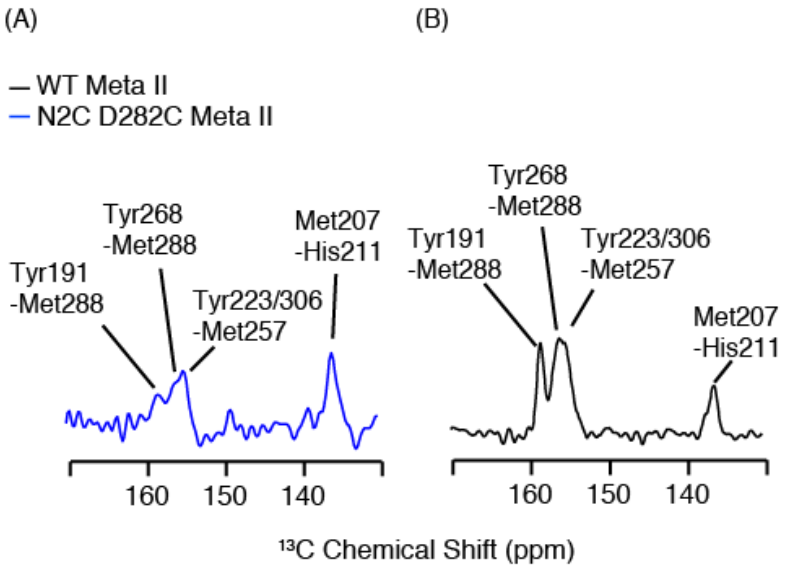

Fig. 5.8. Tyr223$^{5.58}$-Met257$^{6.40}$ and Tyr306$^{7.53}$-Met257$^{6.40}$ contacts in Meta II. *Rows through the Met-^{13}Cε diagonal resonance were extracted from 2D ^{13}C DARR NMR spectra of Meta II for both the N2C, D282C (A) and WT rhodopsin (B) labeled with ^{13}Cζ-Tyr, ^{13}Cε-Met, and ^{13}Cε1-His.*

The perturbed Tyr223/Tyr306/Met257 contacts that are observed in Meta II spectra of the N2C, D282C mutant would suggest that the hydrogen bonding interactions between Tyr223$^{5.58}$,Tyr306$^{7.53}$ and Arg135$^{3.50}$ are weakened. If this were the case, then we would expect to see a decrease in Meta II stability. Figure 5.9 presents kinetic data for N2C, D282C mutant compared to that of wild type rhodopsin. In Panel A, Meta II decay rates are calculated based on monitoring the intensity of Meta II-specific FTIR bands as a function of time post illumination. In WT, the half life of Meta II is 1.7 min, which is reproduced in the N2C, D282C mutant. The pKa of the photoproduct equilibrium between Meta I and Meta II is the same in both wild type

and N2C, D282C mutant. Therefore, it is likely that the interactions which stabilize the active receptor conformation are present in the N2C, D282C mutant as well.

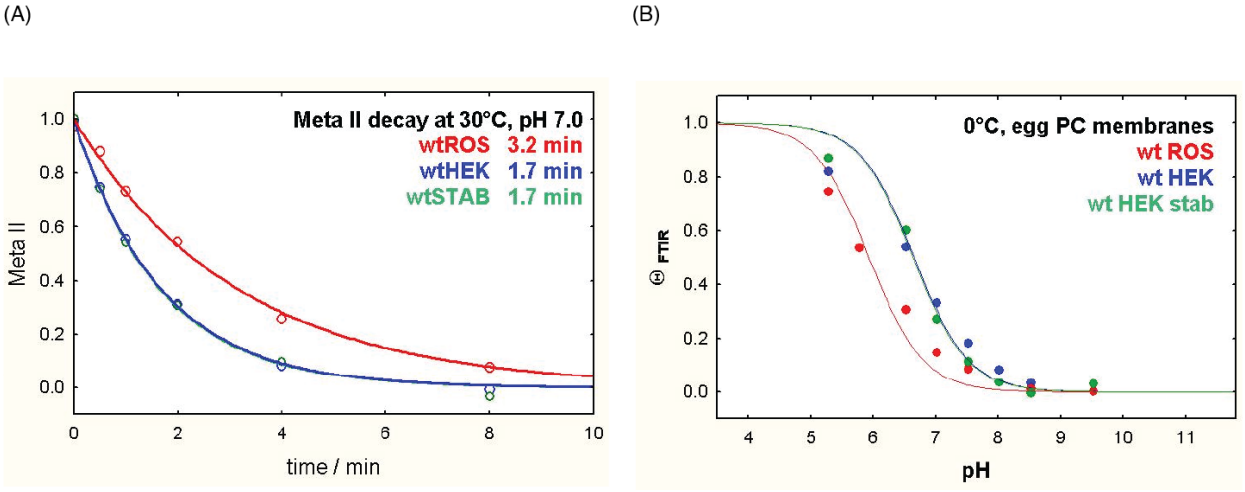

Fig. 5.9. Biochemical characterization of the N2C, D282C mutant. *Meta II decay rates are calculated based on the diminishing intensity of Meta II specific FTIR bands as a function of time after illumination (a). Monoexponential decay curves are shown for wild type (blue) and N2C,D282C (green) rhodopsin solubilized in egg PC. Intensity ratios for Meta II- to Meta I- specific FTIR bands are also presented as function of pH for wild type (blue) and N2CD282C (green) rhodopsin solubilized in egg PC. For comparison Meta II decay and photoproduct titration curves for rhodopsin in ROS membranes are presented. FTIR data were obtained by R. Vogel (Univ. Of Frieburg).*

Previous NMR experiments have established that mutations of EL2 (e.g. E181Q) show a demonstrable difference in markers of H5 motion (i.e. ^{13}Cζ-Tyr206 chemical shift). These observations were used to argue for a coupled motion of H5 and EL2 upon receptor activation (*172*). However, in the case of the N2C, D282C mutant, it appears that EL2 motion has been hampered without affecting the position of H5.

5.3.2 Met288 is a crucial residue at the interface between EL2 and EL3.

In Figure 5.6 panel C, positive peaks in the rhodopsin minus Meta II ^{13}Cε-Met difference spectrum reveal that the ^{13}Cε chemical shift of a single methionine residue at 17.4 ppm undergoes a change in frequency. A ^{13}Cε-Met chemical shift of 17.4 ppm is significantly downfield from the average and consistent with a polar environment. The side chain of Met288 is at the boundary between H7 and EL3 in close proximity to the polar side chain moieties of several neighboring residues including Tyr268$^{6.51}$, Tyr192^{EL2}, Tyr191^{EL2}, Ser198^{EL2} and

Glu181^{EL2} (Fig. 5.10A). On the basis of ^{13}C chemical shift measurements collected on site directed rhodopsin mutants, the dark state ^{13}Cε chemical shift at 17.4 ppm has been assigned to Met288$^{7.35}$ (Fig 5.10B).

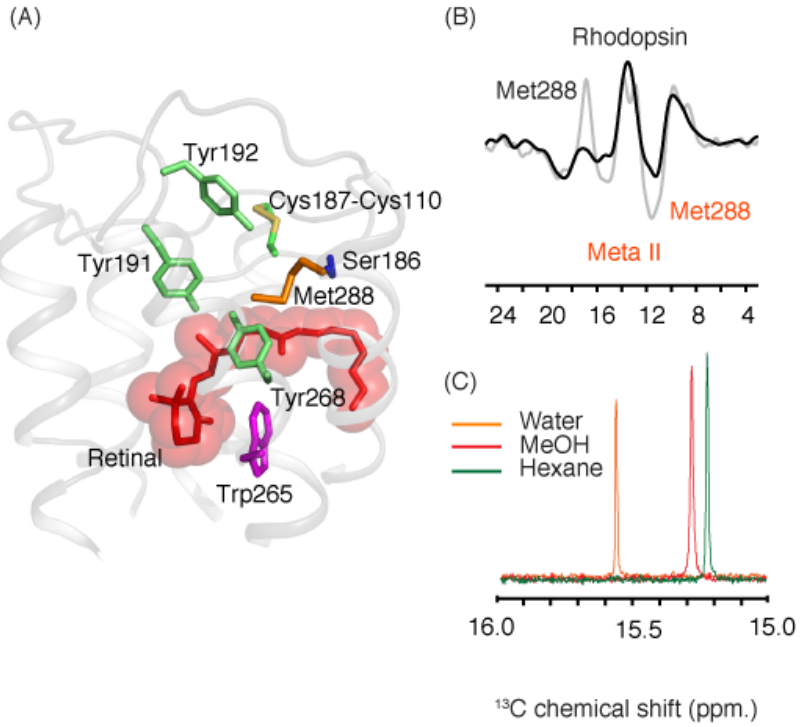

Fig. 5.10. Met288 undergoes a significant chemical shift change upon receptor activation. *A view from the crystal structure of rhodopsin showing the local environment of Met288 in the dark is shown (A). Rhodopsin minus Meta II difference spectra are presented for WT (grey) and the M288L mutant (black) in the region of ^{13}Cε -Met (B). The difference spectra reflect the loss of a single positive peak at 17.4 ppm and a reduction in the intensity of a broad negative band at ~12 ppm upon mutation of Met288. ^{13}Cε-Met chemical shifts were measured in solvents of varying polarity (C). An upfield shift in the ^{13}Cε-Met resonance is consistent with a transition to a more non-polar environment.*

We previously observed that a contact forms between the retinal β-ionone ring and the ^{13}Cε of Met207 in the dark state of the M288L mutant (*172*). NMR contacts between the retinal chromophore and residues on H5 are not observed until the formation of Meta II. The observation of Meta II-like structural elements in the dark state of M288L mutant rhodopsin has consequences for the activation mechanism. Namely, the NMR data suggest that the M288L mutation alters the conformation of H5 in a manner that may facilitate the transition to Meta II. If the energy barrier for adopting the Meta II conformation were to be reduced in the M288L

mutant then we would expect that the photoproduct equilibrium between Meta I and Meta II would be shifted towards Meta II.

In lipid vesicles, the equilibrium between Meta I and Meta II is pH-dependent, with Meta I being stabilized with increased alkalinity. Figure 5.11 presents titration curves for state-specific FTIR difference bands corresponding to Glu122$^{3.37}$, Asp83$^{2.50}$, and the Amide I region of an FTIR spectrum for both WT and the M288L mutant. For WT rhodopsin, the pKa of the Meta I/Meta II equilibrium is 7.7 (at 273 K). At pH 9, nearly all of the receptor populates the Meta I substate (Fig. 5.11B). For M288L, at least 30% of the receptor still exists as Meta II at pH greater than 9. The FTIR data reveal that the photoproduct equilibrium of the M288L mutant never fully populates Meta I, even under alkaline conditions (ie. θ does not go zero), which suggests that Meta II is stabilized in the M288L mutant (Fig. 5.11B). When coupled with the existing NMR data showing a strong contact between Met207 and the C6 carbon of 11-*cis* retinal in the dark, the FTIR data suggest that the M288L mutation alters the conformation of H5 in such a way as to facilitate the transition to Meta II.

For wild type rhodopsin, all three titration curves (Asp83$^{2.50}$, Glu122$^{3.37}$, and Amide I) seem to converge on a pKa of 7.7. In the M288L mutant, the amide I and Glu122$^{3.37}$ titration curves are similar to wild type, but the Asp83 is not. In the dark, Asp83$^{2.50}$ is directly hydrogen bonded to the sidechain of Asn55$^{1.50}$ on H1 and participates in a water-mediated hydrogen bond with Asn302 on H7 (*181, 259*). It has been shown for a number of GPCRs that the conserved H1/H2/H7 hydrogen bonding network is modulated upon receptor activation (*283*). It may be the case that insertion of a leucine at position 288 distorts the conformation of H7 to disrupt the H1/H2/H7 hydrogen bond, which is reported by the unique IR signature of Asp83.

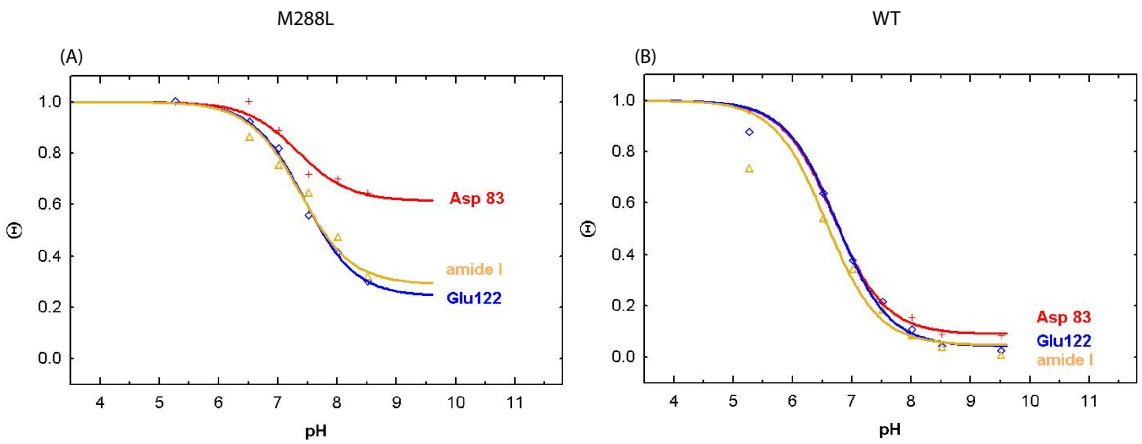

Fig. 5.11. The Meta I/Meta II photoproduct equilibria. *Intensity ratios for Meta II- to Meta I- specific FTIR bands are presented as function of pH for M288L (A) and WT (B) rhodopsin solubilized in egg PC. This data was collected by Katrina Zaitseva in the laboratory of Reiner Vogel at the University of Freiburg.*

Given that the dramatic effects of such a conservative mutation (M288L), we went on to look at the structural consequences of a less conservative mutation (M288A) via FTIR and NMR. When compared with the wild type receptor, the titration curve for the Meta I/Meta II equilibrium is shifted by 1.6 pH units (5.11A). The shift is similar to what was previously observed for the Y223F mutant, which diminishes the stability of Meta II (Chapter 3). As a result, the FTIR data reveal that Meta II is destabilized in the M288A mutant.

In Chapter 4 data were presented which suggest that the conformations of EL2 in Meta I and rhodopsin are similar. As a result, EL2 motion is temporally assigned to the transition from Meta I to Meta II. Met288 is the point of interaction between the start of EL3 and EL2. Given its position, the apparent destabilization of Meta II in the M288A mutant may be associated with restricting the motion of EL2. As such we looked at the two most robust probes for the conformation of EL2: the ^{13}Cβ-cysteine and the ^{13}Cζ-tyrosine chemical shifts.

Figure 5.12 presents rows extracted from 2D ^{13}C DARR spectra, collected on wild type (Panel A) and M288A (Panel B) mutant rhodopsin, at the ^{13}Cβ-Cys110$^{3.25}$ chemical shift. In the wild type spectrum, we observe a single cross peak to ^{13}Cβ-Cys187^{EL2} at 50.1 ppm in the active state. In the M288A mutant however, the ^{13}Cβ-Cys187chemical shift is 46.2 ppm. The implication is that the ^{13}Cβ-Cys187^{EL2} chemical shift has not significantly changed upon activation in the

M288A mutant, which is consistent with a lack of EL2 motion. Interestingly, the N2C, D282C disulfide bond had an analogous affect on the active state ^{13}Cβ-Cys187^{EL2} chemical shift, suggesting that the conformation of EL2 for both mutants is similar.

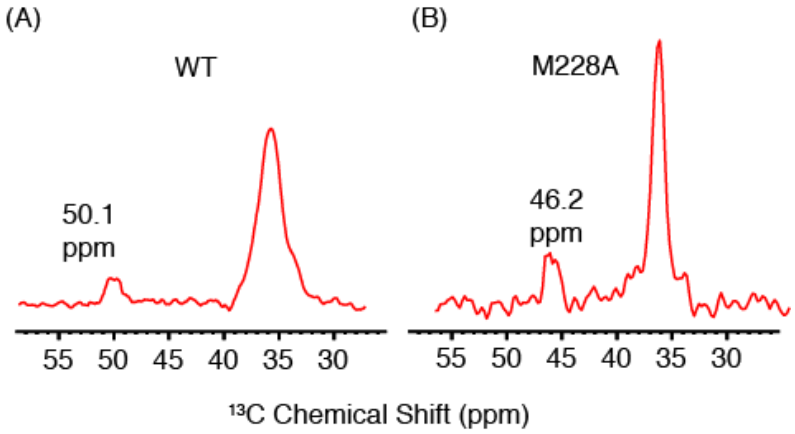

Fig. 5.12. Meta II ^{13}Cβ-Cys187 chemical shift in M288A. *Rows extracted from 2D ^{13}C DARR NMR spectra acquired on the activated Meta II state of wild-type rhodopsin (A) and the M288A mutant (B). The rows show the Cβ region of Cys110$^{3.25}$ and Cys187^{EL2} and were taken through the diagonal resonances of Cys110$^{3.25}$. In the M288A mutant, the chemical shift of Cys187^{EL2} is altered with respect to wild-type rhodopsin*

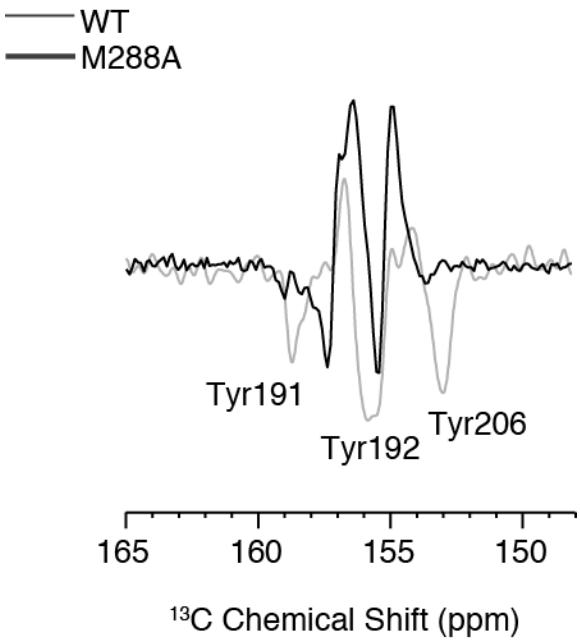

Fig. 5.13. ^{13}Cζ-Tyr difference spectra in M288A. *Rhodopsin minus Meta II difference spectra are presented for both wild type (grey) and the M288A (black) mutant. For clarity, peak assignments are provided only for wild type Meta II frequencies.*

In order to further investigate the influence of the M288A mutation of EL2 motion we looked at the ^{13}Cζ-Tyr difference spectra with an eye towards Tyr191^{EL2} and Tyr192^{EL2} in particular. Figure 5.13 presents rhodopsin minus Meta II difference spectra for wild type and the M288A mutant in the region of ^{13}Cζ-Tyr. When compared with the wild type receptor, the M288A difference spectra show two additional peaks that are not seen in the native sequence. Future efforts can be directed towards assigning the positive difference bands in the M288A spectrum.

For the active state, M288A difference spectrum exhibits two negative peaks at 157.2 ppm and 155.3 ppm. Again, further work is required in order to assign the various peaks in the difference spectrum (i.e. ^{13}C – ^{13}C correlation experiments). Nevertheless the lack of negative peaks at the native frequencies of either ^{13}Cζ-Tyr191^{EL2} or ^{13}Cζ-Tyr206$^{5.41}$ strongly suggest that the active state conformation of EL2 is distorted in the M288A mutant.

CHAPTER 6: OVERALL CONCLUSIONS

6.1 H5 and H6 motion.

The physiological role of GPCRs is to transmit the signal of ligand-binding at the extracellular surface to structural changes in the cytoplasmic moiety of the receptor. These structural changes reveal the binding site for heterotrimeric G proteins in the cytosol. Several studies have demonstrated that IL3 plays a key role in GPCR signal transduction. IL3 contains several residues whose mutation leads to constitutive receptor activity, presumably due to stabilizing the loop region in favor of the active state (*284*). Single molecule fluorescence studies conducted on the β_2AR, in the presence of BI167107, revealed structural changes that were localized to the IL3 (*285*). In rhodopsin, mutations in the IL3 allow weak transducin binding but prohibit guanyl nucleotide exchange, suggesting that the loop serves a mechanistic role for G protein signaling that extends beyond serving as a docking site (*286*). In addition, IL3 is thought to serve as a molecule determinant for the binding of specific G proteins (*287*). G protein-independent signaling in the dopamine D2 receptor is also mediated through cytosolic protein interaction with IL3 (*287*).

The cytosolic domains of transmembrane helices H5 and H6 are bridged by IL3. In 1996, Farrens *et al.* (*43*) observed changes in the EPR spectra of site-directed spin labels incorporated at the cytoplasmic end of transmembrane helix H6 upon activation in rhodopsin. The EPR measurements were consistent with a displacement of the transmembrane helix (*43*). Since the pioneering EPR work, several crystal structures have been determined that capture GPCRs in both their active and inactive conformation (see Chapter 1 for details). The crystal structures confirm that displacement of H6 is a common feature of GPCR activation. In addition, the structures revealed changes in the rotational orientation of H5 between active and inactive receptor conformers. Motion of H5 and H6 provide an explanation for the structural changes that occur in the region of IL3 that allow active receptors to bind downstream signaling targets. The challenge is now to describe a molecular mechanism by which ligand binding at the extracellular surface can induce the H5 and H6 motion.

In Chapters 3 and 4, data are presented that described the motion of transmembrane helices H5 and H6. First, solid-state NMR measurements are presented that temporally separate the

motion of H6 in rhodopsin. In the dark, H6 is held in its inactive conformation via two interactions involving conserved residues: (i) an aromatic stacking interaction between the β-ionone ring of 11-*cis* retinal and the indole side chain of signature conserved residue Trp265$^{6.48}$ (ii) an ionic lock between Glu247$^{6.30}$ and Arg135$^{3.50}$. Upon retinal isomerization the interaction between Trp265$^{6.48}$ and β-ionone ring is lost (*173, 180*). A low-resolution cryo-electron microscopy structure of Meta I reveals changes the electron density assigned to the indole ring of Trp265$^{6.48}$, suggesting that its interaction with the β-ionone ring is lost in Meta I (*117*). The NMR data presented in Chapter 4 reveal that upon formation of the Meta I intermediate, the Arg135$^{3.50}$ – Glu247$^{6.30}$ is broken by a rotation of H6. However, this rotation does not allow H6 to adopt its fully active Meta II conformation. The rotation of H6 in the conversion to Meta I is demonstrated by the appearance of an NMR contact between Met257$^{6.30}$ and Arg135$^{3.50}$ in Meta I, that is not seen in rhodopsin. The change in a single ^{13}Cζ-Arg chemical shift observed between rhodopsin and Meta I provide strong evidence for disruption of the Glu247$^{6.30}$-Arg135$^{3.50}$ salt bridge.

The proposed disruption of the ionic lock in Meta I has implications for non-visual GPCRs. In ligand-activated GPCRs, the state of the ionic lock between Arg$^{3.50}$ and Glu$^{6.30}$ is an open question. Crystal structures of the β_2AR in the presence of inverse agonist carazolol for example do not reveal the formation of a salt bridge between Glu268$^{6.30}$ and Arg131$^{3.50}$ (*87*). However, computation studies of the β_2AR suggest that, in the presence of carazolol, there is conformational exchange between the open and closed states of the Glu268$^{6.30}$ and Arg131$^{3.50}$ interaction (*225*). A crystal structure of the β_1AR in the presence of an inverse agonist shows an ionic lock that is intact (*200, 288*). However, the β_1AR structure was solved using a suite of thermostablizing mutations that significantly reduced the basal activity of the receptor (*97*). As such, the presence of the ionic lock is restricted to receptors that have evolved a mechanism to tightly restrict basal activity. Therefore, we propose that the structural transition between Meta I and Meta II are more representative of what occurs when agonist binds to a ligand activated receptor.

Since the extent of signal amplification is determined, in part, by temporal stability of the signaling competent receptor species, it is also important to understand the interactions that are in place to stabilized the active state of GPCRs. The active state hydrogen bonding interaction

between Tyr223$^{5.58}$ and Arg135$^{3.50}$ provides an explanation for the strict sequence conservation of Tyr$^{5.58}$. Fluorescence spectroscopy demonstrates the role of the Tyr223$^{5.58}$ and Arg135$^{3.50}$ interaction in stabilizing the active conformation of H5. The impact that the Y223F mutant has on Meta II stability is much greater than what is observed in either the Y306F or the Y136F mutant. One interpretation is that the rotational orientation of H5 is important for receptor function. Another conserved residue on H5 is Lys231$^{5.63}$, whose side chain is hydrogen bonded to Glu247$^{6.30}$ upon disruption of the ionic lock. It may be the case that the rotation of Tyr223$^{5.58}$ provides the necessary structural changes in H5 to allow an interaction to form between Lys231$^{5.63}$ and Glu247$^{6.30}$. In this case, mutation of Tyr223$^{5.58}$ may destabilize Meta I, by prohibiting the carboxylate side chain of Glu247$^{6.30}$ from participating in a charge interaction. The end result would be a destabilization of the active state conformation of H6. One experiment that can be done to test this model is to target the Met257$^{6.40}$-Arg135$^{3.50}$ cross peak in Meta II of the Y223F mutant. The prediction would be that the internuclear distance between the side chains of these two residues is more akin to what is seen in Meta I rather than the close packing that we observe in Meta II. It would also be interesting to characterize the phenotype of a K23lL mutant where the rationale is that by eliminating a charged group at this residue, we are not allowing an interaction to stabilize the active state position of Glu247$^{6.30}$. As such, the Meta I/Meta II equilibrium as well as the Arg135$^{3.50}$-Met257$^{6.40}$ crosspeak in the K231L mutant should be probed.

6.2 Role of signature conserved tyrosine residues in rhodopsin activation.

There are three tyrosine residues that are conserved throughout all family A GPCRs. In rhodopsin these are (i) Tyr136$^{3.51}$ of the E/DRY motif of H3, (ii) Tyr223 of the Y(X)$_7$K/R motif, and (iii) Tyr306$^{7.53}$ of the NPxxY motif. The data present in Chapter 3 and recapitulated in the preceding section describe the role of Tyr223 in preserving active state stability to family A GPCRs. FTIR data collected in the lab of Klaus Peter Hofmann reveal that the obligate protonation switch of Glu134$^{3.49}$ is contingent on the presence of Tyr223$^{5.58}$, reflecting its role in satisfying the positive charge of Arg135$^{3.50}$ and disrupting the Glu134$^{3.49}$-Arg135$^{3.50}$ interaction (*289*). Based upon the rate of Meta II decay and transducin activity data, it would appear that Tyr306$^{7.53}$ and Tyr136$^{3.51}$ do not significantly contribute to lowering the energy of the active state. As such, their roles remain to be definitively characterized. Below, models based on the

kinetics of site-directed mutants of rhodopsin are presented for the roles of these two signature conserved residues and experiments are proposed to test them.

Tyr306. There are two features involving Tyr306 that help to stabilize the orientation of H7 in Meta II. The first is a hydrogen bonding interaction that extends through water molecules to H1 and H2. The second is the retinal chromophore. In its all-*trans* configuration, the interactions between retinal and the rest of the receptor are poised to stabilize H7. If the latter were correct, the Tyr306 may have a bigger role in stabilizing the active, low pH, conformation of opsin. In order test this idea, we can look at the pKa of the ops/ops* conformation equilibrium of the Y306F mutant and compare it to that of wild type opsin. The expectation is that the equilibrium is shifted in favor of the inactive conformer.

At physiological pH, the basal activity of opsin is on the order of 15%. The activity of opsin is likely to be proportional to the concentration of the active conformer. As such, if Tyr306 stabilizes the active opsin structure, then by inference it also must regulate the basal activity of opsin. It would be interesting to assess the signaling competence of the Y306F in opsin. Specifically, one can measure the binding affinity of the undecapeptide that corresponds to the carboxy terminal tail from the alpha subunit of transducin. This peptide has been co-crystallized with putative active conformations of rhodopsin. The prediction is that the opsin state of the Y306F mutant will display a weaker affinity for the peptide. Understanding the interactions that stabilize the active opsin structure can begin to elucidate a mechanistic understanding of basal activity in ligand activated family A GPCRs.

Tyr136. Tyr136 is the least conserved residue within the E/DRY motif; serine, histidine, and cysteine are found at this position in other family A GPCRs. Several mutational studies suggest that mutations at position 3.51 do not significantly alter receptor function both in terms of ligand affinity and heterotrimeric G protein binding in the melancortin receptor (*290*) and muscarinic acetylcholine receptor (*291*). Mutation of $Tyr^{3.51}$ has also been shown to decrease receptor expression in the chemokine receptor CCR3 (*196*). In the melanocortin receptor, the presence of serine at 3.51 is coincident with a reduced level of receptor internalization after activation (*290*). Given what appears to be a broad range of marginally altered phenotypes for mutants of $Tyr^{3.51}$, it is likely that the conservation of this residue serves a subfamily specific role and is worthy of further investigation. One possibility, is that in receptors where signaling must be under stringent

control, Tyr$^{3.51}$ is phosphorylated to serve as a binding site for arrestin molecules during clathrin mediated endocytosis. In rhodopsin however, the known phosphotyrosine residues that dock visual arrestin are in the unstructured carboxy terminus after the amphipathic helix H8 (*292*). However, rhodopsin signaling has evolved to be exquisitely regulated. One could use the AMBER (*293-296*) suppressor system to incorporate phosphotyrosine residues at position 136 in rhodopsin and ask the question: does this increase arrestin binding? Moreover does incorporated a phosophotyrosine at position 136 rescue arrestin binding of C terminal truncated mutants of rhodopsin (*297*)?

6.3 Perspectives on the mechanism of rhodopsin activation.

The role of Schiff base deprotonation in H3 motion. The work presented in Chapter 4 reveals that there is a significant change in the local environment of Arg135$^{3.50}$ upon conversion to the Meta I photointermediate. Arg135$^{3.50}$ is part of the signature conserved E/DRY sequence on transmembrane helix H3. In the dark state of rhodopsin, the sidechain of Arg135 forms an ionic interaction with neighboring Glu134$^{3.49}$ and Glu247$^{6.30}$ on H6 (*59*). The Glu134$^{3.49}$-Arg135$^{3.50}$ interaction is essential in preventing the inactive state of rhodopsin from coupling to transducin. As such, this interaction is not disrupted prior to formation of the active Meta II photointermediate (*56*). However, the NMR data in Chapter 4 suggest that ionic interaction between Arg135$^{3.50}$ and Glu247$^{6.30}$ is disrupted upon formation of Meta I, the penultimate photointermediate in rhodopsin activation.

In addition to the proposed rotation of H6, the NMR data are also consistent with structural changes of transmembrane helix H3. While it is true that the major structural changes occurring during GPCR activation are localized to transmembrane helices H5 and H6, there are indications that H3 is also involved. The role of transmembrane helix H3 is underscored by mutational studies that characterize receptor stability of site-directed mutants in the center of the transmembrane domain (*78*). In addition, cysteine scanning reveals changes in solvent accessibility for several residues of H3 upon rhodopsin activation. In the β_2AR, one of the more salient observations that come from comparing the intracellular regions of active and inactive receptor conformations is a ratcheting motion of H3 and H6, where the side chains of Phe282$^{6.42}$ on H6 and Ile123$^{3.42}$ on H3 seem to swap positions upon receptor activation via rotation of both helices. Arg135$^{3.50}$ is part of the conserved E/DRY sequence.

In addition to the signature conserve E/DRY sequence, the counterion of the Schiff base, Glu113$^{3.28}$, is located on H3. An obligate proton transfer between the protonated Schiff base that connects all-*trans* retinal to Lys296$^{7.43}$ in Meta I is transferred to Glu113$^{3.28}$ upon formation of the Meta II photointermediate. Mutation of Glu113$^{3.28}$ imparts constitutive activity in rhodopsin (*82, 298*). In the β_2AR receptor, a similar interaction is forged between the side change of Asp113$^{3.32}$ and the amine nitrogen of aminergic ligands. Mutation of Asp113$^{3.32}$ impaired the ability of partial agonists to activate the β_2AR (*231*). Clearly there is some specific ligand induced conformation change on H3 that modulates receptor activity.

One interpretation of the data is that the structural changes associated with Arg135$^{3.50}$ are coupled to a weakening of the Glu113$^{3.28}$-Lys296$^{7.43}$ interaction up photoactivation. In the dark, pKa of the protonated Schiff base is on the order of 14, due to its close associate of with the carboxylate side chain of Glu113. However, upon retinal isomerization the pKa drops to ~6 (*299*). Necessarily, this corresponds to a weakened interaction between Glu113$^{3.28}$ and Lys296$^{7.43}$. Weakening of the Glu113$^{3.28}$-Lys296$^{7.43}$ interaction may allow a slight rotation of H3 to facilitate disruption of the Arg135$^{3.50}$-Glu247$^{6.30}$ interaction in Meta I. Breaking of the Arg135$^{3.50}$-Glu247$^{6.30}$ interaction in Meta I, allows the subsequent displacement of H6 in the transition to Meta II (see below for a more detailed account of how H6 may be displaced). In Meta I, the charged guanidium group of Arg135$^{3.50}$ is not fully compensated. In Meta II partial charges on the phenol sidechains of Tyr223$^{5.58}$ and 306$^{7.53}$ compensated for the missing Arg135$^{3.50}$-Glu247$^{6.30}$ interaction and allow the sidechain of Glu134$^{3.49}$ to be protonated.

In order to verify this model, markers for H3 motion need to be probed in both Meta I and Meta II. Solid-state NMR data have already been collected that suggest a change in the region around Gly120 and Gly121. In fact, the Ernst crystal structure of reversibly formed Meta II would suggest that the orientation of all-*trans* retinal in Meta II, induces steric contacts between The C20 methyl and residues in the center of transmembrane helix H3. If correct, these contacts provide addition support for a motion of H3. One potential experiment would be to measure the internuclear distance between the side chain of Phe261$^{6.44}$ and the backbone carbonyls of Gly121$^{3.36}$ and Leu125$^{3.40}$ in rhodopsin and Meta I.

The interaction between the β-ionone ring and Trp265$^{6.48}$ acts a 'pin' to restrict the motion of H6. Trp265$^{6.48}$ is signature conserved residue within family A GPCRs and part of CWxP motif that is thought to mediate motion of H6 upon receptor activation (*111*). In ligand activated receptors the side of Trp$^{6.48}$ is packed against the side chain a conserved alanine residue (*115*). The crystal structure of the β_2AR also confirmed that the Phe$^{6.52}$ is in close contact with the ligand, and therefore can transduce small molecule binding to the side chain of Trp286$^{6.48}$. In rhodopsin the residue at position 6.52 is Ala269. The absence of a bulky side chain at position 6.52 is one of the features that let 11-*cis* retinal penetrate deeper into the transmembrane core of the binding pocket and interact directly with the indole side chain of Trp265$^{6.48}$. Substituting a phenylalanine at position 269 in rhodopsin increases basal activity (*300*). In this sense, a direct interaction between Trp265$^{6.48}$ and the retinal chromophore is required in order for the receptor to differentiate between isomeric states and induce receptor activation in the presence of all-*trans* retinal. In rhodopsin, modulating the interaction between the β-ionone ring and Trp265$^{6.48}$ is essential for receptor activation. There are two major details that prevent an accurate understanding of this interaction. First, how is the Trp265$^{6.48}$-retinal interaction altered upon receptor activation? As summarized in Chapter 5, the two competing models call for either a change about the χ_1 torsion angle of Trp265$^{6.48}$ upon retinal isomerization, or a change in the orientation of the β-ionone ring as proposed by the crystal structure of reversibly formed Meta II. The data presented in Chapter 5 suggest a close interaction between Phe261$^{6.44}$ and the C18 methyl group of retinal and argue against the orientation of the β-ionone ring in the crystal structure in Meta II. When coupled with the presence of a strong contact between Trp265$^{6.48}$ and the C19 methyl group in Meta II, the Phe261$^{6.44}$-C18 contact is consistent a change in side chain orientation for Trp265$^{6.48}$.

Phe261$^{6.44}$ is also a signature conserve residue. The NMR data suggest that the β-ionone ring becomes closer to the side chain of Phe261$^{6.44}$. One interpretation of the NMR data is that retinal isomerization drives the C18 methyl within Van der Waals contact with Phe261$^{6.44}$, and helps to induce motion of H6. This idea can be verified by looking for NMR contacts between Phe261$^{6.44}$ and the C18 retinal methyl group in Meta I. If shown to be correct, the interaction would provide insight into why site directed mutations that reduce the side chain volume at position 261 lower light dependent activation of rhodopsin (*301*).

As mentioned earlier, the nuclei in the side chain of Trp265$^{6.48}$ have the lowest thermal factors of all the residues in rhodopsin, indicating a rigid and well-ordered structure. This is likely due to the interaction with the β-ionone ring of retinal. It may by the case that Schiff base formation with 11-*cis* retinal 'pushes' the indole ring in a manner that 'springloads' H6. When retinal isomerizes and the indole-ionone ring packing interaction is lost, the energy is dissipated via slight rotation of transmembrane helix H6. In the dark, H6 contains a 30° kink about signature conserved Pro267$^{6.50}$. Analyzing backbone chemical shifts in this region of the receptor (see Chapter 5) suggest that the overall secondary structure does not change, and the kink is preserved after photoactivation. Due to the persistence of proline kink upon activation, a slight rotation of H6 in the retinal binding pocket is amplified to a displacement of the transmembrane helix at the cytosolic surface. In addition, a water mediated hydrogen bonding network that links the indole nitrogen of Trp265$^{6.48}$ with Asn302$^{7.49}$ of the NPxxY motif on H7 serves to couple the rotation of H6 with the structural changes that allow Tyr306$^{7.53}$ to rotate inwards towards the transmembrane core where it interacts with Arg135$^{3.50}$ in Meta II.

Changes EL2/EL3 interactions are a feature of rhodopsin activation. The extracellular surface of rhodopsin is made up of a well structured random coiled amino-terminus, and three extracellular loops (EL1, EL2 and EL3). The extracellular loops bridge transmembrane helices H2-H3, H4-H5, and H6-H7 respectively. EL1 is relatively short and is part of the stable H1-H4 core. In contrast EL2 is 27 residues long and contains two short stretches of amino acids that adopt β sheet secondary structure β3 and β4. The β4 strand is buried within the transmembrane core and packs against the retinal chromophore in its 11-*cis* conformation. Reconstitution studies that regenerated rhodopsin from two fragments bisected at EL2 showed that proper loop folding is both necessary and sufficient to confer receptor stability (*302*). Given its position relative to the ligand binding pocket, EL2 is thought to be important in receptor function across GPCRs (*303-311*). EL3 is situated between the amino terminal tail and the extracellular surface of EL2.

Previously collected solid-state NMR measurements were interpreted in terms of a motion of EL2 away from the retinal upon rhodopsin activation (*172*). EL2 motion is consistent with an increased solvent accessibility of the retinal Schiff based in Meta II (*269*). However, the

crystal structures of reversibly formed and constitutively active Meta II intermediates do not show a displacement of EL2 with respect to its position in the dark state. As such, the role of EL2 in rhodopsin activation remains an open question.

Given the close association between the EL2 and EL3 – and in turn, the amino terminus – the proposed motion of EL2 requires a rearrangement of the EL3. In Chapter 5 we addressed the motion of EL2 in the context of a stable rhodopsin mutant (N2C, D282C). In the stable mutant a disulfide bridge tethers the amino-terminal tail to EL3 and restricts the motion of EL2. In Chapter 5 we compare NMR markers for EL2 motion (i.e. ^{13}Cζ-Tyr difference spectra and ^{13}Cβ-Cys187 chemical shift) collected on the stable mutant and compared them wildtype data. The observation that our markers for EL2 motion are not reproduced in the stable mutant has several implications. First, it strengthens confidence in their ability to report EL2 motion. In addition, it shows that EL2 motion does not occur in the stable mutant.

However, the N2C, D282C mutant retains over 90% transducin activity when compared to wild type, suggested that EL2 motion is not necessary for signal transduction in rhodopsin. One possibility for the apparent insensitivity of signaling to the activation-induced motion of EL2 in rhodopsin has to do with the unique features of the visual receptor. In rhodopsin, the retinal ligand occupies a deeper binding pocket than ligands observed in crystal structure of other GPCRs and is allowed to interact directly with H5 to induce helix rotation. The NMR data showing the active state Met257$^{6.40}$-Tyr223$^{5.58}$ contact in the stable mutant is consistent with H5 rotation in the absence of EL2 motion.

In ligand activated receptors, EL2 is oriented away from the transmembrane core towards the extracellular surface and has been characterized as having ligand-determining characteristics. One explanation is that in non-visual GPCRs, EL2 does not intercalate into the transmembrane core in order to allow diffusible ligands in the bulk solvent to enter the ligand binding pocket. In this case, specific interactions between individual ligands and EL2 may serve to initiate the motion of associated transmembrane helix H5.

References

1. Kolakowski, L. F. (1994) Gcrdb - a G-protein-coupled receptor database, *Receptors Channels 2*, 1-7.
2. Bockaert, J., and Pin, J. P. (1999) Molecular tinkering of G protein-coupled receptors: An evolutionary success, *EMBO J. 18*, 1723-1729.
3. Foord, S. M., Bonner, T. I., Neubig, R. R., Rosser, E. M., Pin, J. P., Davenport, A. P., Spedding, M., and Harmar, A. J. (2005) International Union of Pharmacology. XLVI. G protein-coupled receptor list, *Pharmacol. Rev. 57*, 279-288.
4. Miller, L. J., Dong, M., Harikumar, K. G., and Gao, F. (2007) Structural basis of natural ligand binding and activation of the Class II G-protein-coupled secretin receptor, *Biochem. Soc. Trans. 35*, 709-712.
5. Markovic, D., and Grammatopoulos, D. K. (2009) Focus on the splicing of Secretin GPCRs transmembrane-domain 7, *Trends Biochem. Sci. 34*, 443-452.
6. Bräuner-Osborne, H., Wellendorph, P., and Jensen, A. A. (2007) Structure, pharmacology and therapeutic prospects of family C G-protein coupled receptors, *Curr. Drug Targets 8*, 169-184.
7. Karakas, E., Simorowski, N., and Furukawa, H. (2009) Structure of the zinc-bound amino-terminal domain of the NMDA receptor NR2B subunit, *EMBO J. 28*, 3910-3920.
8. Kothe, E. (2008) Sexual attraction: On the role of fungal pheromone/receptor systems (A review), *Acta Microbiologica et Immunologica Hungarica 55*, 125-143.
9. Klein, P. S., Sun, T. J., Saxe, C. L., Kimmel, A. R., Johnson, R. L., and Devreotes, P. N. (1988) A chemoattractant receptor controls development in *Dictyostelium discoideum*, *Science 241*, 1467-1472.
10. Johnson, R. L., Saxe, C. L., Gollop, R., Kimmel, A. R., and Devreotes, P. N. (1993) Identification and targeted gene disruption of cAR3, a cAMP receptor subtype expressed during multicellular stages of *Dictyostelium* development, *Genes Dev. 7*, 273-282.
11. Fredriksson, R., Lagerström, M. C., Lundin, L. G., and Schiöth, H. B. (2003) The G-protein-coupled receptors in the human genome form five main families. Phylogenetic analysis, paralogon groups, and fingerprints, *Mol. Pharmacol. 63*, 1256-1272.
12. Huang, H. C., and Klein, P. S. (2004) The Frizzled family: receptors for multiple signal transduction pathways, *Genome Biology 5*, 234.
13. Bayburt, T. H., Vishnivetskiy, S. A., McLean, M. A., Morizumi, T., Huang, C. C., Tesmer, J. J. G., Ernst, O. P., Sligar, S. G., and Gurevich, V. V. (2011) Monomeric rhodopsin is sufficient for normal rhodopsin kinase (GRK1) phosphorylation and arrestin-1 binding, *J. Biol. Chem. 286*, 1420-1428.
14. Tesmer, V. M., Kawano, T., Shankaranarayanan, A., Kozasa, T., and Tesmer, J. J. G. (2005) Snapshot of activated G proteins at the membrane: The $G\alpha_q$-GRK2-$G\beta\gamma$ complex, *Science 310*, 1686-1690.
15. Zhao, X. Y., Huang, J., Khani, S. C., and Palczewski, K. (1998) Molecular forms of human rhodopsin kinase (GRK1), *J. Biol. Chem. 273*, 5124-5131.

16. Peppel, K., Boekhoff, I., Mcdonald, P., Breer, H., Caron, M. G., and Lefkowitz, R. J. (1997) G protein-coupled receptor kinase 3 (GRK3) gene disruption leads to loss of odorant receptor desensitization, *J. Biol. Chem. 272*, 25425-25428.

17. Shukla, A. K., Xiao, K. H., and Lefkowitz, R. J. (2011) Emerging paradigms of β-arrestin-dependent seven transmembrane receptor signaling, *Trends Biochem. Sci. 36*, 457-469.

18. Shenoy, S. K., and Lefkowitz, R. J. (2011) β-arrestin-mediated receptor trafficking and signal transduction, *Trends Pharmacol. Sci. 32*, 521-533.

19. Kim, M., Hanson, S. M., Vishnivetskiy, S. A., Song, X. F., Cleghorn, W. M., Hubbell, W. L., and Gurevich, V. V. (2011) Robust self-association is a common feature of mammalian visual arrestin-1, *Biochemistry 50*, 2235-2242.

20. Hanson, S. M., Gurevich, E. V., Vishnivetskiy, S. A., Ahmed, M. R., Song, X. F., and Gurevich, V. V. (2007) Each rhodopsin molecule binds its own arrestin, *Proc. Natl. Acad. Sci. U. S. A. 104*, 3125-3128.

21. Benovic, J. L., Kühn, H., Weyand, I., Codina, J., Caron, M. G., and Lefkowitz, R. J. (1987) Functional desensitization of the isolated β-adrenergic-receptor by the β-adrenergic-receptor kinase - Potential role of an analog of the retinal protein arrestin (48-kDa protein), *Proc. Natl. Acad. Sci. U. S. A. 84*, 8879-8882.

22. Benovic, J. L., Onorato, J. J., Caron, M. G., and Lefkowitz, R. J. (1990) Regulation of G protein-coupled receptors by agonist-dependent phosphorylation, *Society of General Physiologists Series 45*, 87-103.

23. Overington, J. P., Al-Lazikani, B., and Hopkins, A. L. (2006) Opinion - How many drug targets are there?, *Nature Reviews Drug Discovery 5*, 993-996.

24. Ma, P., and Zemmel, R. (2002) Value of novelty?, *Nature Reviews Drug Discovery 1*, 571-572.

25. Lagerström, M. C., and Schiöth, H. B. (2008) Structural diversity of G protein-coupled receptors and significance for drug discovery, *Nature Reviews Drug Discovery 7*, 339-357.

26. Rao, V. R., and Oprian, D. D. (1996) Activating mutations of rhodopsin and other G protein-coupled receptors, *Annu. Rev. Biophys. Biomol. Struct. 25*, 287-314.

27. Saunders, J. (2005) G-protein-coupled receptors in drug discovery, *Bioorganic & Medicinal Chemistry Letters 15*, 3653-3653.

28. Samson, M., Libert, F., Doranz, B. J., Rucker, J., Liesnard, C., Farber, C. M., Saragosti, S., Lapoumeroulie, C., Cognaux, J., Forceille, C., Muyldermans, G., Verhofstede, C., Burtonboy, G., Georges, M., Imai, T., Rana, S., Yi, Y. J., Smyth, R. J., Collman, R. G., Doms, R. W., Vassart, G., and Parmentier, M. (1996) Resistance to HIV-1 infection in caucasian individuals bearing mutant alleles of the CCR-5 chemokine receptor gene, *Nature 382*, 722-725.

29. Alkhatib, G., Combadiere, C., Broder, C. C., Feng, Y., Kennedy, P. E., Murphy, P. M., and Berger, E. A. (1996) CC CKR5: A RANTES, MIP-1α, MIP-1β receptor as a fusion cofactor for macrophage-tropic HIV-1, *Science 272*, 1955-1958.

30. Feng, Y., Broder, C. C., Kennedy, P. E., and Berger, E. A. (1996) HIV-1 entry cofactor: Functional cDNA cloning of a seven-transmembrane, G protein-coupled receptor, *Science 272*, 872-877.

31. Amara, A., LeGall, S., Schwartz, O., Salamero, J., Montes, M., Loetscher, P., Baggiolini, M., Virelizier, J. L., and Arenzana-Seisdedos, F. (1997) HIV coreceptor downregulation as antiviral principle: SDF-1α-dependent internalization of the chemokine receptor CXCR4 contributes to inhibition of HIV replication, *Journal of Experimental Medicine 186*, 139-146.

32. Dorr, P., Westby, M., Dobbs, S., Griffin, P., Irvine, B., Macartney, M., Mori, J., Rickett, G., Smith-Burchnell, C., Napier, C., Webster, R., Armour, D., Price, D., Stammen, B., Wood, A., and Perros, M. (2005) Maraviroc (UK-427,857), a potent, orally bioavailable, and selective small-molecule inhibitor of chemokine receptor CCR5 with broad-spectrum anti-human immunodeficiency virus type 1 activity, *Antimicrobial Agents and Chemotherapy 49*, 4721-4732.

33. De Lean, A., Stadel, J. M., and Lefkowitz, R. J. (1980) A ternary complex model explains the agonist-specific binding-properties of the adenylate cyclase-coupled β-adrenergic-receptor, *J. Biol. Chem. 255*, 7108-7117.

34. Samama, P., Cotecchia, S., Costa, T., and Lefkowitz, R. J. (1993) A mutation-induced activated state of the β_2-adrenergic receptor, *J. Biol. Chem. 268*, 4625-4636.

35. Hermans, E. (2003) Biochemical and pharmacological control of the multiplicity of coupling at G-protein-coupled receptors, *Pharmacol. Ther. 99*, 25-44.

36. Cordeaux, Y., Nickolls, S. A., Flood, L. A., Graber, S. G., and Strange, P. G. (2001) Agonist regulation of D-2 dopamine receptor/G protein interaction - Evidence for agonist selection of G protein subtype, *J. Biol. Chem. 276*, 28667-28675.

37. Kobilka, B. K., and Deupi, X. (2007) Conformational complexity of G-protein-coupled receptors, *Trends Pharmacol. Sci. 28*, 397-406.

38. Gether, U. (2000) Uncovering molecular mechanisms involved in activation of G protein-coupled receptors, *Endocr. Rev. 21*, 90-113.

39. Sakmar, T. P., Menon, S. T., Marin, E. P., and Awad, E. S. (2002) Rhodopsin: Insights from recent structural studies, *Annu. Rev. Biophys. Biomol. Struct. 31*, 443-484.

40. Palczewski, K. (2006) G protein-coupled receptor rhodopsin, *Annu. Rev. Biochem. 75*, 743-767.

41. Schwartz, T. W., Frimurer, T. M., Holst, B., Rosenkilde, M. M., and Elling, C. E. (2006) Molecular mechanism of 7TM receptor activation - A global toggle switch model, *Annu. Rev. Pharmacol. Toxicol. 46*, 481-519.

42. Rosenbaum, D. M., Rasmussen, S. G. F., and Kobilka, B. K. (2009) The structure and function of G-protein-coupled receptors, *Nature 459*, 356-363.

43. Farrens, D. L., Altenbach, C., Yang, K., Hubbell, W. L., and Khorana, H. G. (1996) Requirement of rigid-body motion of transmembrane helices for light activation of rhodopsin, *Science 274*, 768-770.

44. Altenbach, C., Klein-Seetharaman, J., Cai, K. W., Khorana, H. G., and Hubbell, W. L. (2001) Structure and function in rhodopsin: Mapping light-dependent changes in distance between residue 316 in helix 8 and residues in the sequence 60-75, covering the cytoplasmic end of helices TM1 and TM2 and their connection loop CL1, *Biochemistry 40*, 15493-15500.

45. Altenbach, C., Cai, K. W., Klein-Seetharaman, J., Khorana, F. G., and Hubbell, W. L. (2001) Structure and function in rhodopsin: Mapping light-dependent changes in distance between residue 65 in helix TM1 and residues in the sequence 306-319 at the cytoplasmic end of helix TM7 and in helix H8, *Biochemistry 40*, 15483-15492.

46. Knierim, B., Hofmann, K. P., Ernst, O. P., and Hubbell, W. L. (2007) Sequence of late molecular events in the activation of rhodopsin, *Proc. Natl. Acad. Sci. U. S. A. 104*, 20290-20295.

47. Altenbach, C., Kusnetzow, A. K., Ernst, O. P., Hofmann, K. P., and Hubbell, W. L. (2008) High-resolution distance mapping in rhodopsin reveals the pattern of helix movement due to activation, *Proc. Natl. Acad. Sci. U. S. A. 105*, 7439-7444.

48. Dunham, T. D., and Farrens, D. L. (1999) Conformational changes in rhodopsin - Movement of helix F detected by site-specific chemical labeling and fluorescence spectroscopy, *J. Biol. Chem. 274*, 1683-1690.

49. Yao, X. J., Parnot, C., Deupi, X., Ratnala, V. R. P., Swaminath, G., Farrens, D., and Kobilka, B. (2006) Coupling ligand structure to specific conformational switches in the β_2-adrenoceptor, *Nat. Chem. Biol. 2*, 417-422.

50. Granier, S., Kim, S., Shafer, A. M., Ratnala, V. R. P., Fung, J. J., Zare, R. N., and Kobilka, B. (2007) Structure and conformational changes in the C-terminal domain of the β_2-adrenoceptor - Insights from fluorescence resonance energy transfer studies, *J. Biol. Chem. 282*, 13895-13905.

51. Chabre, M., and Breton, J. (1979) Orientation of aromatic residues in rhodopsin. Rotation of one tryptophan upon the meta I to meta II transition after illumination, *Photochem. Photobiol. 30*, 295-299.

52. Lin, S. W., and Sakmar, T. P. (1996) Specific tryptophan UV-absorbance changes are probes of the transition of rhodopsin to its active state, *Biochemistry 35*, 11149-11159.

53. Fahmy, K., Jäger, F., Beck, M., Zvyaga, T. A., Sakmar, T. P., and Siebert, F. (1993) Protonation states of membrane-embedded carboxylic acid groups in rhodopsin and metarhodopsin II: A Fourier-transform infrared spectroscopy study of site-directed mutants, *Proc. Natl. Acad. Sci. U. S. A. 90*, 10206-10210.

54. Rath, P., DeCaluwe, L. L. J., Bovee-Geurts, P. H. M., Degrip, W. J., and Rothschild, K. J. (1993) Fourier transform infrared difference spectroscopy of rhodopsin mutants: light activation of rhodopsin causes hydrogen-bonding change in residue aspartic acid-83 during meta II formation, *Biochemistry 32*, 10277-10282.

55. Arnis, S., Fahmy, K., Hofmann, K. P., and Sakmar, T. P. (1994) A conserved carboxylic acid group mediates light-dependent proton uptake and signaling by rhodopsin, *J. Biol. Chem. 269*, 23879-23881.

56. Fahmy, K., Sakmar, T. P., and Siebert, F. (2000) Transducin-dependent protonation of glutamic acid 134 in rhodopsin, *Biochemistry 39*, 10607-10612.

57. Vogel, R., Siebert, F., Mathias, G., Tavan, P., Fan, G. B., and Sheves, M. (2003) Deactivation of rhodopsin in the transition from the signaling state Meta II to Meta III involves a thermal isomerization of the retinal chromophore C=N double bond, *Biochemistry 42*, 9863-9874.

58. Lehmann, N., Alexiev, U., and Fahmy, K. (2007) Linkage between the intramembrane H-bond network around aspartic acid 83 and the cytosolic environment of helix 8 in photoactivated rhodopsin, *J. Mol. Biol. 366*, 1129-1141.

59. Vogel, R., Mahalingam, M., Lüdeke, S., Huber, T., Siebert, F., and Sakmar, T. P. (2008) Functional role of the "Ionic Lock" - An interhelical hydrogen-bond network in family a heptahelical receptors, *J. Mol. Biol. 380*, 648-655.

60. Mahalingam, M., Martinez-Mayorga, K., Brown, M. F., and Vogel, R. (2008) Two protonation switches control rhodopsin activation in membranes, *Proc. Natl. Acad. Sci. U. S. A. 105*, 17795-17800.

61. Lüdeke, S., Mahalingam, M., and Vogel, R. (2009) Rhodopsin activation switches in a native membrane environment, *Photochem. Photobiol. 85*, 437-441.

62. Lin, S. W., Sakmar, T. P., Franke, R. R., Khorana, H. G., and Mathies, R. A. (1992) Resonance Raman microprobe spectroscopy of rhodopsin mutants: Effect of substitutions in the third transmembrane helix, *Biochemistry 31*, 5105-5111.

63. Yan, E. C. Y., Kazmi, M. A., Ganim, Z., Hou, J. M., Pan, D. H., Chang, B. S. W., Sakmar, T. P., and Mathies, R. A. (2003) Retinal counterion switch in the photoactivation of the G protein-coupled receptor rhodopsin, *Proc. Natl. Acad. Sci. U. S. A. 100*, 9262-9267.

64. Kukura, P., McCamant, D. W., Yoon, S., Wandschneider, D. B., and Mathies, R. A. (2005) Structural observation of the primary isomerization in vision with femtosecond-stimulated Raman, *Science 310*, 1006-1009.

65. AbdAlla, S., Zaki, E., Lother, H., and Quitterer, U. (1999) Involvement of the amino terminus of the B-2 receptor in agonist-induced receptor dimerization, *J. Biol. Chem. 274*, 26079-26084.

66. Wheatley, M., and Hawtin, S. R. (1999) Glycosylation of G-protein-coupled receptors for hormones central to normal reproductive functioning: its occurrence and role, *Hum. Reprod. Update 5*, 356-364.

67. Tansky, M. F., Pothoulakis, C., and Leeman, S. E. (2007) Functional consequences of alteration of N-linked glycosylation sites on the neurokinin 1 receptor, *Proc. Natl. Acad. Sci. U. S. A. 104*, 10691-10696.

68. Rands, E., Candelore, M. R., Cheung, A. H., Hill, W. S., Strader, C. D., and Dixon, R. A. F. (1990) Mutational analysis of β-adrenergic receptor glycosylation, *J. Biol. Chem. 265*, 10759-10764.

69. Kunishima, N., Shimada, Y., Tsuji, Y., Sato, T., Yamamoto, M., Kumasaka, T., Nakanishi, S., Jingami, H., and Morikawa, K. (2000) Structural basis of glutamate recognition by a dimeric metabotropic glutamate receptor, *Nature 407*, 971-977.

70. Tsuchiya, D., Kunishima, N., Kamiya, N., Jingami, H., and Morikawa, K. (2002) Structural views of the ligand-binding cores of a metabotropic glutamate receptor complexed with an antagonist and both glutamate and Gd3+, *Proc. Natl. Acad. Sci. U. S. A. 99*, 2660-2665.

71. Rajagopalan, L., and Rajarathnam, K. (2006) Structural basis of chemokine receptor function - A model for binding affinity and ligand selectivity, *Bioscience Reports 26*, 325-339.

72. Adams, M. N., Ramachandran, R., Yau, M. K., Suen, J. Y., Fairlie, D. P., Hollenberg, M. D., and Hooper, J. D. (2011) Structure, function and pathophysiology of protease activated receptors, *Pharmacol. Ther. 130*, 248-282.

73. Kaushal, S., Ridge, K. D., and Khorana, H. G. (1994) Structure and function in rhodopsin: The role of asparagine-linked glycosylation, *Proc. Natl. Acad. Sci. U. S. A. 91*, 4024-4028.

74. Cha, K. W., Reeves, P. J., and Khorana, H. G. (2000) Structure and function in rhodopsin: Destabilization of rhodopsin by the binding of an antibody at the N-terminal segment provides support for involvement of the latter in an intradiscal tertiary structure, *Proc. Natl. Acad. Sci. U. S. A. 97*, 3016-3021.

75. Yun, R. H., Anderson, A., and Hermans, J. (1991) Proline in alpha-helix: Stability and conformation studied by dynamics simulation, *Proteins: Structure, Function, and Genetics 10*, 219-228.

76. Williams, K. A., and Deber, C. M. (1991) Proline residues in transmembrane helices: Structural or dynamic role?, *Biochemistry 30*, 8919-8923.

77. Liu, W., Eilers, M., Patel, A. B., and Smith, S. O. (2004) Helix packing moments reveal diversity and conservation in membrane protein structure, *J. Mol. Biol. 337*, 713-729.

78. Han, M., Lin, S. W., Smith, S. O., and Sakmar, T. P. (1996) The effects of amino acid replacements of glycine 121 on transmembrane helix 3 of rhodopsin, *J. Biol. Chem. 271*, 32330-32336.

79. Ballesteros, J. A., and Weinstein, H. (1995) Integrated methods for the construction of three dimensional models and computational probing of structure-function relations in G-protein coupled receptors, *Methods Neurosci. 25*, 366-428.

80. Chelikani, P., Hornak, V., Eilers, M., Reeves, P. J., Smith, S. O., RajBhandary, U. L., and Khorana, H. G. (2007) Role of group-conserved residues in the helical core of β_2-adrenergic receptor, *Proc. Natl. Acad. Sci. U. S. A. 104*, 7027-7032.

81. Sakmar, T. P., Franke, R. R., and Khorana, H. G. (1989) Glutamic acid-113 serves as the retinylidene Schiff base counterion in bovine rhodopsin, *Proc. Natl. Acad. Sci. U. S. A. 86*, 8309-8313.

82. Sakmar, T. P., Franke, R. R., and Khorana, H. G. (1991) The role of the retinylidene Schiff base counterion in rhodopsin in determining wavelength absorbance and Schiff base pKa, *Proc. Natl. Acad. Sci. U. S. A. 88*, 3079-3083.

83. Javitch, J. A., Fu, D., and Chen, J. (1996) Differentiating dopamine D2 ligands by their sensitivities to modification of the cysteine exposed in the binding-site crevice, *Mol. Pharmacol. 49*, 692-698.

84. Javitch, J. A., Fu, D., Chen, J., and Karlin, A. (1995) Mapping the binding-site crevice of the dopamine D2 receptor by the substituted-cysteine accessibility method, *Neuron 14*, 825-831.

85. Javitch, J. A., Li, X., Kaback, J., and Karlin, A. (1994) A cysteine residue in the third membrane-spanning segment of the human D2 dopamine receptor is exposed in the binding-site crevice, *Proc. Natl. Acad. Sci. U. S. A. 91*, 10355-10359.

86. Rasmussen, S. G. F., Choi, H. J., Fung, J. J., Pardon, E., Casarosa, P., Chae, P. S., DeVree, B. T., Rosenbaum, D. M., Thian, F. S., Kobilka, T. S., Schnapp, A., Konetzki, I., Sunahara, R. K., Gellman, S. H., Pautsch, A., Steyaert, J., Weis, W. I., and Kobilka, B. K. (2011) Structure of a nanobody-stabilized active state of the β_2 adrenoceptor, *Nature 469*, 175-180.

87. Rasmussen, S. G. F., Choi, H. J., Rosenbaum, D. M., Kobilka, T. S., Thian, F. S., Edwards, P. C., Burghammer, M., Ratnala, V. R. P., Sanishvili, R., Fischetti, R. F., Schertler, G. F. X., Weis, W. I., and Kobilka, B. K. (2007) Crystal structure of the human β_2 adrenergic G-protein-coupled receptor, *Nature 450*, 383-387.

88. Weiss, E. R., Kelleher, D. J., and Johnson, G. L. (1988) Mapping sites of interaction between rhodopsin and transducin using rhodopsin antipeptide antibodies, *J. Biol. Chem. 263*, 6150-6154.

89. Weiss, E. R., Hadcock, J. R., Johnson, G. L., and Malbon, C. C. (1987) Antipeptide antibodies directed against cytoplasmic rhodopsin sequences recognize the β-adrenergic-receptor, *J. Biol. Chem. 262*, 4319-4323.

90. Krupnick, J. G., Gurevich, V. V., Schepers, T., Hamm, H. E., and Benovic, J. L. (1994) Arrestin-rhodopsin interaction: Multi-site binding delineated by peptide inhibition, *J. Biol. Chem. 269*, 3226-3232.

91. Cheung, A. H., Huang, R. R., and Strader, C. D. (1992) Involvement of specific hydrophobic, but not hydrophilic, amino acids in the third intracellular loop of the β-adrenergic receptor in the activation of G_s, *Mol. Pharmacol. 41*, 1061-1065.

92. Högger, P., Shockley, M. S., Lameh, J., and Sadée, W. (1995) Activating and inactivating mutations in N-terminal and C-terminal I3 loop junctions of muscarinic acetylcholine Hm1 receptors, *J. Biol. Chem. 270*, 7405-7410.

93. Deupi, X., Edwards, P., Singhal, A., Nickle, B., Oprian, D., Schertler, G., and Standfuss, J. (2012) Stabilized G protein binding site in the structure of constitutively active metarhodopsin-II, *Proc. Natl. Acad. Sci. U. S. A. 109*, 119-124.

94. Standfuss, J., Edwards, P. C., D'Antona, A., Fransen, M., Xie, G., Oprian, D. D., and Schertler, G. F. (2011) The structural basis of agonist-induced activation in constitutively active rhodopsin, *Nature 471*, 656-660.

95. Scheerer, P., Park, J. H., Hildebrand, P. W., Kim, Y. J., Krauss, N., Choe, H. W., Hofmann, K. P., and Ernst, O. P. (2008) Crystal structure of opsin in its G-protein-interacting conformation, *Nature 455*, 497-502.

96. Goncalves, J. A., South, K., Ahuja, S., Zaitseva, E., Opefi, C. A., Eilers, M., Vogel, R., Reeves, P. J., and Smith, S. O. (2010) Highly conserved tyrosine stabilizes the active state of rhodopsin, *Proc. Natl. Acad. Sci. U. S. A. 107*, 19861-19866.

97. Warne, T., Serrano-Vega, M. J., Tate, C. G., and Schertler, G. F. X. (2009) Development and crystallization of a minimal thermostabilised G protein-coupled receptor, *Protein Expression Purif. 65*, 204-213.

98. Palczewski, K., Kumasaka, T., Hori, T., Behnke, C. A., Motoshima, H., Fox, B. A., Le Trong, I., Teller, D. C., Okada, T., Stenkamp, R. E., Yamamoto, M., and Miyano, M. (2000) Crystal structure of rhodopsin: A G protein-coupled receptor, *Science 289*, 739-745.

99. Patel, A. B., Crocker, E., Reeves, P. J., Getmanova, E. V., Eilers, M., Khorana, H. G., and Smith, S. O. (2005) Changes in interhelical hydrogen bonding upon rhodopsin activation, *J. Mol. Biol. 347*, 803-812.

100. Patel, A. B., Crocker, E., Eilers, M., Hirshfeld, A., Sheves, M., and Smith, S. O. (2004) Coupling of retinal isomerization to the activation of rhodopsin, *Proc. Natl. Acad. Sci. U. S. A. 101*, 10048-10053.

101. Ambrosio, C., Molinari, P., Cotecchia, S., and Costa, T. (2000) Catechol-binding serines of β_2-adrenergic receptors control the equilibrium between active and inactive receptor states, *Mol. Pharmacol. 57*, 198-210.

102. Liapakis, G., Chan, W. C., Papadokostaki, M., and Javitch, J. A. (2004) Synergistic contributions of the functional groups of epinephrine to its affinity and efficacy at the β_2 adrenergic receptor, *Mol. Pharmacol. 65*, 1181-1190.

103. Liapakis, G., Ballesteros, J. A., Papachristou, S., Chan, W. C., Chen, X., and Javitch, J. A. (2000) The forgotten serine - A critical role for Ser-203(5.42) in ligand binding to and activation of the β_2-adrenergic receptor, *J. Biol. Chem. 275*, 37779-37788.

104. Strader, C. D., Candelore, M. R., Hill, W. S., Sigal, I. S., and Dixon, R. A. F. (1989) Identification of two serine residues involved in agonist activation of the β-adrenergic receptor, *J. Biol. Chem. 264*, 13572-13578.

105. Pollock, N. J., Manelli, A. M., Hutchins, C. W., Steffey, M. E., Mackenzie, R. G., and Frail, D. E. (1992) Serine mutations in transmembrane V of the dopamine D1 receptor affect ligand interactions and receptor activation, *J. Biol. Chem. 267*, 17780-17786.

106. Sheikh, S. P., Zvyaga, T. A., Lichtarge, O., Sakmar, T. P., and Bourne, H. R. (1996) Rhodopsin activation blocked by metal-ion-binding sites linking transmembrane helices C and F, *Nature 383*, 347-350.

107. Park, J. H., Scheerer, P., Hofmann, K. P., Choe, H. W., and Ernst, O. P. (2008) Crystal structure of the ligand-free G-protein-coupled receptor opsin, *Nature 454*, 183-187.

108. Choe, H. W., Kim, Y. J., Park, J. H., Morizumi, T., Pai, E. F., Krauss, N., Hofmann, K. P., Scheerer, P., and Ernst, O. P. (2011) Crystal structure of metarhodopsin II, *Nature 471*, 651-655.

109. Gether, U., Lin, S. S., and Kobilka, B. K. (1995) Fluorescent labeling of purified β_2 adrenergic-receptor - Evidence for ligand-specific conformational changes, *J. Biol. Chem. 270*, 28268-28275.

110. Gether, U., Lin, S., Ghanouni, P., Ballesteros, J. A., Weinstein, H., and Kobilka, B. K. (1997) Agonists induce conformational changes in transmembrane domains III and VI of the β_2 adrenoceptor, *EMBO J. 16*, 6737-6747.

111. Shi, L., Liapakis, G., Xu, R., Guarnieri, F., Ballesteros, J. A., and Javitch, J. A. (2002) β_2 adrenergic receptor activation - Modulation of the proline kink in transmembrane 6 by a rotamer toggle switch, *J. Biol. Chem. 277*, 40989-40996.

112. Rasmussen, S. G. F., DeVree, B. T., Zou, Y., Kruse, A. C., Chung, K. Y., Kobilka, T. S., Thian, F. S., Chae, P. S., Pardon, E., Calinski, D., Mathiesen, J. M., Shah, S. T. A., Lyons, J. A., Caffrey, M., Gellman, S. H., Steyaert, J., Skiniotis, G., Weis, W. I., Sunahara, R. K., and Kobilka, B. K. (2011) Crystal structure of the β_2 adrenergic receptor-Gs protein complex, *Nature 477*, 549-555.

113. Steyaert, J., and Kobilka, B. K. (2011) Nanobody stabilization of G protein-coupled receptor conformational states, *Curr. Opin. Struct. Biol. 21*, 567-572.

114. Rosenbaum, D. M., Cherezov, V., Hanson, M. A., Rasmussen, S. G. F., Thian, F. S., Kobilka, T. S., Choi, H. J., Yao, X. J., Weis, W. I., Stevens, R. C., and Kobilka, B. K. (2007) GPCR engineering yields high-resolution structural insights into β_2-adrenergic receptor function, *Science 318*, 1266-1273.

115. Visiers, I., Ballesteros, J. A., and Weinstein, H. (2002) Three-dimensional representations of G protein-coupled receptor structures and mechanisms, *Methods Enzymol. 343*, 329-371.

116. Hofmann, K. P., Scheerer, P., Hildebrand, P. W., Choe, H.-W., Park, J. H., Heck, M., and Ernst, O. P. (2009) A G protein-coupled receptor at work: The rhodopsin model, *Trends Biochem. Sci. 34*, 540-552.

117. Ruprecht, J. J., Mielke, T., Vogel, R., Villa, C., and Schertler, G. F. X. (2004) Electron crystallography reveals the structure of metarhodopsin I, *EMBO J. 23*, 3609-3620.

118. Nygaard, R., Frimurer, T. M., Holst, B., Rosenkilde, M. M., and Schwartz, T. W. (2009) Ligand binding and micro-switches in 7TM receptor structures, *Trends Pharmacol. Sci. 30*, 249-259.

119. Ahuja, S., and Smith, S. O. (2009) Multiple switches in G protein-coupled receptor activation, *Trends Pharmacol. Sci. 30*, 494-502.

120. Horn, F., Weare, J., Beukers, M. W., Horsch, S., Bairoch, A., Chen, W., Edvardsen, O., Campagne, F., and Vriend, G. (1998) GPCRDB: an information system for G protein-coupled receptors, *Nucleic Acids Res. 26*, 275-279.

121. Madabushi, S., Gross, A. K., Philippi, A., Meng, E. C., Wensel, T. G., and Lichtarge, O. (2004) Evolutionary trace of G protein-coupled receptors reveals clusters of residues that determine global and class-specific functions, *J. Biol. Chem. 279*, 8126-8132.

122. Baranski, T. J., Herzmark, P., Lichtarge, O., Gerber, B. O., Trueheart, J., Meng, E. C., Iiri, T., Sheikh, S. P., and Bourne, H. R. (1999) C5a receptor activation - Genetic identification of critical residues in four transmembrane helices, *J. Biol. Chem. 274*, 15757-15765.

123. Lu, Z. L., and Hulme, E. C. (1999) The functional topography of transmembrane domain 3 of the M_1 muscarinic acetylcholine receptor, revealed by scanning mutagenesis, *J. Biol. Chem. 274*, 7309-7315.

124. Tao, Y. X., Abell, A. N., Liu, X. B., Nakamura, K., and Segaloff, D. L. (2000) Constitutive activation of G protein-coupled receptors as a result of selective substitution of a conserved leucine residue in transmembrane helix III, *Mol. Endocrinol. 14*, 1272-1282.

125. Raman, D., Osawa, S., Gurevich, V. V., and Weiss, E. R. (2003) The interaction with the cytoplasmic loops of rhodopsin plays a crucial role in arrestin activation and binding, *J. Neurochem. 84*, 1040-1050.

126. Smith, S. O. (2010) Structure and activation of the visual pigment rhodopsin, *Annu. Rev. Biophys. 39*, 309-328.

127. Gehret, A. U., Jones, B. W., Tran, P. N., Cook, L. B., Greuber, E. K., and Hinkle, P. M. (2010) Role of helix 8 of the thyrotropin-releasing hormone receptor in phosphorylation by G protein-coupled receptor kinase, *Mol. Pharmacol. 77*, 288-297.

128. Marin, E. P., Krishna, K. G., Zvyaga, T. A., Isele, J., Siebert, F., and Sakmar, T. P. (2000) The amino terminus of the fourth cytoplasmic loop of rhodopsin modulates rhodopsin-transducin interaction, *J. Biol. Chem. 275*, 1930-1936.

129. Kirchberg, K., Kim, T.-Y., Möller, M., Skegro, D., Raju, G. D., Granzin, J., Büldt, G., Schlesinger, R., and Alexiev, U. (2011) Conformational dynamics of helix 8 in the GPCR rhodopsin controls arrestin activation in the desensitization process, *Proc. Natl. Acad. Sci. U. S. A. 108*, 18690-18695.

130. Fritze, O., Filipek, S., Kuksa, V., Palczewski, K., Hofmann, K. P., and Ernst, O. P. (2003) Role of the conserved NPxxY(x)(5,6)F motif in the rhodopsin ground state and during activation, *Proc. Natl. Acad. Sci. U. S. A. 100*, 2290-2295.

131. Reeves, P. J., Thurmond, R. L., and Khorana, H. G. (1996) Structure and function in rhodopsin: High level expression of a synthetic bovine opsin gene and its mutants in stable mammalian cell lines, *Proc. Natl. Acad. Sci. U. S. A. 93*, 11487-11492.

132. Eilers, M., Reeves, P. J., Ying, W. W., Khorana, H. G., and Smith, S. O. (1999) Magic angle spinning NMR of the protonated retinylidene Schiff base nitrogen in rhodopsin: Expression of ^{15}N-lysine and ^{13}C-glycine labeled opsin in a stable cell line, *Proc. Natl. Acad. Sci. U. S. A. 96*, 487-492.

133. Eilers, M., Ying, W. W., Reeves, P. J., Khorana, H. G., and Smith, S. O. (2002) Magic angle spinning nuclear magnetic resonance of isotopically labeled rhodopsin, *Methods Enzymol. 343*, 212-222.

134. Reeves, P. J., Kim, J. M., and Khorana, H. G. (2002) Structure and function in rhodopsin: A tetracycline-inducible system in stable mammalian cell lines for high-level expression of opsin mutants, *Proc. Natl. Acad. Sci. U. S. A. 99*, 13413-13418.

135. Allen, S. J., Ribeiro, S., Horuk, R., and Handel, T. M. (2009) Expression, purification and in vitro functional reconstitution of the chemokine receptor CCR1, *Protein Expression Purif. 66*, 73-81.

136. Arakawa, M., Chakraborty, R., Upadhyaya, J., Eilers, M., Reeves, P. J., Smith, S. O., and Chelikani, P. (2011) Structural and functional roles of small group-conserved amino acids present on helix-H7 in the β_2-adrenergic receptor, *Biochim. Biophys. Acta 1808*, 1170-1178.

137. Chelikani, P., Reeves, P. J., Rajbhandary, U. L., and Khorana, H. G. (2006) The synthesis and high-level expression of a β_2-adrenergic receptor gene in a tetracycline-inducible stable mammalian cell line, *Protein Sci. 15*, 1433-1440.

138. Dulbecco, R., and Freeman, G. (1959) Plaque production by the polyoma virus, *Virology 8*, 396-397.

139. Smith, J. D., Freeman, G., Vogt, M., and Dulbecco, R. (1960) The nucleic acid of polyoma virus, *Virology 12*, 185-196.

140. Dee, K. U., Shuler, M. L., and Wood, H. A. (1997) Inducing single-cell suspension of BTI-TN5B1-4 insect cells .1. The use of sulfated polyanions to prevent cell aggregation and enhance recombinant protein production, *Biotechnol. Bioeng. 54*, 191-205.

141. Navratilova, I., Sodroski, J., and Myszka, D. G. (2005) Solubilization, stabilization, and purification of chemokine receptors using biosensor technology, *Anal. Biochem. 339*, 271-281.

142. Molday, R. S., and MacKenzie, D. (1983) Monoclonal antibodies to rhodopsin: characterization, cross-reactivity, and application as structural probes, *Biochemistry 22*, 653-600.

143. Levitt, M. H. (2001) *Spin Dynamics*, 1 ed., John Wiley & Sons, Ltd, Chichester.

144. Lipfert, J., Columbus, L., Chu, V. B., Lesley, S. A., and Doniach, S. (2007) Size and shape of detergent micelles determined by small-angle x-ray scattering, *J. Phys. Chem. B 111*, 12427-12438.

145. Fahmy, K., and Sakmar, T. P. (1993) Light-dependent transducin activation by an ultraviolet-absorbing rhodopsin mutant, *Biochemistry 32*, 9165-9171.

146. Jastrzebska, B., Goc, A., Golczak, M., and Palczewski, K. (2009) Phospholipids are needed for the proper formation, stability, and function of the photoactivated rhodopsin-transducin complex, *Biochemistry 48*, 5159-5170.

147. Weiss, H. M., and Grisshammer, R. (2002) Purification and characterization of the human adenosine A_{2a} receptor functionally expressed in *Escherichia coli*, *Eur. J. Biochem. 269*, 82-92.

148. Navratilova, I., Besnard, J., and Hopkins, A. L. (2011) Screening for GPCR ligands using surface plasmon resonance, *ACS Med. Chem. Lett. 2*, 549-554.

149. Navratilova, I., Pancera, M., Wyatt, R. T., and Myszka, D. G. (2006) A biosensor-based approach toward purification and crystallization of G protein-coupled receptors, *Anal. Biochem. 353*, 278-283.

150. Navratilova, I., Dioszegi, M., and Myszka, D. G. (2006) Analyzing ligand and small molecule binding activity of solubilized GPCRs using biosensor technology, *Anal. Biochem. 355*, 132-139.

151. Devesa, F., Chams, V., Dinadayala, P., Stella, A., Ragas, A., Auboiroux, H., Stegmann, T., and Poquet, Y. (2002) Functional reconstitution of the HIV receptors CCR5 and CD4 in liposomes, *Eur. J. Biochem. 269*, 5163-5174.

152. Kobilka, B. K. (1995) Amino and carboxyl-terminal modifications to facilitate the production and purification of a g-protein-coupled receptor, *Anal. Biochem. 231*, 269-271.

153. Kobilka, B. K. (2011) Structural insights into adrenergic receptor function and pharmacology, *Trends Pharmacol. Sci. 32*, 213-218.

154. Farrens, D. L., and Khorana, H. G. (1995) Structure and function in rhodopsin. Measurement of the rate of metarhodopsin II decay by fluorescence spectroscopy, *J. Biol. Chem. 270*, 5073-5076.

155. Lowe, I. J. (1959) Free induction decays of rotating solids, *Physical Review Letters 2*, 285-287.

156. Andrew, E. R., Bradbury, A., and Eades, R. G. (1958) Nuclear magnetic resonance spectra from a crystal rotated at high speed, *Nature 182*, 1659.

157. Bjerring, M., and Nielsen, N. C. (2003) Solid-state NMR heteronuclear dipolar recoupling using off- resonance symmetry-based pulse sequences, *Chemical Physics Letters 370*, 496-503.

158. Ernst, M., Samoson, A., and Meier, B. H. (2001) Low-power decoupling in fast magic-angle spinning NMR, *Chemical Physics Letters 348*, 293-302.

159. Bennett, A. E., Rienstra, C. M., Auger, M., Lakshmi, K. V., and Griffin, R. G. (1995) Heteronuclear decoupling in rotating solids, *J. Chem. Phys. 103*, 6951-6958.

160. Gan, Z., and Ernst, R. R. (1997) Frequency- and phase-modulated heteronuclear decoupling in rotating solids, *Solid State Nucl. Magn. Reson. 8*, 153-159.

161. Fung, B. M., Khitrin, A. K., and Ermolaev, K. (2000) An improved broadband decoupling sequence for liquid crystals and solids, *J. Magn. Reson. 142*, 97-101.

162. Mayo, K. H., Daragan, V. A., Idiyatullin, D., and Nesmelova, I. (2000) Peptide internal motions on nanosecond time scale derived from direct fitting of ^{13}C and ^{15}N NMR spectral density functions, *J. Magn. Reson. 146*, 188-195.

163. Larsson, G., Martinez, G., Schleucher, J., and Wijmenga, S. S. (2003) Detection of nano-second internal motion and determination of overall tumbling times independent of the time scale of internal motion in proteins from NMR relaxation data, *J. Biomol. NMR 27*, 291-312.

164. Pervushin, K., Riek, R., Wider, G., and Wüthrich, K. (1997) Attenuated T-2 relaxation by mutual cancellation of dipole-dipole coupling and chemical shift anisotropy indicates an avenue to NMR structures of very large biological macromolecules in solution, *Proc. Natl. Acad. Sci. U. S. A. 94*, 12366-12371.

165. Hartmann, S. R., and Hahn, E. L. (1962) Nuclear double resonance in the rotating frame, *Physical Review 128*, 2042-2053.

166. Pines, A., Gibby, M. G., and Waugh, J. S. (1973) Proton-enhanced NMR of dilute spins in solids, *J. Chem. Phys. 59*, 569-590.

167. Peersen, O. B., Wu, X., and Smith, S. O. (1994) Enhancement of CP-MAS signals by variable amplitude cross polarization. Compensation for inhomogeneous B1 fields, *J. Magn. Reson. 106*, 127-131.

168. Metz, G., Ziliox, M., and Smith, S. O. (1996) Towards quantitative CP-MAS NMR, *Solid State Nucl. Magn. Reson. 7*, 155-160.

169. Schneider, R., Schumacher, M. C., Mueller, H., Nand, D., Klaukien, V., Heise, H., Riedel, D., Wolf, G., Behrmann, E., Raunser, S., Seidel, R., Engelhard, M., and Baldus, M. (2011) Structural characterization of polyglutamine fibrils by solid-state NMR spectroscopy, *J. Mol. Biol. 412*, 121-136.

170. Ahuja, S., Eilers, M., Hirshfeld, A., Yan, E. C. Y., Ziliox, M., Sakmar, T. P., Sheves, M., and Smith, S. O. (2009) 6-s-cis conformation and polar binding pocket of the retinal chromophore in the photoactivated state of rhodopsin, *J. Am. Chem. Soc. 131*, 15160–15169.

171. Ahuja, S., Crocker, E., Eilers, M., Hornak, V., Hirshfeld, A., Ziliox, M., Syrett, N., Reeves, P. J., Khorana, H. G., Sheves, M., and Smith, S. O. (2009) Location of the retinal chromophore in the activated state of rhodopsin, *J. Biol. Chem. 284*, 10190-10201.

172. Ahuja, S., Hornak, V., Yan, E. C. Y., Syrett, N., Goncalves, J. A., Hirshfeld, A., Ziliox, M., Sakmar, T. P., Sheves, M., Reeves, P. J., Smith, S. O., and Eilers, M. (2009) Helix movement is coupled to displacement of the second extracellular loop in rhodopsin activation, *Nat. Struct. Mol. Biol. 16*, 168-175.

173. Crocker, E., Eilers, M., Ahuja, S., Hornak, V., Hirshfeld, A., Sheves, M., and Smith, S. O. (2006) Location of Trp265 in metarhodopsin II: Implications for the activation mechanism of the visual receptor rhodopsin, *J. Mol. Biol. 357*, 163-172.

174. Herzfeld, J., Das Gupta, S. K., Farrar, M. R., Harbison, G. S., McDermott, A. E., Pelletier, S. L., Raleigh, D. P., Smith, S. O., Winkel, C., Lugtenburg, J., and Griffin, R. G. (1990) Solid-state ^{13}C NMR study of tyrosine protonation in dark-adapted bacteriorhodopsin, *Biochemistry 29*, 5567-5574.

175. Raleigh, D. P., Levitt, M. H., and Griffin, R. G. (1988) Rotational resonance in solid state NMR, *Chemical Physics Letters 146*, 71-76.

176. Gullion, T., and Schaefer, J. (1989) Detection of weak heteronuclear dipolar coupling by rotational-echo double-resonance NMR, In *Advances in Magnetic Resonance, Vol. 13; Conference on "High Resolution NMR in Solids", January 19-21, 1989* (Warren, W. S., Ed.), pp 57-84, Academic Press, Inc., San Diego, California, USA; London, England, UK.

177. Bennett, A. E., Rienstra, C. M., Griffiths, J. M., Zhen, W. G., Lansbury, P. T., and Griffin, R. G. (1998) Homonuclear radio frequency-driven recoupling in rotating solids, *J. Chem. Phys. 108*, 9463-9479.

178. Sodickson, D. K., Levitt, M. H., Vega, S., and Griffin, R. G. (1993) Broad-band dipolar recoupling in the nuclear-magnetic-resonance of rotating solids, *J. Chem. Phys. 98*, 6742-6748.

179. Takegoshi, K., Nakamura, S., and Terao, T. (2001) ^{13}C-^{1}H dipolar-assisted rotational resonance in magic-angle spinning NMR, *Chemical Physics Letters 344*, 631-637.

180. Crocker, E., Patel, A. B., Eilers, M., Jayaraman, S., Getmanova, E., Reeves, P. J., Ziliox, M., Khorana, H. G., Sheves, M., and Smith, S. O. (2004) Dipolar assisted rotational resonance NMR of tryptophan and tyrosine in rhodopsin, *J. Biomol. NMR 29*, 11-20.

181. Okada, T., Sugihara, M., Bondar, A. N., Elstner, M., Entel, P., and Buss, V. (2004) The retinal conformation and its environment in rhodopsin in light of a new 2.2 Å crystal structure, *J. Mol. Biol. 342*, 571-583.

182. Attwood, P. V., and Gutfreund, H. (1980) The application of pressure relaxation to the study of the equilibrium between metarhodopsin-I and metaphodopsin-II from bovine retinas, *FEBS Lett. 119*, 323-326.

183. Mielke, T., Alexiev, U., Gläsel, M., Otto, H., and Heyn, M. P. (2002) Light-induced changes in the structure and accessibility of the cytoplasmic loops of rhodopsin in the activated M-II state, *Biochemistry 41*, 7875-7884.

184. Okada, T., and Palczewski, K. (2001) Crystal structure of rhodopsin: implications for vision and beyond, *Curr. Opin. Struct. Biol. 11*, 420-426.

185. Salom, D., Le Trong, I., Pohl, E., Ballesteros, J. A., Stenkamp, R. E., Palczewski, K., and Lodowski, D. T. (2006) Improvements in G protein-coupled receptor purification yield light stable rhodopsin crystals, *J. Struct. Biol. 156*, 497-504.

186. Salom, D., Lodowski, D. T., Stenkamp, R. E., Le Trong, I., Golczak, M., Jastrzebska, B., Harris, T., Ballesteros, J. A., and Palczewski, K. (2006) Crystal structure of a photoactivated deprotonated intermediate of rhodopsin, *Proc. Natl. Acad. Sci. U. S. A. 103*, 16123-16128.

187. Arnis, S., and Hofmann, K. P. (1993) Two different forms of metarhodopsin II: Schiff base deprotonation precedes proton uptake and signaling state, *Proc. Natl. Acad. Sci. U. S. A. 90*, 7849-7853.

188. Jäger, S., Palczewski, K., and Hofmann, K. P. (1996) Opsin/all-trans-retinal complex activates transducin by different mechanisms than photolyzed rhodopsin, *Biochemistry 35*, 2901-2908.

189. Vogel, R., and Siebert, F. (2001) Conformations of the active and inactive states of opsin, *J. Biol. Chem. 276*, 38487-38493.

190. Kisselev, O. G., Kao, J., Ponder, J. W., Fann, Y. C., Gautam, N., and Marshall, G. R. (1998) Light-activated rhodopsin induces a structural binding motif in G protein α subunit, *Proc. Natl. Acad. Sci. U. S. A. 95*, 4270-4275.

191. Koenig, B. W., Kontaxis, G., Mitchell, D. C., Louis, J. M., Litman, B. J., and Bax, A. (2002) Structure and orientation of a G protein fragment in the receptor bound state from residual dipolar couplings, *J. Mol. Biol. 322*, 441-461.

192. Petkova, A. T., Hu, J. G. G., Bizounok, M., Simpson, M., Griffin, R. G., and Herzfeld, J. (1999) Arginine activity in the proton-motive photocycle of bacteriorhodopsin: Solid-state NMR studies of the wild-type and D85N proteins, *Biochemistry 38*, 1562-1572.

193. Kanamori, K., and Roberts, J. D. (1983) A nitrogen-15 NMR study of the barriers to isomerization about guanidinium and guanidino carbon-nitrogen bonds in L-arginine, *J. Am. Chem. Soc. 105*, 4698-4701.

194. Andres, A., Garriga, P., and Manyosa, J. (2003) Altered functionality in rhodopsin point mutants associated with retinitis pigmentosa, *Biochem. Biophys. Res. Commun. 303*, 294-301.

195. Hawtin, S. R. (2005) Charged residues of the conserved DRY triplet of the vasopressin V1a receptor provide molecular determinants for cell surface delivery and internalization, *Mol. Pharmacol. 68*, 1172-1182.

196. Auger, G. A., Pease, J. E., Shen, X. Y., Xanthou, G., and Barker, M. D. (2002) Alanine scanning mutagenesis of CCR3 reveals that the three intracellular loops are essential for functional receptor expression, *Eur. J. Immunol. 32*, 1052-1058.

197. Eilers, M., Patel, A. B., Liu, W., and Smith, S. O. (2002) Comparison of helix interactions in membrane and soluble α-bundle proteins, *Biophys. J. 82*, 2720-2736.

198. Imai, H., Kojima, D., Oura, T., Tachibanaki, S., Terakita, A., and Shichida, Y. (1997) Single amino acid residue as a functional determinant of rod and cone visual pigments, *Proc. Natl. Acad. Sci. U. S. A. 94*, 2322-2326.

199. Jaakola, V. P., Griffith, M. T., Hanson, M. A., Cherezov, V., Chien, E. Y. T., Lane, J. R., Ijzerman, A. P., and Stevens, R. C. (2008) The 2.6 Angstrom crystal structure of a human A_{2A} adenosine receptor bound to an antagonist, *Science 322*, 1211-1217.

200. Warne, T., Serrano-Vega, M. J., Baker, J. G., Moukhametzianov, R., Edwards, P. C., Henderson, R., Leslie, A. G., Tate, C. G., and Schertler, G. F. X. (2008) Structure of a β_1-adrenergic G-protein-coupled receptor, *Nature 454*, 486-491.

201. Janz, J. M., and Farrens, D. L. (2004) Role of the retinal hydrogen bond network in rhodopsin Schiff base stability and hydrolysis, *J. Biol. Chem. 279*, 55886-55894.

202. Kuwayama, S., Imai, H., Hirano, T., Terakita, A., and Shichida, Y. (2002) Conserved proline residue at position 189 in cone visual pigments as a determinant of molecular properties different from rhodopsins, *Biochemistry 41*, 15245-15252.

203. Sharma, D., and Rajarathnam, K. (2000) ^{13}C NMR chemical shifts can predict disulfide bond formation, *J. Biomol. NMR 18*, 165-171.

204. Ballesteros, J., Kitanovic, S., Guarnieri, F., Davies, P., Fromme, B. J., Konvicka, K., Chi, L., Millar, R. P., Davidson, J. S., Weinstein, H., and Sealfon, S. C. (1998) Functional microdomains in G-protein-coupled receptors - the conserved arginine-cage motif in the gonadotropin-releasing hormone receptor, *J. Biol. Chem. 273*, 10445-10453.

205. Ballesteros, J. A., Jensen, A. D., Liapakis, G., Rasmussen, S. G. F., Shi, L., Gether, U., and Javitch, J. A. (2001) Activation of the β_2-adrenergic receptor involves disruption of an ionic lock between the cytoplasmic ends of transmembrane segments 3 and 6, *J. Biol. Chem. 276*, 29171-29177.

206. Baltensperger, K., Karoor, V., Paul, H., Ruoho, A., Czech, M. P., and Malbon, C. C. (1996) The β-adrenergic receptor is a substrate for the insulin receptor tyrosine kinase, *J. Biol. Chem. 271*, 1061-1064.

207. Han, M., Smith, S. O., and Sakmar, T. P. (1998) Constitutive activation of opsin by mutation of methionine 257 on transmembrane helix 6, *Biochemistry 37*, 8253-8261.

208. Davidson, F. F., Loewen, P. C., and Khorana, H. G. (1994) Structure and function in rhodopsin: Replacement by alanine of cysteine residues 110 and 187, components of a conserved disulfide bond in rhodopsin, affects the light-activated metarhodopsin II state, *Proc. Natl. Acad. Sci. U. S. A. 91*, 4029-4033.

209. Cohen, G. B., Oprian, D. D., and Robinson, P. R. (1992) Mechanism of activation and inactivation of opsin: Role of Glu113 and Lys296, *Biochemistry 31*, 12592-12601.

210. Kobilka, B. K. (2007) G protein coupled receptor structure and activation, *Biochim. Biophys. Acta 1768*, 794-807.

211. Dixon, R. A. F., Kobilka, B. K., Strader, D. J., Benovic, J. L., Dohlman, H. G., Frielle, T., Bolanowski, M. A., Bennett, C. D., Rands, E., Diehl, R. E., Mumford, R. A., Slater, E. E., Sigal, I. S., Caron, M. G., Lefkowitz, R. J., and Strader, C. D. (1986) Cloning of the gene and cDNA for mammalian β-adrenergic receptor and homology with rhodopsin, *Nature 321*, 75-79.

212. Dixon, R. A. F., Sigal, I. S., Rands, E., Register, R. B., Candelore, M. R., Blake, A. D., and Strader, C. D. (1987) Ligand binding to the β-adrenergic receptor involves its rhodopsin-like core, *Nature 326*, 73-77.

213. Franke, R. R., Sakmar, T. P., Graham, R. M., and Khorana, H. G. (1992) Structure and function in rhodopsin. Studies of the interaction between the rhodopsin cytoplasmic domain and transducin, *J. Biol. Chem. 267*, 14767-14774.

214. Lai, R. K., Perezsala, D., Cañada, F. J., and Rando, R. R. (1990) The γ-subunit of transducin is farnesylated, *Proc. Natl. Acad. Sci. U. S. A. 87*, 7673-7677.

215. Vuong, T. M., Chabre, M., and Stryer, L. (1984) Millisecond activation of transducin in the cyclic nucleotide cascade of vision, *Nature 311*, 659-661.

216. Daaka, Y., Luttrell, L. M., Ahn, S., Della Rocca, G. J., Ferguson, S. S. G., Caron, M. G., and Lefkowitz, R. J. (1998) Essential role for G protein-coupled receptor endocytosis in the activation of mitogen-activated protein kinase, *J. Biol. Chem. 273*, 685-688.

217. Carman, C. V., and Benovic, J. L. (1998) G-protein-coupled receptors: Turn-ons and turn-offs, *Curr. Opin. Neurobiol. 8*, 335-344.

218. Kenakin, T. (2005) New concepts in drug discovery: Collateral efficacy and permissive antagonism, *Nature Reviews Drug Discovery 4*, 919-927.

219. Cherezov, V., Rosenbaum, D. M., Hanson, M. A., Rasmussen, S. G. F., Thian, F. S., Kobilka, T. S., Choi, H. J., Kuhn, P., Weis, W. I., Kobilka, B. K., and Stevens, R. C. (2007) High-resolution crystal structure of an engineered human β_2-adrenergic G protein-coupled receptor, *Science 318*, 1258-1265.

220. Rosenbaum, D. M., Zhang, C., Lyons, J. A., Holl, R., Aragao, D., Arlow, D. H., Rasmussen, S. G. F., Choi, H. J., DeVree, B. T., Sunahara, R. K., Chae, P. S., Gellman, S. H., Dror, R. O., Shaw, D. E., Weis, W. I., Caffrey, M., Gmeiner, P., and Kobilka, B. K. (2011) Structure and function of an irreversible agonist-β_2 adrenoceptor complex, *Nature 469*, 236-240.

221. Deupi, X., and Kobilka, B. K. (2010) Energy landscapes as a tool to integrate GPCR structure, dynamics, and function, *Physiology 25*, 293-303.

222. Swaminath, G., Xiang, Y., Lee, T. W., Steenhuis, J., Parnot, C., and Kobilka, B. K. (2004) Sequential binding of agonists to the β_2 adrenoceptor: Kinetic evidence for intermediate conformational states, *J. Biol. Chem. 279*, 686-691.

223. Dror, R. O., Pan, A. C., Arlow, D. H., Borhani, D. W., Maragakis, P., Shan, Y. B., Xu, H. F., and Shaw, D. E. (2011) Pathway and mechanism of drug binding to G-protein-coupled receptors, *Proc. Natl. Acad. Sci. U. S. A. 108*, 13118-13123.

224. Dror, R. O., Arlow, D. H., Maragakis, P., Mildorf, T. J., Pan, A. C., Xu, H., Borhani, D. W., and Shaw, D. E. (2011) Activation mechanism of the β_2-adrenergic receptor, *Proc. Natl. Acad. Sci. U. S. A. 108*, 18684-18689.

225. Dror, R. O., Arlow, D. H., Borhani, D. W., Jensen, M. O., Piana, S., and Shaw, D. E. (2009) Identification of two distinct inactive conformations of the β_2-adrenergic receptor reconciles structural and biochemical observations, *Proc. Natl. Acad. Sci. U. S. A. 106*, 4689-4694.

226. Li, J., Edwards, P. C., Burghammer, M., Villa, C., and Schertler, G. F. X. (2004) Structure of bovine rhodopsin in a trigonal crystal form, *J. Mol. Biol. 343*, 1409-1438.

227. Bokoch, M. P., Zou, Y. Z., Rasmussen, S. G. F., Liu, C. W., Nygaard, R., Rosenbaum, D. M., Fung, J. J., Choi, H. J., Thian, F. S., Kobilka, T. S., Puglisi, J. D., Weis, W. I., Pardo, L., Prosser, R. S., Mueller, L., and Kobilka, B. K. (2010) Ligand-specific regulation of the extracellular surface of a G-protein-coupled receptor, *Nature 463*, 108-121.

228. Ye, S. X., Zaitseva, E., Caltabiano, G., Schertler, G. F. X., Sakmar, T. P., Deupi, X., and Vogel, R. (2010) Tracking G-protein-coupled receptor activation using genetically encoded infrared probes, *Nature 464*, 1386-1389.

229. Vanni, S., Neri, M., Tavernelli, I., and Rothlisberger, U. (2009) Observation of "ionic lock" formation in molecular dynamics simulations of wild-type β_1 and β_2 adrenergic receptors, *Biochemistry 48*, 4789-4797.

230. Romo, T. D., Grossfield, A., and Pitman, M. C. (2010) Concerted interconversion between ionic lock substates of the β_2 adrenergic receptor revealed by microsecond timescale molecular dynamics, *Biophys. J. 98*, 76-84.

231. Strader, C. D., Candelore, M. R., Hill, W. S., Dixon, R. A. F., and Sigal, I. S. (1989) A single amino acid substitution in the β-adrenergic receptor promotes partial agonist activity from antagonists, *J. Biol. Chem. 264*, 16470-16477.

232. Del Carmine, R., Molinari, P., Sbraccia, M., Ambrosio, C., and Costa, T. (2004) "Induced-fit" mechanism for catecholamine binding to the β_2-adrenergic receptor, *Mol. Pharmacol. 66*, 356-363.

233. Ballesteros, J. A., Deupi, X., Olivella, M., Haaksma, E. E. J., and Pardo, L. (2000) Serine and threonine residues bend α-helices in the $c_1 = g^-$ conformation, *Biophys. J. 79*, 2754-2760.

234. Deupi, X., Olivella, M., Govaerts, C., Ballesteros, J. A., Campillo, M., and Pardo, L. (2004) Ser and Thr residues modulate the conformation of Pro-kinked transmembrane α-helices, *Biophys. J. 86*, 105-115.

235. Dawson, J. P., Weinger, J. S., and Engelman, D. M. (2002) Motifs of serine and threonine can drive association of transmembrane helices, *J. Mol. Biol. 316*, 799-805.

236. Xu, F., Wu, H. X., Katritch, V., Han, G. W., Jacobson, K. A., Gao, Z. G., Cherezov, V., and Stevens, R. C. (2011) Structure of an agonist-bound human A_{2A} adenosine receptor, *Science 332*, 322-327.

237. Warne, T., Moukhametzianov, R., Baker, J. G., Nehmé, R., Edwards, P. C., Leslie, A. G. W., Schertler, G. F. X., and Tate, C. G. (2011) The structural basis for agonist and partial agonist action on a β_1-adrenergic receptor, *Nature 469*, 241-244.

238. Eyring, G., Curry, B., Broek, A., Lugtenburg, J., and Mathies, R. (1982) Assignment and interpretation of hydrogen out-of-plane vibrations in the resonance Raman spectra of rhodopsin and bathorhodopsin, *Biochemistry 21*, 384-393.

239. Cooper, A. (1979) Energy uptake in the first step of visual excitation, *Nature 282*, 531-533.

240. Doukas, A. G., Aton, B., Callender, R. H., and Ebrey, T. G. (1978) Resonance raman studies of bovine metarhodopsin I and metarhodopsin II, *Biochemistry 17*, 2430-2435.

241. Verdegem, P. J. E., Bovee-Geurts, P. H. M., De Grip, W. J., Lugtenburg, J., and de Groot, H. J. M. (1999) Retinylidene ligand structure in bovine rhodopsin, metarhodopsin-I, and 10-methylrhodopsin from internuclear distance measurements using C-13-labeling and 1-D rotational resonance MAS NMR, *Biochemistry 38*, 11316-11324.

242. Feng, X., Verdegem, P. J. E., Eden, M., Sandström, D., Lee, Y. K., Bovee-Geurts, P. H. M., De Grip, W. J., Lugtenburg, J., de Groot, H. J. M., and Levitt, M. H. (2000) Determination of a molecular torsional angle in the metarhodopsin-I photointermediate of rhodopsin by double-quantum solid-state NMR, *J. Biomol. NMR 16*, 1-8.

243. Pan, D. H., and Mathies, R. A. (2001) Chromophore structure in lumirhodopsin and metarhodopsin I by time-resolved resonance Raman microchip spectroscopy, *Biochemistry 40*, 7929-7936.

244. Parkes, J. H., and Liebman, P. A. (1984) Temperature and pH dependence of the metarhodopsin I-metarhodopsin II kinetics and equilibria in bovine rod disk membrane suspensions, *Biochemistry 23*, 5054-5061.

245. Beck, M., Sakmar, T. P., and Siebert, F. (1998) Spectroscopic evidence for interaction between transmembrane helices 3 and 5 in rhodopsin, *Biochemistry 37*, 7630-7639.

246. Paulsen, R., and Bentrop, J. (1983) Activation of rhodopsin phosphorylation is triggered by the lumirhodopsin−metarhodopsin I transition, *Nature 302*, 417-419.

247. Pulvermüller, A., Palczewski, K., and Hofmann, K. P. (1993) Interaction between photoactivated rhodopsin and its kinase: stability and kinetics of complex formation, *Biochemistry 32*, 14082-14088.

248. Tachibanaki, S., Imai, H., Mizukami, T., Okada, T., Imamoto, Y., Matsuda, T., Fukada, Y., Terakita, A., and Shichida, Y. (1997) Presence of two rhodopsin intermediates responsible for transducin activation, *Biochemistry 36*, 14173-14180.

249. Tachibanaki, S., Imai, H., Terakita, A., and Shichida, Y. (1998) Identification of a new intermediate state that binds but not activates transducin in the bleaching process of bovine rhodopsin, *FEBS Lett. 425*, 126-130.

250. Spooner, P. J. R., Sharples, J. M., Goodall, S. C., Seedorf, H., Verhoeven, M. A., Lugtenburg, J., Bovee-Geurts, P. H. M., DeGrip, W. J., and Watts, A. (2003) Conformational similarities in the β-ionone ring region of the rhodopsin chromophore in its ground state and after photoactivation to the metarhodopsin-I intermediate, *Biochemistry 42*, 13371-13378.

251. Salgado, G. F. J., Struts, A. V., Tanaka, K., Krane, S., Nakanishi, K., and Brown, M. F. (2006) Solid-state ^{2}H NMR structure of retinal in metarhodopsin I, *J. Am. Chem. Soc. 128*, 11067-11071.

252. Resek, J. F., Farahbakhsh, Z. T., Hubbell, W. L., and Khorana, H. G. (1993) Formation of the meta II photointermediate is accompanied by conformational changes in the cytoplasmic surface of rhodopsin, *Biochemistry 32*, 12025-12032.

253. Matthews, R. G., Hubbard, R., Brown, P. K., and Wald, G. (1963) Tautomeric forms of metarhodopsin, *J. Gen. Physiol. 47*, 215-240.

254. Kusnetzow, A. K., Altenbach, C., and Hubbell, W. L. (2006) Conformational states and dynamics of rhodopsin in micelles and bilayers, *Biochemistry 45*, 5538-5550.

255. Nakamichi, H., and Okada, T. (2006) Local peptide movement in the photoreaction intermediate of rhodopsin, *Proc. Natl. Acad. Sci. U. S. A. 103*, 12729-12734.

256. Katayama, K., Furutani, Y., and Kandori, H. (2010) FTIR study of the photoreaction of bovine rhodopsin in the presence of hydroxylamine, *J. Phys. Chem. B 114*, 9039-9046.

257. Ratner, V. L., Bagirov, I. G., and Fesenko, E. E. (1981) Metarhodopsin I can react with hydroxylamine, *Vision Res. 21*, 251-253.

258. Unal, H., Jagannathan, R., Bhat, M. B., and Karnik, S. S. (2010) Ligand-specific conformation of extracellular loop-2 in the angiotensin II type 1 receptor, *J. Biol. Chem. 285*, 16341-16350.

259. Okada, T., Fujiyoshi, Y., Silow, M., Navarro, J., Landau, E. M., and Shichida, Y. (2002) Functional role of internal water molecules in rhodopsin revealed by x-ray crystallography, *Proc. Natl. Acad. Sci. U. S. A. 99*, 5982-5987.

260. Lüdeke, S., Beck, R., Yan, E. C. Y., Sakmar, T. P., Siebert, F., and Vogel, R. (2005) The role of Glu181 in the photoactivation of rhodopsin, *J. Mol. Biol. 353*, 345-356.

261. Struts, A. V., Salgado, G. F. J., Martínez-Mayorga, K., and Brown, M. F. (2011) Retinal dynamics underlie its switch from inverse agonist to agonist during rhodopsin activation, *Nat. Struct. Mol. Biol. 18*, 392-394.

262. Hornak, V., Ahuja, S., Eilers, M., Goncalves, J. A., Sheves, M., Reeves, P. J., and Smith, S. O. (2010) Light activation of rhodopsin: Insights from molecular dynamics simulations guided by solid-state NMR distance restraints, *J. Mol. Biol. 396*, 510-527.

263. Grossfield, A., Pitman, M. C., Feller, S. E., Soubias, O., and Gawrisch, K. (2008) Internal hydration increases during activation of the G-protein-coupled receptor rhodopsin, *J. Mol. Biol. 381*, 478-486.

264. Nakamichi, H., and Okada, T. (2006) Crystallographic analysis of primary visual photochemistry, *Angew. Chem.-Int. Edit. 45*, 4270-4273.

265. Ye, S. X., Huber, T., Vogel, R., and Sakmar, T. P. (2009) FTIR analysis of GPCR activation using azido probes, *Nat. Chem. Biol. 5*, 397-399.

266. Chien, E. Y. T., Liu, W., Zhao, Q. A., Katritch, V., Han, G. W., Hanson, M. A., Shi, L., Newman, A. H., Javitch, J. A., Cherezov, V., and Stevens, R. C. (2010) Structure of the human dopamine D3 receptor in complex with a D2/D3 selective antagonist, *Science 330*, 1091-1095.

267. Moukhametzianov, R., Warne, T., Edwards, P. C., Serrano-Vega, M. J., Leslie, A. G., Tate, C. G., and Schertler, G. F. X. (2011) Two distinct conformations of helix 6 observed in antagonist-bound structures of a β_1-adrenergic receptor, *Proc. Natl. Acad. Sci. U. S. A. 108*, 8228-8232.

268. Longstaff, C., Calhoon, R. D., and Rando, R. R. (1986) Deprotonation of the Schiff base of rhodopsin is obligate in the activation of the G-protein, *Proc. Natl. Acad. Sci. U. S. A. 83*, 4209-4213.

269. Zhukovsky, E. A., and Oprian, D. D. (1989) Effect of carboxylic acid side chains on the absorption maximum of visual pigments, *Science 246*, 928-930.

270. Sansom, M. S. P., and Weinstein, H. (2000) Hinges, swivels and switches: The role of prolines in signalling via transmembrane α-helices, *Trends Pharmacol. Sci. 21*, 445-451.

271. Salgado, G. F. J., Struts, A. V., Tanaka, K., Fujioka, N., Nakanishi, K., and Brown, M. F. (2004) Deuterium NMR structure of retinal in the ground state of rhodopsin, *Biochemistry 43*, 12819-12828.

272. Feng, X., Verdegem, P. J. E., Lee, Y. K., Sandström, D., Eden, M., Bovee-Geurts, P., Degrip, W. J., Lugtenburg, J., Degroot, H. J. M., and Levitt, M. H. (1997) Direct determination of a molecular torsional angle in the membrane protein rhodopsin by solid-state NMR, *J. Am. Chem. Soc. 119*, 6853-6857.

273. Wishart, D. S., and Sykes, B. D. (1994) Chemical-shifts as a tool for structure determination, *Methods Enzymol. 239*, 363-392.

274. Röhrig, U. F., Guidoni, L., and Rothlisberger, U. (2002) Early steps of the intramolecular signal transduction in rhodopsin explored by molecular dynamics simulations, *Biochemistry 41*, 10799-10809.

275. Schreiber, M., Sugihara, M., Okada, T., and Buss, V. (2006) Quantum mechanical studies on the crystallographic model of bathorhodopsin, *Angew. Chem.-Int. Edit. 45*, 4274-4277.

276. Nakayama, T. A., and Khorana, H. G. (1991) Mapping of the amino acids in membrane-embedded helices that interact with the retinal chromophore in bovine rhodopsin, *J. Biol. Chem. 266*, 4269-4275.

277. Bright, J. N., and Sansom, M. S. P. (2003) The flexing/twirling helix: Exploring the flexibility about molecular hinges formed by proline and glycine motifs in transmembrane helices, *J. Phys. Chem. B 107*, 627-636.

278. Tieleman, D. P., Shrivastava, I. H., Ulmschneider, M. R., and Sansom, M. S. P. (2001) Proline-induced hinges in transmembrane helices: Possible roles in ion channel gating, *Proteins: Structure, Function, and Genetics 44*, 63-72.

279. Xie, G. F., Gross, A. K., and Oprian, D. D. (2003) An opsin mutant with increased thermal stability, *Biochemistry 42*, 1995-2001.

280. Xie, G., D'Antona, A. M., Edwards, P. C., Fransen, M., Standfuss, J., Schertler, G. F. X., and Oprian, D. D. (2011) Preparation of an activated rhodopsin/transducin complex using a constitutively active mutant of rhodopsin, *Biochemistry 50*, 10399-10407.

281. Standfuss, J., Xie, G. F., Edwards, P. C., Burghammer, M., Oprian, D. D., and Schertler, G. F. X. (2007) Crystal structure of a thermally stable rhodopsin mutant, *J. Mol. Biol. 372*, 1179-1188.

282. Doi, T., Molday, R. S., and Khorana, H. G. (1990) Role of the intradiscal domain in rhodopsin assembly and function, *Proc. Natl. Acad. Sci. U. S. A. 87*, 4991-4995.

283. Nygaard, R., Valentin-Hansen, L., Mokrosinski, J., Frimurer, T. M., and Schwartz, T. W. (2010) Conserved water-mediated hydrogen bond network between TM-I, -II, -VI, and -VII in 7TM receptor activation, *J. Biol. Chem. 285*, 19625-19636.

284. Arvanitakis, L., Geras-Raaka, E., Varma, A., Gershengorn, M. C., and Cesarman, E. (1997) Human herpesvirus KSHV encodes a constitutively active G-protein-coupled receptor linked to cell proliferation, *Nature 385*, 347-350.

285. Bockenhauer, S., Fürstenberg, A., Yao, X. J., Kobilka, B. K., and Moerner, W. E. (2011) Conformational dynamics of single G protein-coupled receptors in solution, *J. Phys. Chem. B 115*, 13328-13338.

286. Franke, R. R., König, B., Sakmar, T. P., Khorana, H. G., and Hofmann, K. P. (1990) Rhodopsin mutants that bind but fail to activate transducin, *Science 250*, 123-125.

287. Liu, Y., Buck, D. C., and Neve, K. A. (2008) Novel interaction of the dopamine D-2 receptor and the Ca2+ binding protein S100B: Role in D-2 receptor function, *Mol. Pharmacol. 74*, 371-378.

288. Warne, T., Edwards, P. C., Leslie, A. G. W., and Tate, C. G. (2012) Crystal Structures of a Stabilized beta(1)-Adrenoceptor Bound to the Biased Agonists Bucindolol and Carvedilol, *Structure 20*, 841-849.

289. Elgeti, M., Kazmin, R., Heck, M., Morizumi, T., Ritter, E., Scheerer, P., Ernst, O. P., Siebert, F., Hofmann, K. P., and Bartl, F. J. (2011) Conserved Tyr223(5.58) plays different roles in the activation and G-protein interaction of rhodopsin, *J. Am. Chem. Soc. 133*, 7159-7165.

290. Arora, K. K., Cheng, Z. Y., and Catt, K. J. (1997) Mutations of the conserved DRS motif in the second intracellular loop of the gonadotropin-releasing hormone receptor affect expression, activation, and internalization, *Mol. Endocrinol. 11*, 1203-1212.

291. Lu, Z. L., Curtis, C. A., Jones, P. G., Pavia, J., and Hulme, E. C. (1997) The role of the aspartate-arginine-tyrosine triad in the m1 muscarinic receptor: Mutations of aspartate 122 and tyrosine 124 decrease receptor expression but do not abolish signaling, *Mol. Pharmacol. 51*, 234-241.

292. Zhang, Y. P., Lewis, R. N., Hodges, R. S., and McElhaney, R. N. (1995) Peptide models of helical hydrophobic transmembrane segments of membrane proteins. 2. Differential scanning calorimetric and FTIR spectroscopic studies of the interaction of Ac-K2-(LA)12-K2-amide with phosphatidylcholine bilayers, *Biochemistry 34*, 2362-2371.

293. Cornish, V. W., Benson, D. R., Altenbach, C. A., Hideg, K., Hubbell, W. L., and Schultz, P. G. (1994) Site-specific incorporation of biophysical probes into proteins, *Proc. Natl. Acad. Sci. U. S. A. 91*, 2910-2914.

294. Mendel, D., Ellman, J. A., Chang, Z., Veenstra, D. L., Kollman, P. A., and Schultz, P. G. (1992) Probing protein stability with unnatural amino acids, *Science 256*, 1798-1802.

295. Ellman, J., Mendel, D., Anthony-Cahill, S., Noren, C. J., and Schultz, P. G. (1991) Biosynthetic method for introducing unnatural amino acids site-specifically into proteins, *Methods Enzymol. 202*, 301-336.

296. Noren, C. J., Anthony-Cahill, S. J., Suich, D. J., Noren, K. A., Griffith, M. C., and Schultz, P. G. (1990) In vitro suppression of an amber mutation by a chemically aminoacylated transfer RNA prepared by runoff transcription, *Nucleic Acids Res. 18*, 83-88.

297. Zhang, L. R., Sports, C. D., Osawa, S., and Weiss, E. R. (1997) Rhodopsin phosphorylation sites and their role in arrestin binding, *J. Biol. Chem. 272*, 14762-14768.

298. Lewis, J. W., Szundi, I., Fu, W. Y., Sakmar, T. P., and Kliger, D. S. (2000) pH dependence of photolysis intermediates in the photoactivation of rhodopsin mutant E113Q, *Biochemistry 39*, 599-606.

299. Vogel, R., Fan, G. B., Siebert, F., and Sheves, M. (2001) Anions stabilize a metarhodopsin II-like photoproduct with a protonated Schiff base, *Biochemistry 40*, 13342-13352.

300. Tsukamoto, H., Terakita, A., and Shichida, Y. (2010) A Pivot between helices V and VI near the retinal-binding site is necessary for activation in rhodopsins, *J. Biol. Chem. 285*, 7351-7357.

301. Han, M., Lin, S. W., Minkova, M., Smith, S. O., and Sakmar, T. P. (1996) Functional interaction of transmembrane helices 3 and 6 in rhodopsin - Replacement of phenylalanine 261 by alanine causes reversion of phenotype of a glycine 121 replacement mutant, *J. Biol. Chem. 271*, 32337-32342.

302. Sakai, K., Imamoto, Y., Yamashita, T., and Shichida, Y. (2010) Functional analysis of the second extracellular loop of rhodopsin by characterizing split variants, *Photochemical & Photobiological Sciences 9*, 1490-1497.

303. Samson, M., LaRosa, G., Libert, F., Paindavoine, P., Detheux, M., Vassart, G., and Parmentier, M. (1997) The second extracellular loop of CCR5 is the major determinant of ligand specificity, *J. Biol. Chem. 272*, 24934-24941.

304. Willett, B. J., Adema, K., Heveker, N., Brelot, A., Picard, L., Alizon, M., Turner, J. D., Hoxie, J. A., Peiper, S., Neil, J. C., and Hosie, M. J. (1998) The second extracellular loop of CXCR4 determines its function as a receptor for feline immunodeficiency virus, *Journal of Virology 72*, 6475-6481.

305. Wurch, T., Colpaert, F. C., and Pauwels, P. J. (1998) Chimeric receptor analysis of the ketanserin binding site in the human 5-hydroxytryptamine$_{1D}$ receptor: Importance of the second extracellular loop and fifth transmembrane domain in antagonist binding, *Mol. Pharmacol. 54*, 1088-1096.

306. Brelot, A., Heveker, N., Adema, K., Hosie, M. J., Willett, B., and Alizon, M. (1999) Effect of mutations in the second extracellular loop of CXCR4 on its utilization by human and feline immunodeficiency viruses, *Journal of Virology 73*, 2576-2586.

307. Kajumo, F., Thompson, D. A. D., Guo, Y., and Dragic, T. (2000) Entry of R5X4 and X4 human immunodeficiency virus type 1 strains is mediated by negatively charged and tyrosine residues in the amino-terminal domain and the second extracellular loop of CXCR4, *Virology 271*, 240-247.

308. Shi, L., and Javitch, J. A. (2002) The binding site of aminergic G protein-coupled receptors: The transmembrane segments and second extracellular loop, *Annu. Rev. Pharmacol. Toxicol. 42*, 437-467.

309. Shi, L., and Javitch, J. A. (2004) The second extracellular loop of the dopamine D-2 receptor lines the binding-site crevice, *Proc. Natl. Acad. Sci. U. S. A. 101*, 440-445.

310. Klco, J. M., Wiegand, C. B., Narzinski, K., and Baranski, T. J. (2005) Essential role for the second extracellular loop in C5a receptor activation, *Nat. Struct. Mol. Biol. 12*, 320-326.

311. Avlani, V. A., Gregory, K. J., Morton, C. J., Parker, M. W., Sexton, P. M., and Christopoulos, A. (2007) Critical role for the second extracellular loop in the binding of both orthosteric and allosteric G protein-coupled receptor ligands, *J. Biol. Chem. 282*, 25677-25686.